Ministry of Higher Education & Scientific Research
University of Kerbala
College of Engineering
Mechanical Engineering Department

Design and Construction a Novel Solar Water Collector with Air Bubble Injection

A Thesis
Submitted to the Mechanical Engineering Department / College of Engineering /University of Kerbala, in Partial Fulfillment of the Requirements for the Degree of Master of Sciences in Mechanical Engineering

Written By:

Zahraa Mohammed Kadhum
(B.Sc. University of Kufa 2012)

Supervised By:

Asst. Prof. Dr. Mohammed Wahhab Al-Jibory

Asst. Prof. Dr. Farhan Lafta Rashid

2023   1444

بسم الله الرحمن الرحيم

﴿اللَّهُ نُورُ السَّمَاوَاتِ وَالْأَرْضِ مَثَلُ نُورِهِ كَمِشْكَاةٍ فِيهَا مِصْبَاحٌ الْمِصْبَاحُ فِي زُجَاجَةٍ الزُّجَاجَةُ كَأَنَّهَا كَوْكَبٌ دُرِّيٌّ يُوقَدُ مِنْ شَجَرَةٍ مُبَارَكَةٍ زَيْتُونَةٍ لَا شَرْقِيَّةٍ وَلَا غَرْبِيَّةٍ يَكَادُ زَيْتُهَا يُضِيءُ وَلَوْ لَمْ تَمْسَسْهُ نَارٌ نُورٌ عَلَى نُورٍ يَهْدِي اللَّهُ لِنُورِهِ مَنْ يَشَاءُ وَيَضْرِبُ اللَّهُ الْأَمْثَالَ لِلنَّاسِ وَاللَّهُ بِكُلِّ شَيْءٍ عَلِيمٌ﴾.

صدق الله العلي العظيم

سورة النور 35

Linguistic Certificate

I certify that the thesis entitled " **Design and Construction a Novel Solar Water Collector with Air Bubble Injection,** " which has been submitted by **Zahraa Mohammed Kadhum,** has been proofread and its language has been amended to meet the English style.

Signature: *sahib*

Dr. Sahib Shihab Ahmed

Date: 24/1/2023

Supervisor's Certificate

We certify that the thesis entitled "**Design and Construction a Novel Solar Water Collector with Air Bubble Injection**" was prepared by **Zahraa Mohammed Kadhum** under our supervision at the Department of Mechanical Engineering, College of Engineering, University of Kerbala (as part of the fulfilment of the requirements for the degree.) of Master of Science in Mechanical Engineering.

Signature:

Dr. Mohammed Wahhab Kadhum

Signature:

Dr. Farhan Lafta Rashid

Undertaking

I certify that the research work entitled "**Design and Construction a Novel Solar Water Collector with Air Bubble Injection**" is my own work. The work has not been presented elsewhere for assessment. Where material has been used from other sources, it has been properly acknowledged / referred to.

Signature: *Zahraa Mohammed*

2023

Examination committee certification

We certify that we have read the thesis entitled "**Design and Construction a Novel Solar Water Collector with Air Bubble Injection**" and as an examining committee, we examined the student "**Zahraa Mohammed Kadhum**" in its content and in what is connected with it, and that in our opinion it is adequate as a thesis for the degree of Master of Science in Mechanical Engineering.

Supervisor

Signature:
Name: Asst. Prof. Dr. Mohammed W. Kadhum
Date: /   / 2023

Supervisor

Signature:
Name: Asst. Prof. Dr. Farhan Lafta Rashid
Date: /   / 2023

Member

Signature:
Name: Asst. Prof. Dr. Hayder Jabar Kurji
Date: 30 / 3 / 2023

Member

Signature:
Name: Asst. Prof. Dr. Hasan Talib Hashim
Date: /   / 2023

Chairman

Signature:
Name: Prof. Dr. Riyadh S. AL-Turaihi
Date: 30 / 3 / 2023

Signature:
Name:
Head of the Department   of Mechanical
Engineering
Date: 10 / 4 / 2023

Signature:
Name:
Dean of the Engineering College
Date: /   / 2023

Acknowledgements

Dedication

To My Husband Murtadha

Thanks for Your Great Supports and Continuous Care without them I wouldn't have been able to accomplish this work

To My Parents

The Reason of What I Became Today.

To My Brother and Sisters

Thanks for Your Supports in My Life.

To My Children Aya and Ahmed

You Are the Reason of My Strength in Life

Zahraa Mohammed

2023

Abstract

This study presented two investigation ways (numerically and experimentally) that used a venturi mechanism to inject air bubbles into a wavy pipe solar water collector to improve its performance. This technique allows air to move through the pipes, mixing with water and then flowing together inside the solar collector's pipe. Two systems were used in each part, an opened and closed system. The numerical part was accomplished by generating the geometric model with SOLID WORKS 2021, followed by being simulated with using the simulation program ANSYS 21. While the experimental part was executed by constructing a rig of the solar water collector system with collector dimensions of (120 x 80 x 24) cm^3 that is inclined by 45º, which includes a wavy copper pipe shape with a diameter of 0.0125 m and a length of 8 m that is painted with matt black color. The test rig was construct in Karbala city to figure out the effect of air bubble injection under the weather conditions of the city of Holy Karbala in Iraq with latitude and longitude of 32.616° N and 44.0249° E during the first months of the year (January, February, March and April). The water as a working fluid was used with multiple flowrates to determine the collector efficiency of each system, then the air bubbles were injected with several discharges to the most efficient water flowrate for each system (closed and opened), thus knowing the best flowrate of the air-water mixture for each system.

In this work, fourteen cases were simulated and experimented to find out the collector performance and the most efficient case, which consisted of four various levels of only water flowrates of (0.5, 1, 1.5 and 2) L/min as a working fluid for an opened and closed system. The air bubbles were injected at three air flowrates of (0.15, 0.25 and 0.35) L/min mixed with the most efficient water flowrate at each system.

However, the system efficiency was calculated after the numerical and experimental tests were done for the four water flowrates for both systems. The calculation shows that the most efficient case for the opened system occurred when the water flowrate was 1 L/min, with an average efficiency of (31.8) %, whereas the most efficient case for the closed system was at 2 L/min, with an average efficiency of (45.5) %. The three different flowrates of air were injected into the efficient casing for each system. The result showed that the closed system efficiency was enhanced by (24.98%), (37.28%), and (53.71%), whereas the opened system efficiency enhanced by (30.89%), (37.92%), and (20.03%) after adding air at flowrates of (0.15, 0.25, and 0.35) L/min respectively.

Numerical simulation, by ANSYS FLUENT software and experimental results, for the model were found, to have a fairly, good agreement, under the same, conditions. For the both systems (with and without air bubbles injection), the maximum percentage of difference in the results is no more than 13.5%.

Table of Content

SUBJECT	Page No.

Nomenclature

Symbol	*Description*	*Units*
A	Collector Area	m^2
Cp	Specific heat capacity at constant pressure	kJ/kg.c
D	Pipe diameter	m
f	Friction factor	…….
F	Force by body	N
g	Gravitation acceleration	m/s^2
G	Turbulence kinetic energy production	J/kg
H	Hight of solar water collector	cm
h	High of solar water collector	m
I	Hourly solar intensity	W/m^2
K	Thermal Conductivity	W/m.k
l	Pipe length	m
MF	Mass flowrate	kg/s
q	Fluid volumetric flowrate	m^3/s
Q	Energy gain	W
S	Total entropy	J/k
T	Temperature	^{o} C
U	Overall heat transfer coefficient	W/m^2.c
V	Velocity	m/s
W	Width of solar water collector	m
L	Length	m
X	Thickness of insulation	cm
ṁ	Mass flow rate	kg/s

Greek Symbols

Symbol	Description	Units
∇	Gradient (vector operator)	……..
α	Volume fraction	……..
β	Angle of elbow	
ΔP	Pressure drops	kpa
ΔT	Temperature difference	^{o} C
ε	Effectiveness	……..
θ	Tilt angle	Degree
μ	Viscosity	N.s/m^2
ρ	Density	kg/m^3
σ	turbulent Prandtl number	……..
v	averaged velocity	m/s
η	Efficiency	……..
∂	Partial differential operator	……..

Subscripts

Symbol	Description
a	Ambient, air
c	Collector
E	Total energy
eff	effective
h	hot
in	Inlet
k	Phase different characters
m	Mixture
out	Outlet
p	plate
s	Shell side
t	Turbulent
u	Useful
w	water

Abbreviation

Symbol	Description
ANSYS	Analysis System
CFD	Computational Fluid Dynamics
cm	Centimeter
FLUENT	Fluid and Heat Transfer Code
FPSC	Flat plate solar collectors
L/min	Litter per minute
m	Mater
mm	Millimeter
NTU	Number of the thermal unit
Nu	Nusselt number
RANS	Reynolds Averaged Naiver–Stokes equations
Re	Reynold number

Chapter one

Introduction

1

<div align="center">

Chapter One

Introduction

</div>

Overview

Current energy production from coal and oil is unsustainable and bad for the environment. Many developing nations are unable to supply these energy sources. Sustainable energy, also known as renewable or alternative energy, is obtained from naturally occurring phenomena like wind, biomass, solar, and hydroelectric power. They are environmentally friendly and sustainable. Because it can meet human energy needs, has no negative environmental effects, and can be converted into other forms of energy, including electrical, mechanical, and thermal energy. Renewable energy has become the first choice among the sources.

One type of clean and sustainable energy is solar energy. In recent years, new technologies that are environmentally friendly, have low operating capacities, and are inexpensive, such as Solar Collectors, these technologies include the solar water heater, which effectively uses solar energy resources to supply hot water.

1.1 Solar Energy Collectors

Solar energy collectors are special kinds of heat exchangers that transform solar radiation energy into the internal energy of the transport medium. The major component of any solar system is the solar collector. This is a device that absorbs the incoming solar radiation, converts it into heat, and transfers this heat to a fluid (usually air, water, or oil) flowing through the collector. The solar energy thus collected is carried by the circulating fluid either directly to the hot water or to a thermal energy storage tank, which can be drawn for use at night and/or cloudy days.

Concentrating and non-concentrating solar collectors are the two most common types. A sun-tracking concentrating solar collector typically has concave reflecting surfaces to intercept and focus the sun's beam radiation to a smaller receiving area, increasing the radiation flux, as opposed to a non-concentrating collector, which has the same area for intercepting and absorbing solar radiation [1]. The solar collector can be classified as below:

- Non – concentrating collectors
  - Flat plate collector
  - Evacuated tube collector
  - Solar chimney
- Concentrating collectors
  - Parabolic dish
  - Parabolic trough
  - Solar tower

1.2 Flat Plate Collector (FPC)

The most efficient and suitable solar technology for low-and medium-temperature thermal applications in fluid heating are flat plate, solar collector. Heat is transferred from the absorber, which has been heated by solar radiation, to the working fluid. Flat plate solar collectors are available for a low price, have a well-developed construction, and are widely used in solar technology. Flat plate collectors can produce enough temperature for household hot water, buildings, and swimming pools in both residential and commercial applications [2]. Figure (1.1) represents a traditional single- glazed flat plate solar collector, which can used both beam and diffuse solar radiation as a heating source [3].
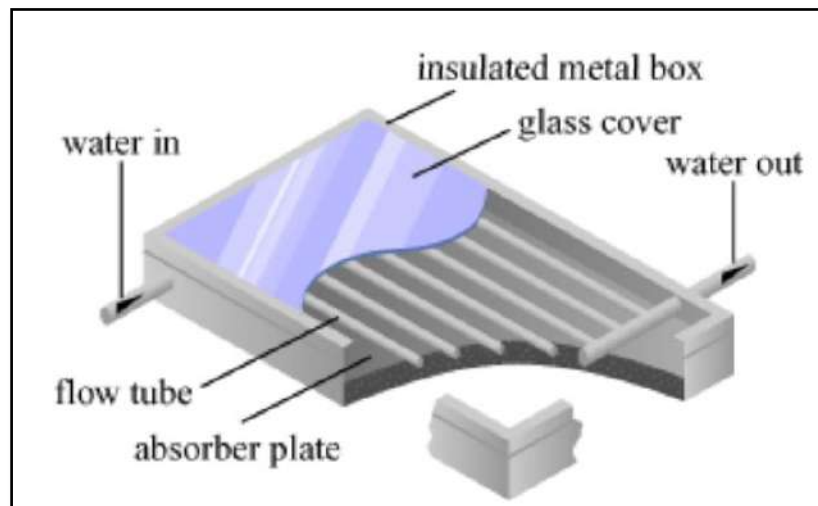
Figure 1-1: Solar Flat Plat Collector [3].

The effectiveness of solar collection can be increased by the careful technical design of the materials and heat transfer system. Basic parts of standard flat plate collectors include:

• A transparent covering made of one or more layers of glass or plastic that transmits visible and near-infrared radiation (wavelengths shorter than 3 μm) while absorbing far-infrared radiation (wavelengths longer than 3 μm). There are three main benefits to the cover in flat plate collectors, first one is to increase the absorber's absorptance and return the solar radiation beam that was reflected from it. The thermal radiation emitted from the black absorber is trapped by the cover, which reduces thermal loss from the collection systems and is the cover's second benefit. The last one is to separate the black absorber from the ambient temperature so that it decreases the heat loss.

• An absorber plate with a high solar absorptance and a low thermal emissivity that is coated with a material with high thermal conductivity.

• Metal tubes or channels that the heat transfer fluid flows through and that are usually coated in the same substance as the absorber plate.

• A container or casing surrounding the above parts, with insulating material covering the sides and rear of the absorber plate to reduce heat losses[4].

1.3 Solar Water Heating Systems

Heating water with solar energy can be a cost effective and environmentally responsible way to generate hot water, minimizing the expense of electricity or fossil fuels to heat water and reducing the associated environmental impacts.

Solar water heating systems use solar collectors to capture sunlight to heat water (or an antifreeze liquid) that is then moved from the collector to storage and then to its point of use. There are two types of systems, active and passive[5].

1.3.1 Active Systems

Active systems pump water or other heat-transfer fluids through the collectors that would use electric pumps, valves, and controllers. They are typically more expensive but also more effective than passive systems. Because active systems' storage tanks do not need to be put above or close to the collectors, they are typically simpler to construct than passive systems. However, they require electricity, so when the power goes off, they won't work [6].

This type of system can be classified into two categories:

- Open-loop (Direct) Active System
- Closed-loop (Indirect) Active System

1.3.1.1 The Open Loop Active Systems

Pumps are used in open-loop active systems to circulate residential water through the collectors. Although this design is effective and lowers operational costs, it is not recommended for use with hard or acidic water since scale and corrosion would quickly making the system unworkable. In nonfreezing climates, these open-loop systems are common. They should never be set up in regions that regularly experience below-freezing temperatures [6]. These open-loop systems are common as shown in figure (1.3) [7].
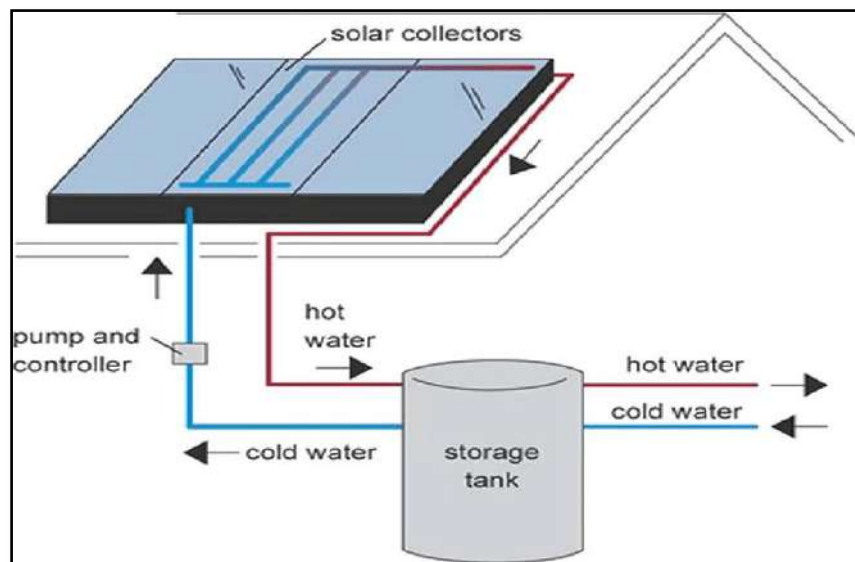
Figure 1-3: Open Loop System [7]

1.3.1.2 The Closed Loop Active Systems

These systems circulate heat-transfer fluids (often an antifreeze solution of glycol and water) through collectors. Household water that is kept in tanks is heated by using heat exchangers. Considering that they provide effective freeze protection [7], closed-loop glycol systems are common in regions that experience prolonged cold temperatures as shown in figure (1.4)[6].
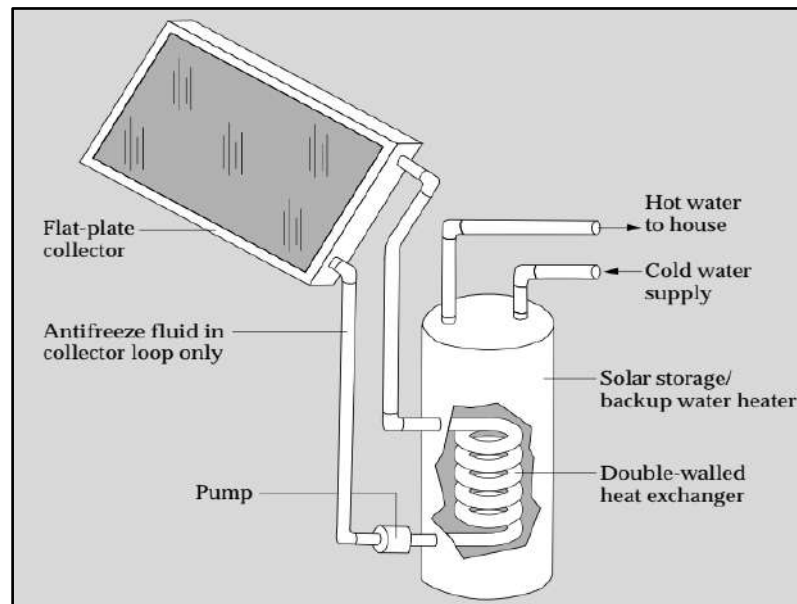
Figure 1-4: Closed Loop Systems [6]

1.3.2 Passive Systems

In passive systems, hot water is either kept in the collector itself or moved through a thermosyphon to a storage tank above the collectors. Pumps are not used in passive systems to move collector fluid or water. there are two types of passive systems[8]:

- Thermosyphon systems.
- Integral collector storage systems

1.4 The Two-Phase Flow

The majority of two-phase flow occurs in systems with two phases (usually gas and liquid) separated by a meniscus. Two-phase flows include solid-gas, solid-liquid, and liquid-liquid flows in addition to gas-liquid flows. Numerous systems in the chemical, petroleum, bio-medical, refrigeration, and air conditioning industries, among others, use two-phase flows[9].

1.4.1 Definitions and Classifications of Flow-Pattern

A- Description of Flow Patterns in Horizontal Tubes

The presence of flow patterns and flow regimes in two-phase flow is the most important distinction between single-phase flows and gas-liquid two-phase flows. The overall geometrical structure of the gas and liquid phases in the pipe is referred to as the flow pattern. The two phases can actively distribute themselves in a variety of various flow patterns when gas and liquid are flowing through a pipe at the same time. Due to varying flow characteristics and velocities, the flow configurations differed significantly from one another in terms of interface spatial distribution. Figure (1.5) show the flow characteristics or flow regimes for horizontal flows[9].
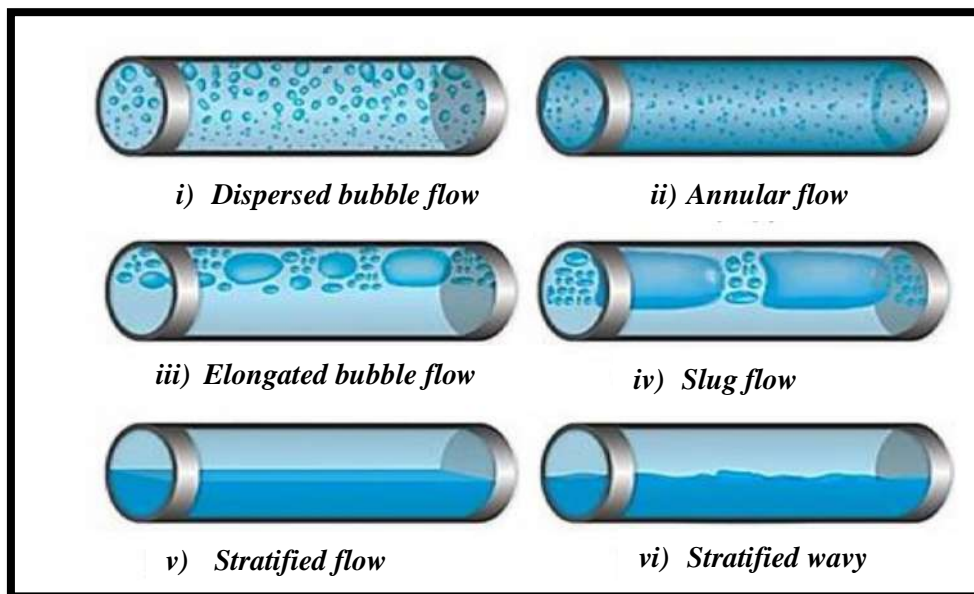
Figure 1-5: Flow Characteristics or Flow Regimes for Horizontal Flows[9].

Gravity forces the gas, the less dense phase, to migrate to the top of the channel in horizontal two-phase flow as a result of the density difference between the air and water phases.

As a result, horizontal two phase flow has the following flow patterns that are not axisymmetrical [10]:

1- **Bubble flow**: This type shows that the flow pattern is characterized by bubbles of air that are distributed randomly in a continuous liquid phase. The bubbles are quite small in comparison with the pipe's diameter. The gas bubbles typically move in the upper half of the tube due to gravity.

2- **Annular flow regime**: In this regime, the liquid is swept up in an annular pattern around the tube's perimeter, while the faster-moving air flows inside the tube's core and picks up tiny droplets of liquid that have been distributed into a mist. The liquid film may contain tiny gas bubbles as well. This regime manifests at a reasonably high gas phase mass flow rate.

3- **Elongated bubbly (slug) flow**: The upper half of the tube contains an aerated continuous liquid phase that is carrying the air phase in the form of elongated bubbles.

4- **Stratified smooth flow**: The liquid phase flows along the bottom of the tube while the air phase goes along the top without any significant interfacial waves. At low air and liquid mass flow rates, the gravity separation is complete, and the stratified flow regime occurs.

5- **Stratified wavy flow**: A wavy flow pattern develops as the air velocity rises because the faster-moving air creates waves at the air-water interfaces. The faster moving liquid slugs are typically accompanied by high pressure pulses and oscillations that can harm equipment further downstream.

B- Description of Flow Patterns in Vertical Tubes

Systems in which a gaseous phase is dispersed throughout a liquid are commonly encountered in both nature and industry. Known as gas-liquid flows, these systems occur in situations as diverse as the bow wave of a ship to the cooling system in a nuclear power plant. Figure (1.6) show the structure of a gas-liquid flow depends upon the relative flow-rates of the two phases, and, for flow in a vertical pipe, can be categorized into regimes[11].
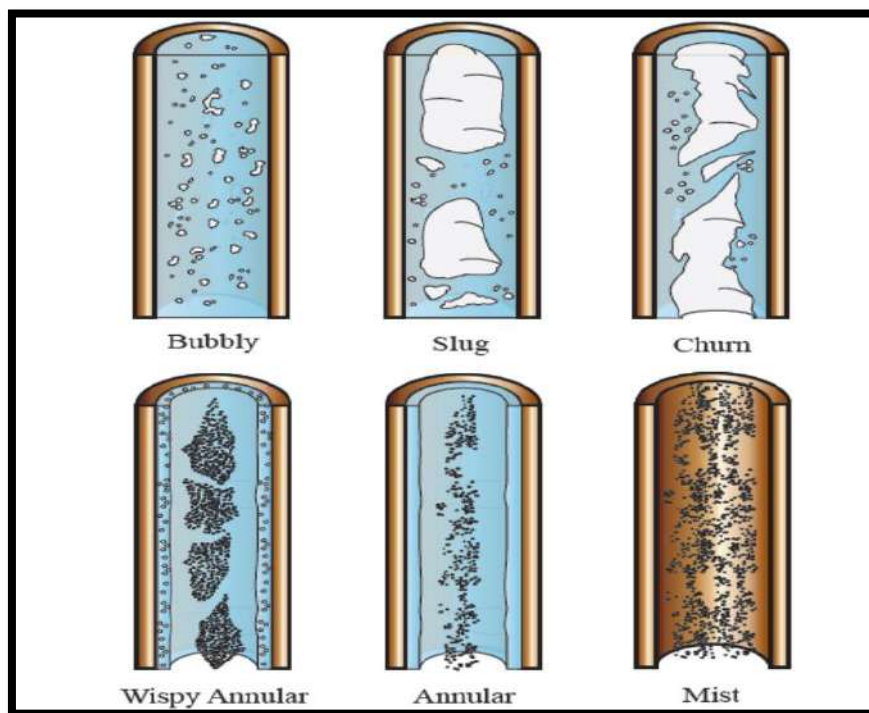
Figure 1-6: Flow Characteristics or Flow Regimes for vertical Flow [12]

1- **Bubbly flow:** In this regime, a large number of small bubbles, notably smaller than the channel diameter, are observed in the continuous liquid phase. The bubbles may vary widely in size and shape but they are typically rather densely packed and flowing side-by-side and one after another, creating a very complex flow.

2- **Slug flow:** This regime is characterized by large bubbles that span nearly the entire channel cross-section and are separated by distinct

liquid slugs, the latter giving this regime its name. These bubbles have a cylindrical shape with a hemispherical nose and a blunt fluctuating tail; they are commonly referred to as Taylor bubbles after the instability of that name. The bubbles are typically about 1.5 to 3.0 times longer in length than the tube diameter.

3- **Churn flow:** This regime is a very chaotic fluctuating type of flow that is passed through during the transition from a stable slug flow to a stable annular flow. Churn flow is typically to be avoided in two-phase piping, because of the pressure and flow oscillations that it induces. Some flow pattern maps treat this regime as part of the transition region between slug flow and annular flow.

4- **Annular flow:** This regime is named after the continuous annular liquid film that flows on the internal perimeter of the channel with a higher velocity gas (or vapor) core in the center. The interface of the annular liquid film is disturbed by high frequency waves and ripples.

5- **Mist flow:** A mist flow has the gas (or vapor) as the continuous phase and numerous very small droplets entrained in it. Mist flow is encountered at high vapor qualities at the point where the annular film is thinned by the shear of the gas core on the interface until it becomes unstable, such that all the liquid is entrained as droplets in the continuous gas phase, or during flow boiling when the critical heat flux has been surpassed. Impinging liquid droplets intermittently wet the tube wall locally but heat transfer is significantly decreased with respect to an annular flow[12].

1.4.2 Injection of Air Bubbles

Air bubble injection has recently been proposed as one of the promising methods for improving the thermal performance of heat exchangers. However, the injection method and the fluid's characteristics have an influence on the number, size and distribution of these bubbles. Once bubbles have formed in the liquid, they will naturally float to the surface due to the buoyancy force created by the difference in densities between the liquid and the air. The liquid will be mixed and the hydrodynamic and thermal boundary layers will be broken down by the random motion of the bubbles, improving heat exchange in thermal systems such solar collectors. However, many of variables including the air bubble flow velocity, number of bubbles, the bubbles size, and the collector design affect the mixing level [13].

1.5 Statement of the Problem

The purpose of this experimental and numerical study was to explain how adding air bubbles to solar collectors improved the parameters (ΔT, Qu and η) and numerical performance parameters (temperature distribution, water flowmeter distribution, ΔT, ΔP) of a wavy pipe solar water collector for demonstrating various ratios (air - water) in Karbala conditions.

1.6 The Objectives and Plan of this Work

This study was focused on the flat plate solar collector system because it offers a potential way to use solar energy. Which in this thesis can be attained by doing the following:

A. Start by researching the development of this type of solar collector as well as the researchers who are involved in experimental or numerical research in this area. Chapter 2 contains this information.

B. Chapter three takes up the numerical design for this system. This design included two parts:

1- Part I: The flow field in a solar collector under a heat flux was examined using numerical simulation, a finite volume, numerical methodologies, and the ANSYS FLUENT package code R.21. These equations for continuity, momentum, and energy were solved as part of the analysis.

2- Part II: Analytical calculations can be used to determine the efficiency of the collector.

C. A scale model of the solar collector was created in order to investigate the performance of a solar collector experimentally. This design was covered in chapter four, which deals with the creation of the experimental setup and instruments needed to validate the concept.

D. The numerical and experimental results are discussed in Chapter 5.

E. In chapter six, the performance and analysis of a scale model of a solar collector are discussed. From the cases that were analyzed, conclusions and recommendations were made.

Chapter Two

Literature Review

2

Chapter Two

Literature Review

Introduction

Solar technology has been used by mankind since ancient times, but the development in this field was in the recent decades when our need for clean and sustainable energy sources to replace our use of fossil fuel was realized. Solar energy can be used for many applications. The climate of a region specifies which applications are useful for that region. In Iraq and other regions with similar climates solar energy is mainly used for space heating, water heating, agricultural drying and electricity generation. Solar energy can also be used in air conditioning and refrigeration.

The reason for writing the literature review is to present a large portion of the discussions and examinations completed by the researchers. The literature review can be divided into two categories, starting with flat plate collectors and following by air bubble injection technique.

2.1 Flat Plate Collectors

Solar water collectors, aim to transfer heat from the sun to the fluids, like water, which is one of the most common fluid uses. The most typical solar water collectors are flat plate collectors, which are consists of differently shaped pipes attached to a fixed plate and covered in glass. Researchers hope to increase efficiency and effectiveness by modifying the collector's shapes, cover glass, coating, liquid type, and other characteristics.

Jinwei Ma.et al. (2012)[14] Design of solar collector that is able to provide both hot water and hot air has been proposed to increase annual thermal conversion ratio of solar energy. By modifying the conventional flat-plate solar water heater, the collector with L-shape fins can also function as a double flow solar air heater. Experiments have been

conducted to investigate the dual functions of the collector. It is shown that the thermal efficiency of the collector reached 50% in water heating, and varied from 41% to 55% in air heating depending on the ambient condition and flow rate. Mathematical model has been presented for the collector working in air heating mode. The theoretical results are in good agreement with the experiment results. Theoretical results show that the air flow rate is a dominant factor to determine the efficiency. The enhancement of the L-shape fins on the performance of the collector in air heating is also proved from the theoretic results.

Oliva.al. (2012) [15] In this work, proposed a low-cost material to be used as an excellent absorber for solar collectors, to increase its thermal efficiency by the high capacity to absorb solar radiation. The material, known as "smoke black" (soot) can be obtained by the incomplete combustion of organic materials, such as the oxygen-acetylene, paraffin, or candles. A comparative analysis between the optical properties (reflectance, absorbance, and emissivity) measured on three covered copper surfaces (without paint, with a commercial matte black paint, and with smoke black) shows amazing optical results for the smoke black. Reflectance values of the smoke black applied over copper surfaces improves 56 times the values obtained from commercial black paints. High values of emissivity (0.9988) were measured on the surface covered with smoke black by spectrophotometry in the UV-VIS range, which represents about 7% of increment as compared with the value obtained for commercial black paints (0.938). The proposed high absorbance material can be easily applied on any kind of surfaces at low cost.

Bakari et al.(2014) [16] The effect of glass thickness on the performance of flat plate solar collectors was studied. Where design four models of solar collectors with an area of 0.72 m² and a depth of 0.15m

and an angle of inclination of 10 degrees towards the ground level and to the north, were built with different glass thicknesses and experimentally tested for their performance. Low-iron (extra-pure) glass was used with thicknesses (3, 4, 5 and 6) mm. The results showed that the change in the thickness of the glass leads to a variation in the efficiency of the compound. The compound with a thickness of 4 mm glass gave the best efficiency of 35.4% compared to 27.8% for glass with a thickness of 6 mm. However, 4mm thick glass is more prone to breakage so care must be taken during use and installation.

Hossain et al. (2014) [17] A two-sided parallel solar water heater has been proposed to improve the thermal efficiency of the system. As it is easy to manufacture as well as lower cost and gives high thermal efficiency. The experimental results showed that the average efficiency during two months is 75.5% and the average temperature is 98 $^{\circ}$C, where the proposed shape of the solar collector was proven in the increase of collector efficiency, especially in areas where there is plenty of sunlight to benefit from it, especially in Malaysia.

Noghrehabadi et al. (2016) [18] experimentally investigated the performance of a symmetric square flat-plate solar collector employing water and a SiO2/water nanofluid with a mass fraction of 1% as working fluids, without surfactants. The experiments were performed according to ASHRAE Standard 93-86 at different flow rates between 0.35 and 2.8 L/min. The result shows the SiO2/water nanofluid increased the efficiency of the square flat-plate solar collector compared with net water.

Hashim et al.(2018) [19] described the performance of flat plate collector for solar water heating. The thermal performance system was created with dimensions of (125×110) cm^2 and 25 cm width, with a pipe length of 15.9 m. It was developed in a lope square pattern and using water

as the fluid flow that operated at two different flow rates (5.3 and 6.51 L/min). The results demonstrate that the water heated faster at flow rates of 5.3 L/min compared to 6.51 L/min, which increased the collector's efficiency. As a result, the maximum temperature was respectively 51.4 °C and 49 °C at these flow rates respectively.

Esdras Nshimyumuremyi and Wang Junqi (2019) [20] In three different regions, solar water heaters were manufactured and installed, and all measurements were made under the same conditions and using the same measuring tools. The absorbent plate was made of aluminum sheets instead of galvanized iron because it has a high thermal conductivity, the absorber plate was (960 * 1300 * 0.6) mm^3 and the base of the solar collector was insulated to avoid thermal losses. The system also consists of a tank with a capacity of 200 L and two solar collectors with an area of 1.385 m^2. The results showed that the thermal efficiency depends on the design of the solar collector and the materials used in the absorption plate, and the efficiency ranged between 60 and 76%.

Moravej et al. (2019)[21] Enhanced the performance of solar water heaters can be by number of different methods. One such method involves altering the geometry of the collector. In this study, a symmetrical flat-panel solar collector with circular geometry has been experimentally evaluated. The collector has an area of one square meter, is free of risers and features spiral tubes that flow into the collector from the side and exit from the center. The collector was tested according to ASHRAE standards in Aghajari, southern Iran. The experiments focused on quantifying the efficiency and thermal performance of the collector at various conditions, such as different water flow rates and solar radiation. The results show that, like other flat-panel collectors, the collector efficiency increases with increase in water flow rate and solar radiation. The efficiency increase in

this collector is higher than that of rectangular collectors owing to the presence of secondary currents. Furthermore, the maximum efficiency of this collector is around 75.3%, with a maximum temperature difference between the inlet and outlet of around 19 °C. This study offers a simple way to improve the performance of solar water heaters.

Saffarian et al. (2020) [22] The effect of changing the flow direction of a flat plate solar collector on raising the convective heat transfer coefficient is being investigated numerically. Three shapes of pipes can be used with flat plate collectors with identical pipe lengths: U-shaped, wavy, and spiral. Nanofluids of Al2O3/water and CuO/water is utilized in volume fractions of 1% and 4%, respectively. The heat transfer coefficient and Nusselt number can be increased by using wavy and spiral pipes, according to the results. Additionally, it has been noted that wavy pipes have the highest pressure drop. Using nanofluid instead of water improves the heat transfer coefficient in every situation, with the exception of the CuO 4%. By adding nanoparticles to water, thermal conductivity was remarkable increased, which resulted in a decrease in the Nusselt number. According to the result, the heat transfer coefficient can rise to 78.25% when wavy pipes and a 4% volume fraction of CuO/water nanofluid are used.

Mohammad et al. (2020)[23]compare between two scenarios of spiral collector; the first one without lens and the other with lens. In the two scenarios, the spiral collector was fabricated from copper tube with 10 mm inner diameter, 15 m length and absorber area 0.5 m2. The lens was selected as acrylic flat lens with transmittance (80 to 90)% and focal distance is 1.3 m. Experiments were carried out at water mass flow rate 0.5 kg/min under the period between 1st to 31th of December over the ambient temperature range of 12 to 17 °C and hourly solar radiation range of 525 to

654 W/m2. The experimental results show that the maximum outlet-temperature, useful energy and efficiency was found to be about 19 °C, 109 W, 35% respectively in scenario of spiral collector without lens. While, in the scenario of spiral with lens was found to be about 21 °C, 178 W, 60% respectively. As compared between the two scenarios, the lens was enhanced the efficiency of spiral collector by 25%.

Muthuraman et al.(2021) [24] modified the tube geometry of solar water collector flow to be straight, curved, and spiral to enhance the system's performance. The flow pipes of the solar water heater are made of copper material, which has higher thermal conductivity to recover the water's heat as thermal energy. The influence of the mass flow rate on the flow pipes with respect to the surface temperature for various configurations of the flow tubes is investigated. The mass flow rate of 0.0045 kg/s and 0.006 kg/s are tested. The mass flow rate of 0.006 kg/s yields the maximum efficiency of 73% compared to the other mass flow rate. The straight, curved, and spiral tubes yielded the highest efficiencies of 58%, 62%, and 69%, respectively, at 0.0045 kg/s. Similarly, the mass flow rate of 0.006 kg/s obtained an efficiency of 62%, 65%, and 73% for straight, curved, and spiral flow tubes, respectively.

2.2 Air Bubble Injection Technique

A novel experimental technique will be proposed for injecting small air bubbles into a solar flat plate collector's riser tube. It will be compared the changes in solar radiation intensity to find out how the forced water flow rates, tube design, and air bubble injection effect on the thermal efficiency of solar flat plates.

Baylar. et al. (2009) [25]The water passes through a restriction in a pipe, it forms a vacuum at the end of the restriction. A hole bored into the pipe at a point where this vacuum occurs will cause air to be drawn into

the main flow. One example of this mechanism is seen in the venturi tube. When a minimal amount of differential pressure exists between the inlet and outlet sides of the venturi tube, a vacuum occurs at suction holes of the venturi tube. Venturi aeration is a method of aeration that has become popular in recent years. In present paper, air injection rates of venturi tubes are analyzed using Computational Fluid Dynamics modeling. These analyses are carried out by means of the program FLUENT V6.2 that uses finite volume theory. There is a good agreement between the measured air injection rates and the values computed from FLUENT CFD program. The results obtained from CFD analyses will lead air suction mechanism of a venturi tobe understood better. There is a good agreement between the measured air injection rates and the values computed from FLUENT V6.2 CFD program. Therefore, CFD analyses can be used to determine optimum dimensions of venturi to get higher air injection rate. The harmful effect of cavitation can be prevented by watching changes in velocity and pressure. The pressure-velocity characteristics of venturi are not affected too much by changing of venturi and throat diameters. But the diameters affect the length of non-aerated flow region of venturi.

Moosavi. et al. (2016) [26] focuses on improving the efficiency of the shell-and-coiled-tube heat exchangers by air bubble injection (with a constant air flow rate) inside the heat exchangers. Only the shell side of the heat exchanger, not the coil side, has had air flow pumped inside it. The range of the air flow rate was 1 to 5 L/min. Shell side water flow rate was adjusted between 1L/min and 5L/min (inlet temperature of 15 ^{0}C), while coil side water flow rate was maintained at 1L/min (inlet temperature of 40 ^{0}C). The pressure drop is also measured. Observations revealed that the effect of bubble injection into heat exchangers is significantly influenced by the air flow rate and injection side (shell and coil). The outcome

demonstrated that an increase in air flow rate results in an improvement in the total heat transfer coefficient.

Panthalookaran and George (2016)[27]developed a novel technique of solar collector cooling that uses a humidification-dehumidification cycle to simultaneously make hot water and saturate air, enabling an effective sun distillation unit to operate .The impacts of the air-to-water ratio and the inner diameters of the absorber tubes in the solar collector were studied in detail. The results showed that air-water flows can successfully cool solar collectors, resulting in superior cooling of solar collector absorber plates.

Heyhat et al. (2018) [28] focused on an experimental analysis of the influence of air bubble injection as an active technique in the thermal efficiency of a twin pipe heat exchanger. Air bubbles are injected into the annulus side using various injectors. Experimental data are compiled for a range of tube and annulus side flow rates. The effect of air flow rate and heat exchanger positioning angle on thermal performance is investigated using energetic analysis. The results show that air bubble injection can increase the overall coefficient of the heat transfer with 10.3% to 14.9%.

Kreem. et al. (2019)[29] studied the impact of the influence of introducing small air bubbles on heat exchanger temperature distribution with a vertical shell and helical coiled tubes. There were four thermocouples installed along the shell side of the heat exchange unit in addition to the inlet and exit thermocouples. At a constant air temperature of 18 ^{0}C for each flow rate, experiments were carried out with three different shell water flow rates (4, 6, and 8 L/min) and five different air flow rates (2, 4, 6, 8, and 10 L/min). Both the coiled tube and the shell's fluid (water) input temperatures were maintained at 37 °C and 17 °C, respectively. The findings demonstrated that there was reciprocal thermal

mixing. As a result, a considerable heat transfer rate was seen, as shown by the heat exchanger's temperature rising quickly.

Viacheslav Shemelin and Tomas Matuska (2019)[30]In the present work, the detailed mathematical model of a dual air/water solar collector has been developed and experimentally verified. To demonstrate the application of Thea dual air/water solar collector, three buildings with different energy performance levels and three building locations were chosen in analyzed case studies. Four solar collector systems were compared with one another. The solar yield of the described systems was determined by simulation using the detailed theoretical model of a dual air/water solar collector. The results indicate that in the case of combining a domestic hot water preparation system and recirculating-air heating system based on a dual air/water solar collector, it is possible to achieve up to 30% higher solar energy yield compared to a conventional solar domestic hot water preparation system dependent on climate and building performance.

Mohammed et al. (2020) [31] Investigate experimentally the influence of small air bubble injection on a flat plate solar collector's efficiency with tube rises in an opened system. Both the change in water flow rate and the variation in the air bubble injection with air flow rates have an effect on the thermal efficiency of the solar flat plate collector. When solar radiation intensity varied, the effects of forced water flow rates and air bubble injection on the thermal efficiency of solar flat plates were compared. With intake water temperatures ranging from (19 to 23.5) °C, water and air flow rates were varied between (1.5 - 2.5) L/min. The thermal efficiency is improved by injecting small air bubbles, and it increased by (3.5–5.25) %.

Hasan et al. (2021)[13] Experimental research is done to determine the effect of air bubble size on the thermal efficiency of a vertical counter-current shell and coiled tube heat exchanger. The studies were carried out in a cylinder-shaped heat exchanger with an outer diameter of 15 cm and a height of 50 cm. The heated water was transported using a copper coil with an outer diameter of 0.6 cm and an equivalent length of 3.939 meters. Constant hot (coil side) flow rate fluid rates 1 L/min, four different injected air flow rates (0.5, 1, 1.5, and 2) L/min, and four varied cold fluid (shell side) flow rates (2, 4, 6 and 8) L/min under laminar flow conditions ($316 \leq$ Re $\leq$ 1223), and constant bubble's number (1400). The experimental results clearly showed that the heat exchanger's thermal efficiency significantly improved with increasing the shell side flow rate and the injected air flow rate. The maximum improvement in U, NTU, and effectiveness was 153%, 153%, and 68%, respectively. The thermal performance of the heat exchanger was shown to be improved with increasing the bubble size.

Sajida Lafta Ghashim, Ayser Muneer Flayh (2021)[32] investigated the addition of air bubbles influenced on the enhancement of heat transfer and the turbulent flow pressure drop in two helical coil heat exchangers. The experiment used a turbulent hot water flow with a Reynolds number (Re) ranging from 9000 to 50000 and a constant mass flow rate of cold water at 0.0331 kg/s. Injection of air bubbles into hot water at rates of (1.5, 2.5, and 3.5) L/min. The effectiveness is increased by adding air bubbles to the hot water, and at a flow rate of 3.5 L/min it reaches its maximum value of 0.22. With increasing bubble injection, the friction factor tends to rise from 0.1 to 0.31 at Reynolds number 9823. Injection of air bubbles increases the Nusselt number in all cases where the flow rate of the air bubbles is present. The greatest enhancement ratio of

the Nusselt number was determined to be between 2.4 and 3.1 at an injected air flow rate of 3.5 L/min with Reynolds number between 9823 and 48028.

Jawad et al. (2022)[33] In their study, the impact of adding small bubbles of air to a water stream that was flowing through two copper spiral tubes that 15 m long, 0.012 m diameter, and had 11 coils was investigated. A matte black paint with a nanomaterial mixture was also coated on the internal surface of the solar collector (thermal dye with 5 % of TiN). Using a venturi mechanism, the air and water were combined and then flowed together inside the tube of the solar water collector at different water flowrates (1, 1.5, 2, 2.5) L/min used. The result show that the outgoing temperature increases as mass flow rate decreases, widening the difference between inlet and outlet temperatures in both the opened and closed systems. In the closed system, the largest temperature difference was 36.1ºC. The greatest temperature difference in the opened system was 12.5 ºC for water and air bubble flow rates of 1 L/min and 0.3 L/min, respectively.

The table (2.1) illustrate a brief for the previous researches for the researchers in this field.

Table 2-1: Literature Reviews for Experimental and Numerical Studies.

No.	Researches	Country	System type	Investigation Type
1.	Jinwei Ma.et al. (2011)	China	solar collector for both hot water and hot air	Experimental
2.	Oliva.al. (2012)	México	Three surfaces of copper for solar collector	Theoretical
3.	Bakari. et al. (2014)	Tanzania	Flat plate solar collectors	Experimental
4.	Hossain.et al. (2014)	Malaysia	Flat plate solar water heater concerning the two-sided parallel serpentine flow	Experimental
5.	Noghrehabadi. et al. (2016)	Iran	Square flat-plate solar collector	Experimental
6.	Hashim et al. (2018)	Iraq	Solar water heater type square flow	Experimental

7.	Esdras Nshimyumuremyi and Wang Junqi (2019)	China	Solar water heating	Experimental
8.	Moravej et al. (2019)	Hungary	Solar water heating with circular geometry	Experimental
9.	Saffarian et al. (2020)	Iran	Changed the flow direction, U-shaped, wavy and spiral pipes	Numerical
10.	Mohammad et al. (2020)	Iraq	spiral solar collector without lens and with lens	Experimental
11.	Muthuraman. et al. (2021)	India	Solar water collector, curved and spiral type flow	Experimental
12.	Baylar. et al. (2009)	Turkey	Numerical Modeling of Venturi Flows.	Numerical
13.	Moosavi. et al. (2016)	Iran	Heat exchangers with shell-and-coiled-tube that have air bubble injection.	Experimental
14.	Panthalookaran and George (2016)	India	solar collectors using a single fluid to cool it with water or with air only.	Experimental
15.	Heyhat. et al. (2018)	Iran	Double Pipe Heat Exchanger with Air Bubble Injection.	Experimental
16.	Kreem. et al. (2019)	Iraq	Air bubble injection on Helical Coiled Tube Heat Exchanger.	Experimental
17.	Viacheslav Shemelin and Tomas Matuska (2019)	Czech	A dual air/water solar collector.	Experimental and Theoretical
18.	Mohammed. et al. (2020)	Iraq	Air bubble injection	Experimental
19.	Hasan. et al. (2021)	Iraq	The effect of injecting air bubble size.	Experimental
20.	Sajida Lafta Ghashim and Ayser Muneer Flayh (2021)	Iraq	Air bubble injection in a heat exchanger with two helical coils.	Experimental
21.	Jawad. et al. (2022)	Iraq	Closed and open system Spiral tube.	Experimental and numerical
22.	Zahraa Mohammed	Iraq	Air bubble injection in wavy pipe.	Experimental and numerical

2.3 Aim of This Work

The current thesis focuses on the air bubble injection technique for wavy pipe of solar water flat plate collector. Investigating the effects of adding tiny air bubbles to a model that was examined numerically and experimentally. A flat plate solar collector's efficiency for both opened and closed systems with multi water flowrate.

Chapter Three

Theoretical Model

3

Chapter Three

Theoretical Model

Introduction

ANSYS Fluent gives extensive modeling capabilities for a large variety of incompressible and compressible, laminar and turbulent fluid flow issues. It is possible to accomplish steady-state or transient analysis. In ANSYS Fluent, a wide range of mathematical models for transport phenomena (such as heat transmission and chemical reactions) is connected with the ability to represent complicated geometries[34].

Simulation programs have been very helpful in the development of various scientific applications. These programs have made it much easier and less expensive for researchers to create simulations that would help them solve many problems involving the design and operation of different systems

3.1 Part I: Numerical Simulation

3.1.1 System Geometry

Geometric models created with the SOLID WORKS 2021 application are used to depict the real dimensions of study case geometries. The system's configuration is shown in figure (3.1) and detailed in table (3.1), which contains a (120*80) cm^2 rectangle area with a wavy tube that is designed to cover the largest possible collector area by taking into account the symmetrical pitch and pipe bending and curves to each line with the other pipe lines. Eight-meter-long copper tubes are placed on top of the aluminum plate with 1 mm thickness.
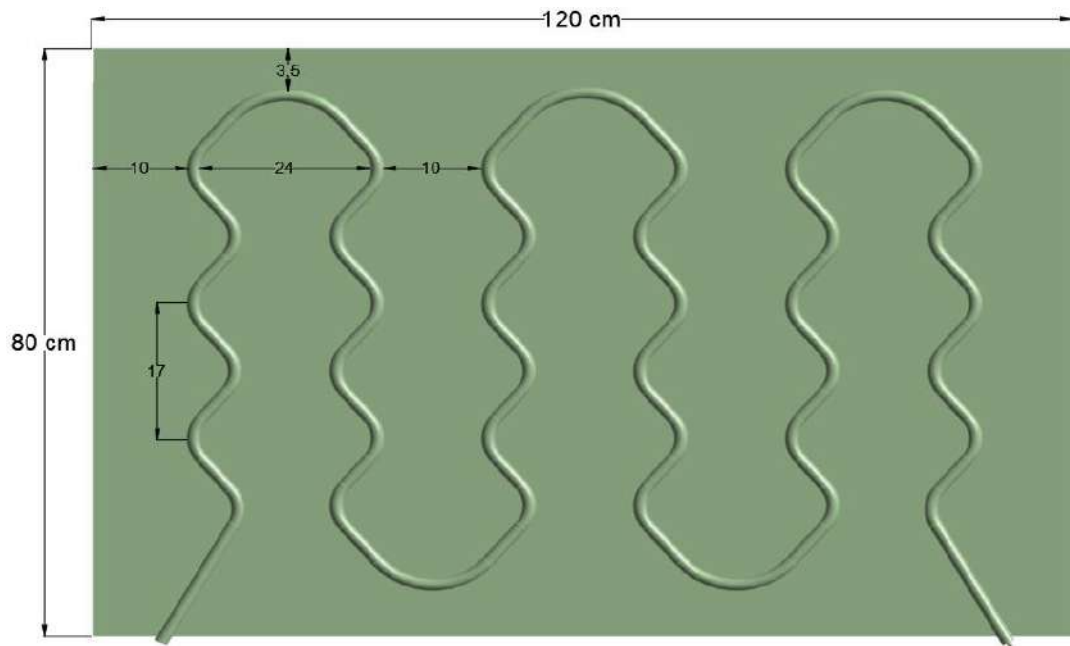
Figure 3-1: Solar Water Collector

Table 3-1: Designed Dimensions of Flat Plate Solar Collector.

No.	Parameters	Symbol	Values
1.	Collector length	L_c	120 cm
2.	Collector width	w	80 cm
3.	Collector height	H	24 cm
4.	Thickness of insulation	X	3 cm
5.	Tilt angle	Θ	45°
6.	Pipe diameter	D	0.0125 m
7.	Pipe length	l	8 m

3.1.2 Basic Governing Equations

In order to evaluate and create a mathematical model, the mathematical formula for water flow and heat transfer in the forced convection of a solar water collector was established according to the following assumptions:

1. Steady state.

2. Incompressible fluid.

3. Newtonian fluid.

4. Turbulent flow.

5. Three-dimensional.

6. Gravity on

The continuity, momentum and energy conservation equations for each phase were solved using a mixture model, which is particularly useful when the phases move at different speeds.

The mixture model is the simplest multiphase model which can be used in a variety of applications. It has the ability to simulate multiphase flows in which the phases move at various speeds but remain in local equilibrium over small spatial length scales. Moreover, mixture models can be used to calculate non-Newtonian viscosity for homogenous multiphase flows with very strong coupling and phases moving at the same velocity. The mixture model solves the following equations: continuity equation, momentum equation, energy equation, and the volume fraction equation for the secondary phases [34].

3.1.2.1 Conservation of Mass (Continuity)

A control volume's internal mass growth must be equal to the mass inflow minus the mass outflow through the surface. For an incompressible fluid, this may mathematically be stated as[34]:

$$\frac{\partial}{\partial_t}(\rho_m) + \nabla.(\rho_m \vec{v}_m) = 0 \tag{3-1}$$

The averaged mass velocity, $\vec{v}_m$, is denoted as

$$\vec{v}_m = \frac{\sum_{k=1}^{n} \alpha_k \rho_k \vec{v}_k}{\rho_m} \tag{3-2}$$

And ρ_m is the mixture density:

$$\rho_m = \sum_{k=1}^{n} \alpha_k \rho_k \tag{3-3}$$

α_k is the volume fraction of phase k.

3.1.2.2 Momentum Equation

The second law of Newton is the source of the other fundamental set of equations that regulate fluid flow (the conservation of momentum). The equations are known as the Navier-Stokes equations, and they have the following form for incompressible fluids[34]:

$$\frac{\partial}{\partial_t}(\rho_m \vec{v}_m) + \nabla \cdot (\rho_m \vec{v}_m \vec{v}_m)$$
$$= -\nabla_P + \nabla \cdot [\mu_m (\nabla \vec{v}_m + \nabla \vec{v}_m^T)] + \rho_m \vec{g} + \vec{F}$$
$$+ \nabla \cdot \left(\sum_{k=1}^{n} \alpha_k \rho_k \vec{v}_{dr,k} \vec{v}_{dr,k} \right) \tag{3-4}$$

Where μ_m is the mixture viscosity $\vec{F}$ is a force by body, n is the phases number; μ_m is given by:

$$\mu_m = \sum_{k=1}^{n} \alpha_k \mu_k \tag{3-5}$$

where $\vec{v}_{dr,k}$ is the secondary phase k drift velocity.

$$\vec{v}_{dr,k} = \vec{v}_k - \vec{v}_m \tag{3-6}$$

3.1.2.3 Energy Equation

The transfer of heat inside the flow field is represented in the following equation[34]:

$$\frac{\partial}{\partial_t} \sum_{k=1}^{n} (\alpha_k \rho_k E_k) + \nabla \cdot \sum_{k=1}^{n} (\alpha_k \vec{v}_k (\rho_k E_k + p)) = \nabla \cdot (k_{eff} \nabla T) + S_E \tag{3-7}$$

The original term in the correct side of equation (3-7) denotes the conduced energy transfer.

S_E includes all other heat volumetric sources, where k_{eff} is the conductivity effective, $\sum \alpha_k (k_k + k_t))$ and k_t is the thermal conductivity turbulent.

3.1.2.4   The k-ε Turbulence Model

The main purpose of using turbulence modeling is to prompt the equations to anticipate the time-averaged velocity, pressure, and temperature fields, without calculating the complete turbulent flow pattern as a function of time. The following equations were used to set the turbulence k- ε parameter of the conventional mixture model to the discrepancy between the computational and experimental data based on the two-phases model [34]:

$$\frac{\partial}{\partial_t}(\rho_m k) + \nabla.(\rho_m \vec{v}_m k) = \nabla.\left(\frac{\mu_{t,m}}{\sigma k}\nabla k\right) + G_{k,m} - \rho_m \epsilon \qquad (3\text{-}8)$$

$$\frac{\partial}{\partial_t}(\rho_m \epsilon) + \nabla.(\rho_m \vec{v}_m \epsilon)$$
$$= \nabla.\left(\frac{\mu_{t,m}}{\sigma_\epsilon}\nabla\epsilon\right) + \frac{\epsilon}{k}(c_{1\epsilon}G_{k,m} - c_{2\epsilon}\rho_m \epsilon \qquad (3\text{-}9)$$

where ϵ is the turbulent dissipation percentage, and G_k is the generation of turbulence kinetic energy, σ for k and ϵ, is the turbulent Prandtl number. The following formulas are used to calculate the mixture's density and speed:

$$\rho_m = \sum_{k=1}^{n} \alpha_i \rho_i \qquad (3\text{-}10)$$

$$\vec{v}_m = \frac{\sum_{i=1}^{n} \alpha_i \rho_i \vec{v}_i}{\sum_{i=1}^{n} \alpha_i \rho_i} \qquad (3\text{-}11)$$

The turbulence kinetic energy production, $G_{k,m}$, and turbulent viscosity, $\mu_{t,m}$, are calculated as follows:

$$\mu_{t,m} = \rho_m C_m \frac{k^2}{\varepsilon} \qquad (3\text{-}12)$$

$$G_{k,m} = \mu_{t,m}(\nabla\vec{v}_m + (\nabla\vec{v}_m)^T):\nabla\vec{v}_m \qquad (3\text{-}13)$$

3.1.2.5   The Secondary Phases Volume Fraction Equation

The secondary phase p volume fraction equation can be obtained from the continuity equation for secondary phase p [34]:

$$\frac{\partial}{\partial_t}(\alpha_p \rho_p) + \nabla.(\alpha_p \rho_p \vec{v}_m)$$

$$= -\nabla.(\alpha_p \rho_p \vec{v}_{dr,p}) + \sum_{q=1}^{n}(\dot{m}_{qp} - \dot{m}_{pq}) \tag{3-14}$$

3.1.3 The Boundary Conditions

The flow and thermal variables on the physical model's boundaries are specified by boundary conditions. Thus, it is an important component of the FLUENT simulations and must be properly specified. The Table (3.2) displays the zone's boundary conditions for model elements.

Table 3-2: Demonstrating the Boundary Conditions

Boundary – Inlet Water	
Inlet	Mass flowrate: Water Flow rate (0.5, 1, 1.5 and 2) L/min Air Flow rate (0.15, 0.25 and 0.35) L/min
Water Inlet Temperature	Estimated upon the weather conditions for the first four months in Holy Karbala.
Boundary – Outlet water	
Outlet	Mass flowrate
Pressure (Gauge pressure)	0 Pa
Boundary – Wall	
Type	Walls
Heat Flux (Solar intensity)	Calculated from equations as in [35]

3.1.4 Mesh Generation

The solution in ANSYS is based on the finite element method, commonly known as a grid, which divides the geometry into small parts. This means that a liquid or solid body can be created from a network of elements connected to points and lines, which could in turn forms the network necessary for the program to proceed with the solution beginning

with Point one to first-line to the first item, and etc., to run thousands or hundreds of computations which verify each iteration.

Tetrahedrons that shown in figure (3.2) are the suggested lattice type for this simulation. Choosing a network, or more precisely, understanding how to select a network that is appropriate for the current case, is the key to each stage of a numerical solution. Having a better network is the key to developing the ANSYS network in the 3D example. Geometric patterns must be specified in as many blocks as possible in order to obtain trustworthy results. After multiple iterations of testing, the feature network findings were created as depicted in table (3.3). The figure (3.3) shows computational grid for the flat plate solar water collector that using in this study, while figure (3.4) illustrates megascopic mesh for sections (A and B) that was taking from figure (3.3).
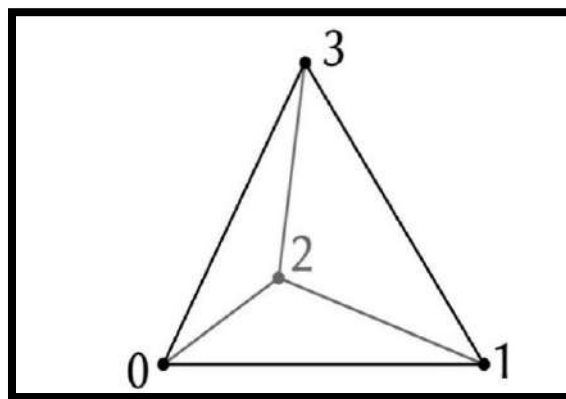
Figure 3-2: Tetrahedron Cells [36].
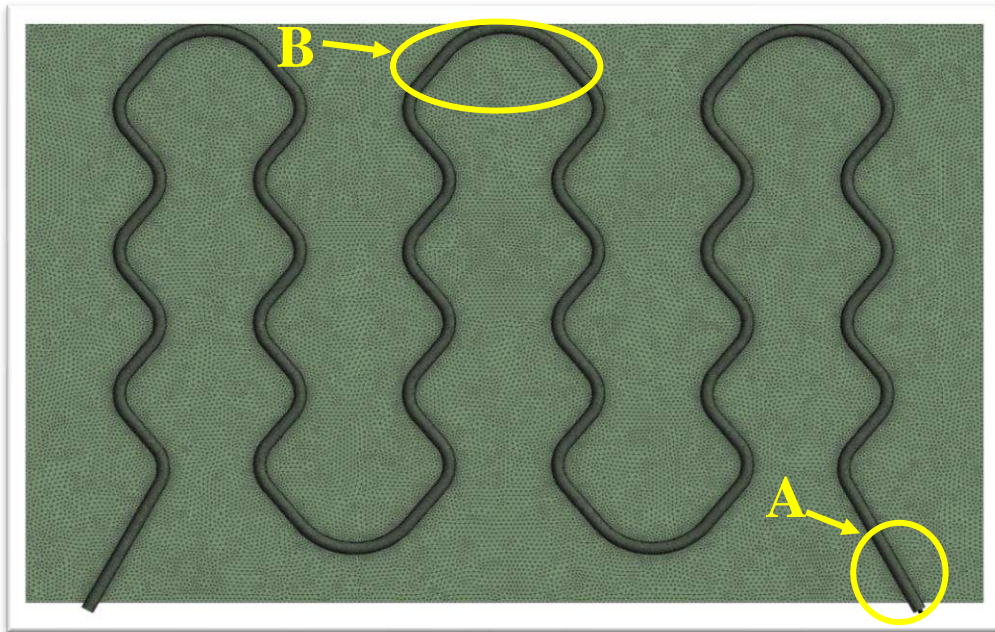
Figure 3-3: Computational Grid for Solar Water Collector
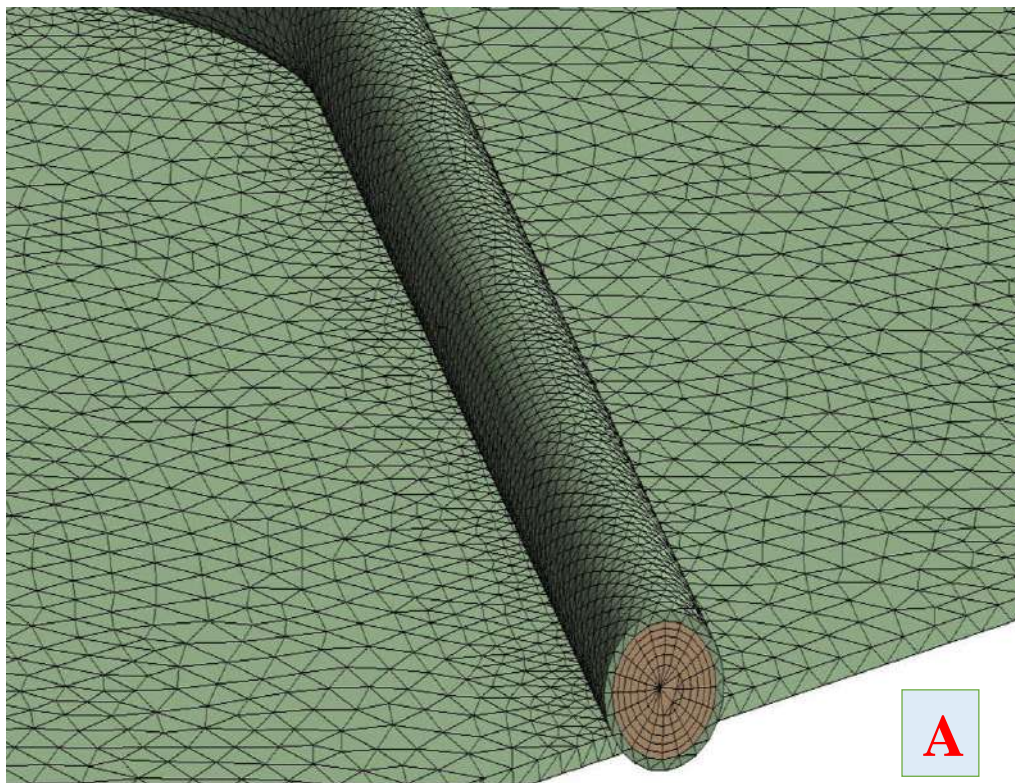
Figure 3-4: Megascopic Mesh Section from Figure (3-3)
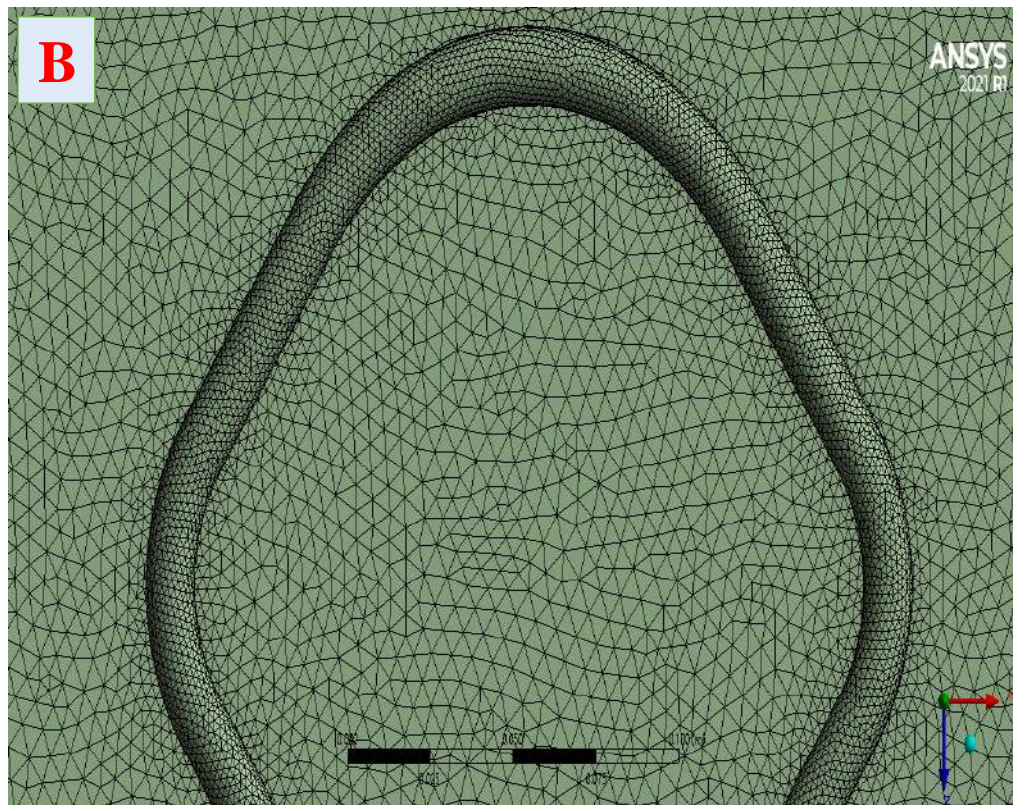
Figure 3-4: Contd.

Table 3-3: Mesh Details

Details of the Mesh	Values
Number of Elements	2870905
Number of Nodes	968084
Rate of Growth	1.2
Normal Curvature Angle	18.0˚
Diagonal Bounding Box	1314.1 mm^2
The Average Surface Area	7999.1 mm^2
Length Edge	2.0 mm

3.1.5 Simulation Procedure

FLUENT solves the governing, integral equations for, the conservation of mass, momentum, energy, and other scalers. There are two processors, used to solve the flow and heat transfer equations. The first preprocessor is the program structure, which creates the geometry, and grid by using the SOLID WORKS 2021 application. The second post-processor is solving Navier-Stokes equations, that include continuity, momentum, and energy. The Simulation procedure for the fluent was

shown in Appendix (A) and these procedures were illustrated in the numerical simulation chart (3.5).

	Modeling Gemometry
	Mesh Generation
	Selection Model Equation
	Initial and Boundary Condition Settings
	Problem Solving
	Results Analysis
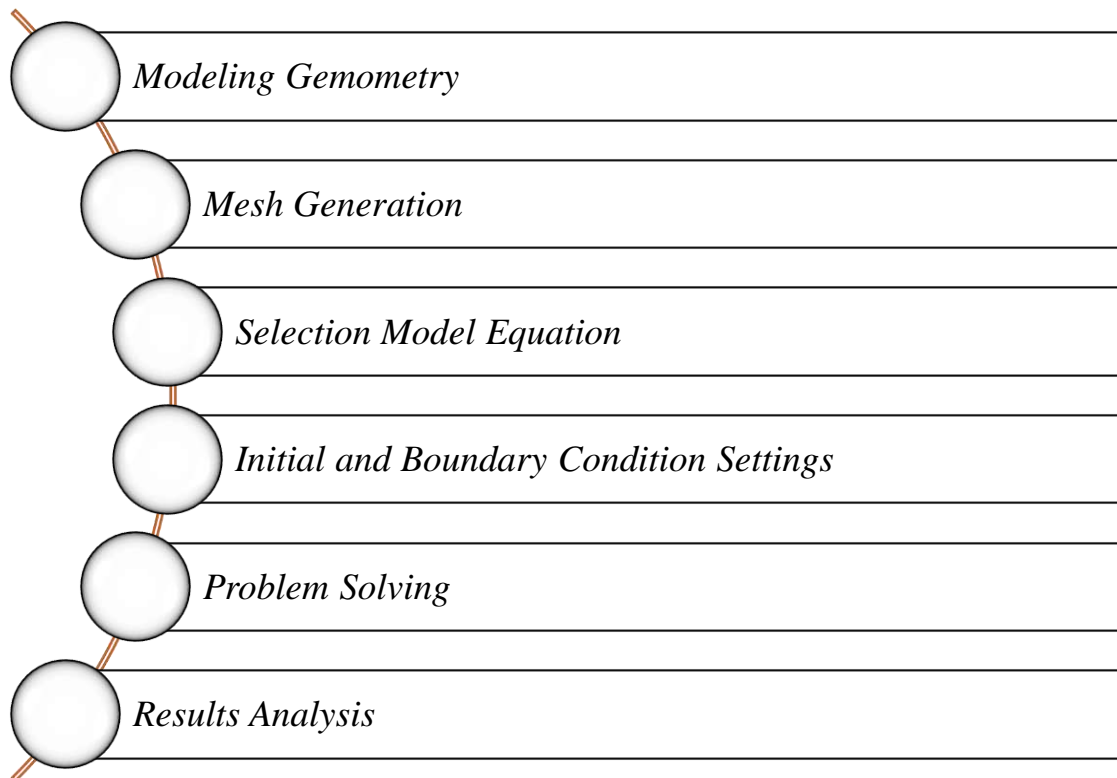
Figure 3-5: Numerical Simulation Chart

3.1.6 Grid Independence Mesh

For the grid independence study, working substance has been taken as water and the simulation was run at flowrate of 0.5 L/min. Grid independence test was carried out to discover the optimum grid size for the present study. Six different elements of mesh from (9.5×10^5 to 4×10^6) were tested to find out the effect on the outlet temperature. It has been found that there is no significant change in outlet temperature beyond the mesh elements of 2.87×10^6, which is shown in figure (3.6) and table (3.4). Therefore, for the present study, the mesh elements of 2.87×10^6 has been used to perform all the simulations.

Table 3-4: Grid Independence Mesh Test

No.	No. of element	T out (˚C)
1	9560000	36.2
2	1578443	37.6
3	2147566	38.45
4	2870000	39.02
5	3453222	39.07
6	3984775	39.1
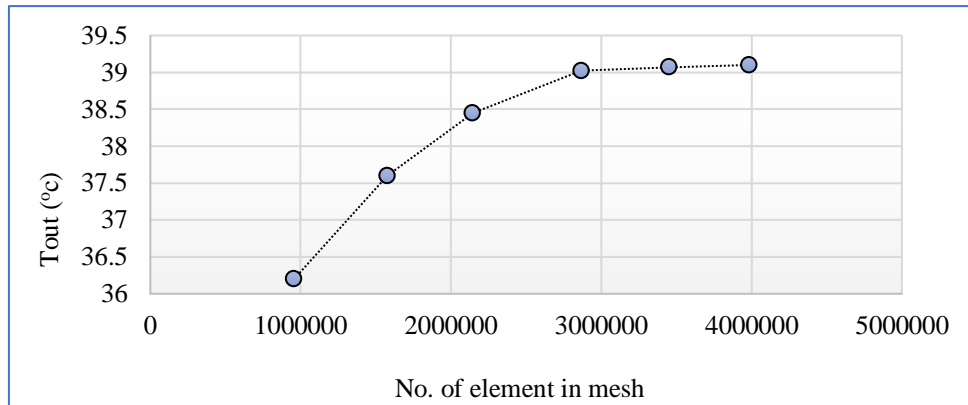
Figure 3-6: Grid Independence Mesh Test

3.2 Part II: Collector Performance Calculations

The thermal properties of the collector materials and collector design can be thoroughly analyzed under controlled settings. Solar radiation mainly depends on local weather and location. In for the first months (January, February, March and April), the experimentations were carried out with clear sky conditions. The performance of a flat plate solar collector with various flowrates was evaluated. The energy collected is converted to the thermal energy of water in the pipes [24]. The following variables need to be known for the tests:

1. Solar radiation at the collector plane, I.
2. Ambient air temperature, Ta.
3. Water temperature at the collector inlet, T_{in}.
4. Water temperature at the collector outlet, T_{out}.
5. Fluid volumetric flowrate, q.

The amount of useful energy gained is calculated using the following equation:

$$Q_u = \dot{m}\, C_p\, \Delta T \tag{3-15}$$

where:

C_p is water specific heat capacity (kJ/kg. °C),

ΔT = The temperature difference between the outlet and inlet of water (°C), $\Delta T = (T_{out} - T_{in})$.

$\dot{m}$ is the fluid mass flow rate (kg/sec) which can be calculated from the equation (3-16).

$$\dot{m} = \rho q \tag{3-16}$$

Where q is the fluid volumetric flowrate (m³/s) and ρ is the water density (kg/m3) and that can be calculated for the air-water mixture from the equation (3-17).

$$\rho = \alpha_{water}\rho_{water} + \alpha_{air}\, \rho_{air} \tag{3-17}$$

Where α is the volumetric void fraction which is the ratio of the air volumetric flowrate over the mixture volumetric flow rate written as [10]:

$$\alpha_a = \frac{Q_a}{Q_w + Q_a} \tag{3-18}$$

Where Q_a and Q_w are air flow rate and water flow rate, respectively.

The efficiency, η of the transform the radiation of solar energy into functioning heat in the collector results from the ratio of beneficial transported medium of thermal flow by the of heat transfer Q_u to the total radiation occurrence on the collector area, as in equation (3-19)

$$\eta = \frac{Q_u}{I\, A_c} \tag{3-19}$$

Q_u = useful energy gained (watt)

I = solar radiation (w/m²)

A_c = collector area (m)

Chapter Four

Experimental Work

4

Chapter Four

Experimental Work

Introduction

The most important studies on thermal performance and various methods for improving the performance of solar water collectors were covered in chapter two. The use of bubble injection technology through the solar water collector has not been studied widely in the previous literature. This technique has studied the effects of the air bubbles on the thermal performance of the solar water collector in two situations; opened and closed. The solar system has been installed with tilt angle 45°[37] based on the location of experiments, (32.6160 ⁰N) and (44.0249 ⁰E) latitude and longitude respectively for Karbala city (Iraq). Several parameters are taken into consideration to achieve the objectives of this work, such as inlet temperature, outlet temperature, plate temperature, air flow rate, water flow rate, pressure drop, efficiency.

4.1 Design Consideration

A new model was designed, and manufactured. As illustrated in table (4.1), the dimension of the solar water collector was chosen from the research [38]which was an experimented in Babylon city that has almost the similar weather condition in Karbala city. Determining angle of tilt taking latitude of location and adding 15⁰ for winter season [37].The wavy shape design by adoption of [22] and [39]and manufactured and tested experimentally for the first time with pipe copper with diameter 0.5 inch.

Table (4.1): Model Solar collector System

Property	This work
Collector dimensions	$(120 \times 80 \times 24)$ cm^3
Pipe diameter	0.0125 m
Pipe length	8 m
Inclination angle	45 degree
Pipe Arc angle	45 degree

4.2 Opened and Closed Systems Working Principle

The working principle of the opened system which sketched in figure (4.1), started when the pump draws water from the tank and pumps it to the solar collector passing through the water flowmeter to control the amount of water that through a one-way valve to prevent the water from returning in reverse and then enters the solar collector from the bottom, which is tilted at an angle of 45°. The collector contains wavy pipes, a shape that was not used practically before in the previous researches. The absorbing surface of the collector was coated by black paint to ensure that the maximum amount of solar radiation is absorbed. The water will then be heated by the solar radiation that fall on the collector area and exited from the upper side of the collector then stored in an isolated storage tank for use whenever it needed.

For the closed system, the working principle is the same procedure at the opened system except that exit water is return to the tank that the water was drawing from, which pumped to the collector again and again. for many applications, the tank in the closed system was contained heat exchanger to transfer the heat from the water to the fluid in the heat exchanger as shown in figure (4.2).

To inject the air bubble into the systems (opened and closed), an air compressor was used to supply the air to the system. The air was passed through into air flowmeter to control the amount of air entering, then passed through a venturi as shown in figures (4.1) and (4.2) to create an air bubble that mixed with the water that flowed in the system. A data logger with twelve sensors for digital temperature, solar power meter to measure the intensity of solar radiation, a manometer to measure the pressure difference and a computer for saving data were used in this experiment.
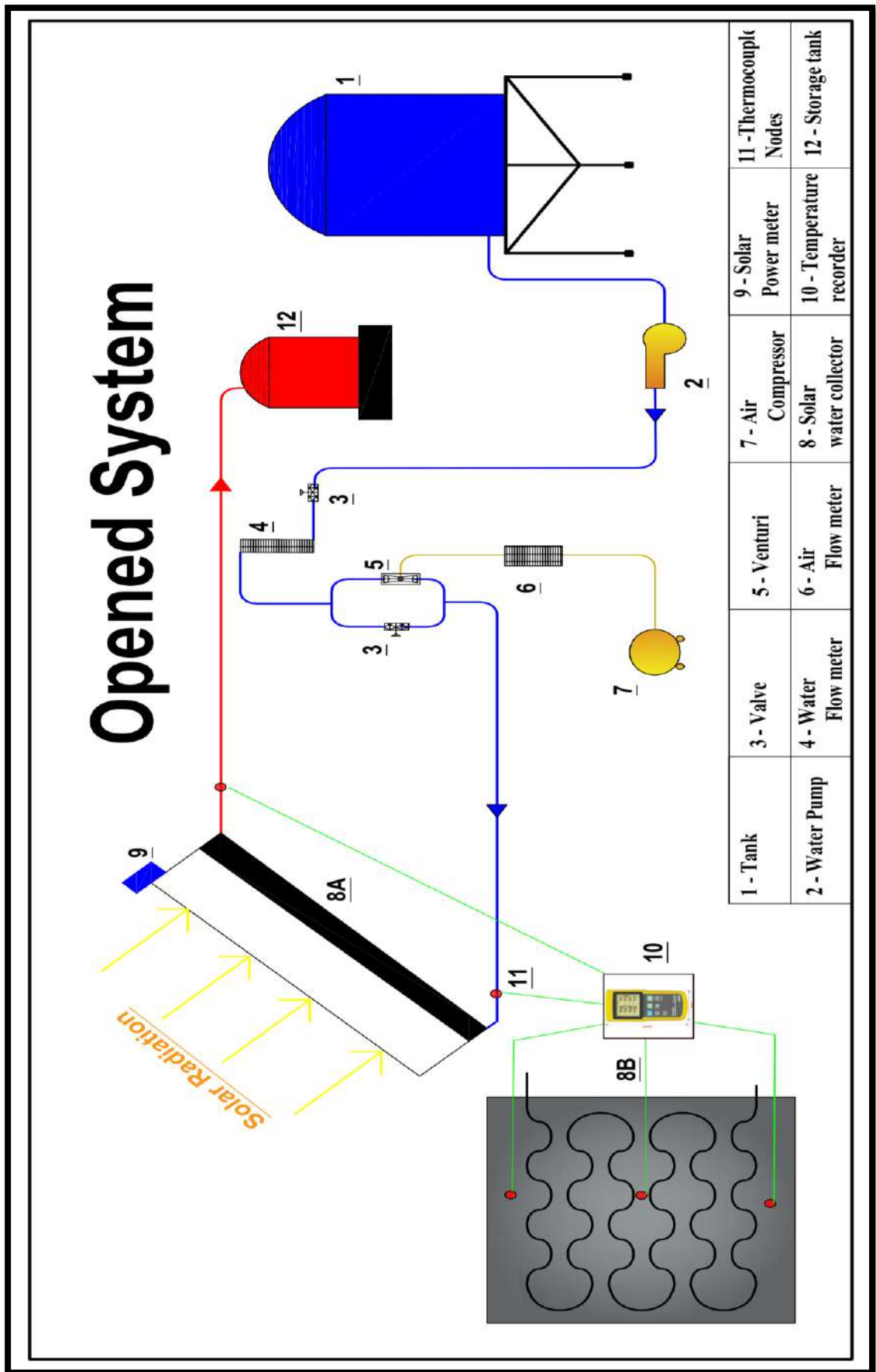
Figure 4-1: Schematic Diagram of the Experimental Rig for Opened System
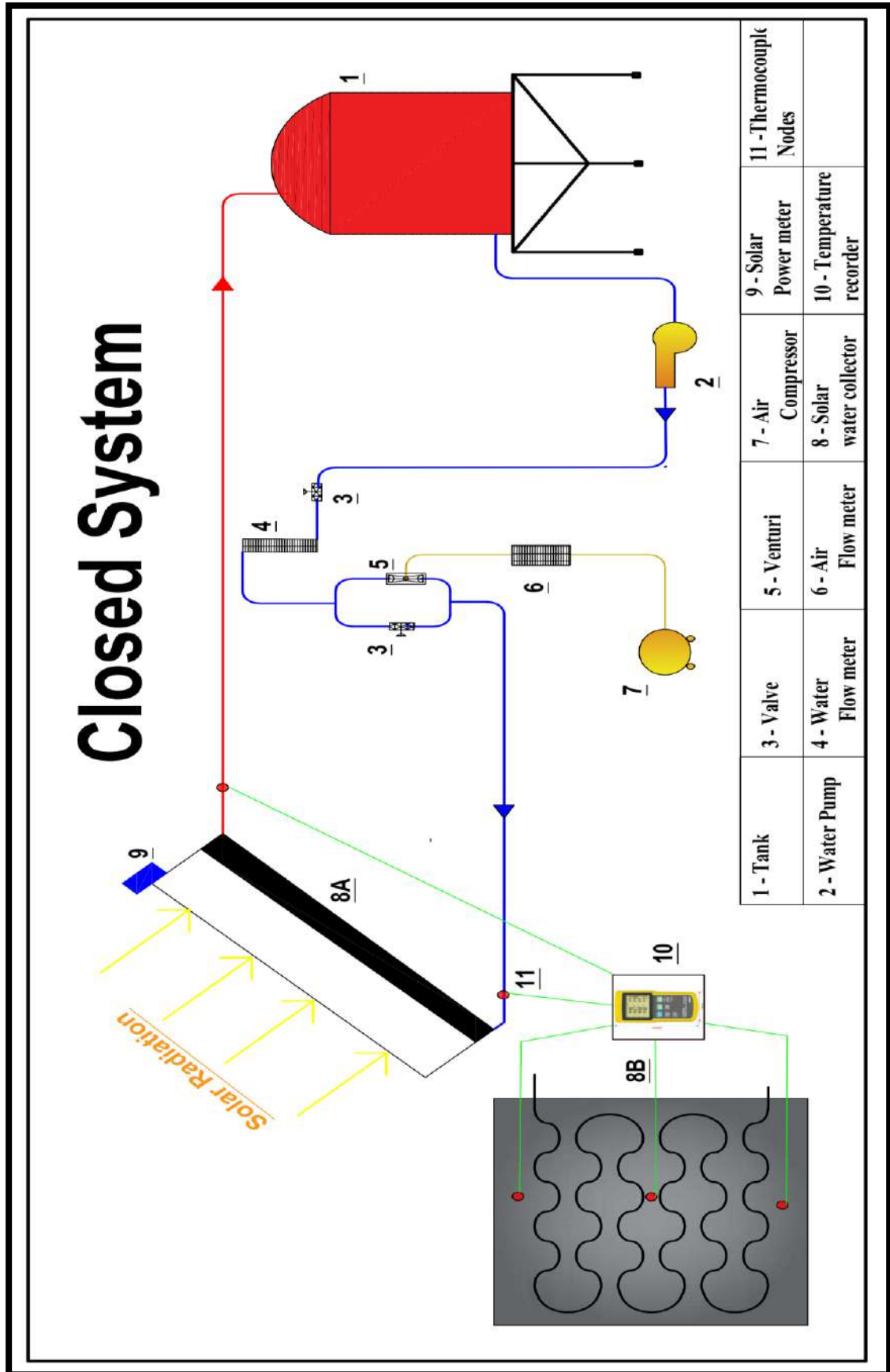
Figure 4-2: Schematic Diagram of the Experimental Rig for Closed System

4.3 Experimental Rig Components

The main components of the system are:

1. The collector.

2. Tanks.

3. Water pump.

4. Check valve.

5. Venturi.

6. Air compressor.

4.3.1 The Collector

The main components of the solar collector are the casing, the glass cover, the absorber plate, the pipe, and the insulation. Figure (4.3) shows the construction of the collector frame by using angle iron bars, which consists of a base for the storage tank welded by a rectangular frame tilted 45º from the horizon, that is used to hold the collector that consists of aluminum alloy/white box with (120*80*24) cm^3 with a 6 mm thick glass top, inside which is an absorbent plate made of aluminum and coated with a matte black paint to increase the absorption ability.

Figure (4-3). Steps of Collector Construction

In order to design pipe shape, the unique wavy shape was chosen to complete the collector design requirement. For the first time, such a shape was manufactured and experimentally tested, and only a similar shape has been tested numerically as in research [22]. A copper pipe with 0.0125 m diameter was selected with 8 m long. The pipe was corrugated by using special tool to make the wavy shape. The wavy pipe located in the pipeline is expected to be able to modify the way of interaction between air and water and further affect the flow behavior in the whole pipeline system. The angle of elbow (β) is selected to allow the wavy pipe to match the pipelines upstream and downstream. Therefore, the elbow angle, β, is 45°[39].The wavy tubes are installed in the absorber plate using metal pieces fixed with screws and fixed on the absorber plate to ensure a high conduction ability as shown in figure (4.4) while table (4.2) show the specifications of the flat plate solar collector.

Figure 4-4: Wavy Shape Pipe Manufacturing.
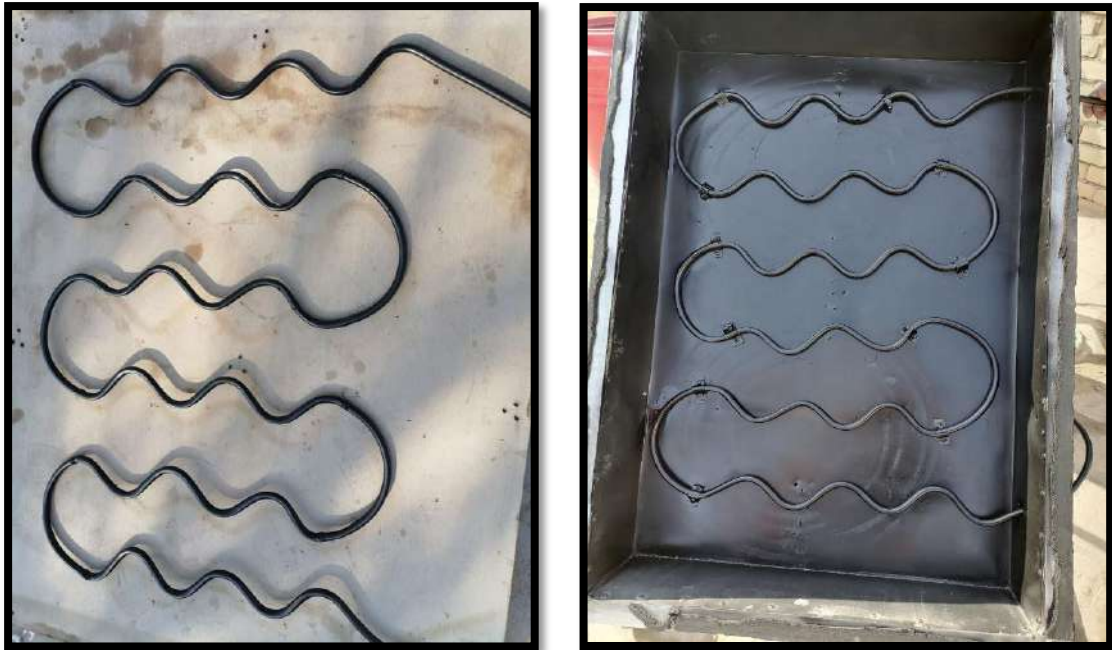
Figure 4-4: Contd.

Table 4-2: The Solar Collector's Specifications

Parameters	Specification
Sizes of the collector	(120 x 80 x 24) cm^3
The Casing	White aluminum alloy
Cross-sectional area	0.9600 m^2
Material for Absorber	Aluminum with black coating
Material of the tube	Copper
Specifications for tubes	Length: 8 m Diameter: 0.0125 m
Material for insulating	Fiberglass, Thickness:3cm
Covered glass	Thickness: 6 mm
Angle of tilt	45˚

4.3.2 Tanks

There are two kinds of tanks, the first tank (capacity 250 liters) was used as a reservoir to contain the water. Before operation of the system, it prefers to fill the tank more than half to get almost constant inlet temperature for the system. The second tank was a storage tank (an isolated tank) that stores hot water after it has left the solar water collector so it can stay warm before it is used for other purposes, as shown in Figure (4.5).

Figure 4-5: Isolated Tank

4.3.3 Water Pump

To discharge water from the tank to the water flowmeter, which is attached to the flat plate solar collector system, the water pump TM20 type was used. Table (4.3) contains a list of its specs.

Table 4-3: Specifications of the electric water pump

Parameter	Comment
Power	150 W
Frequency	50 Hz
Maximum head	12 m
Flow rate	25 LPM
Voltage	220 V
Pressure	10 bar
Type	TM20

4.3.4 Check Valve

The system used the check valve to ensure maximum accuracy in the work and that no water or air bubbles returned to the storage tank as indicated in figure (4.6).

Figure 4-6: Check Valve

4.3.5 Venturi Meter

Microbubble generation techniques have been proposed in former investigations. An effective technique using air bubbly flow into a convergent-divergent nozzle (venturi tube), which consist of the intake cylinder, converging section, ring, and diverging section as shown in figure (4.7). Venturi injectors work by forcing water through a conical body which initiates a pressure differential between the inlet and outlet ports. This creates a vacuum inside the injector body, which initiates air suction through the suction port. Water flow from up to down; air is introduced into the middle. Air is sucked into a venturi injector then small bubbles present after the suction port. The injector bubbles, greatly increasing the surface area of air in contact with the water [38].
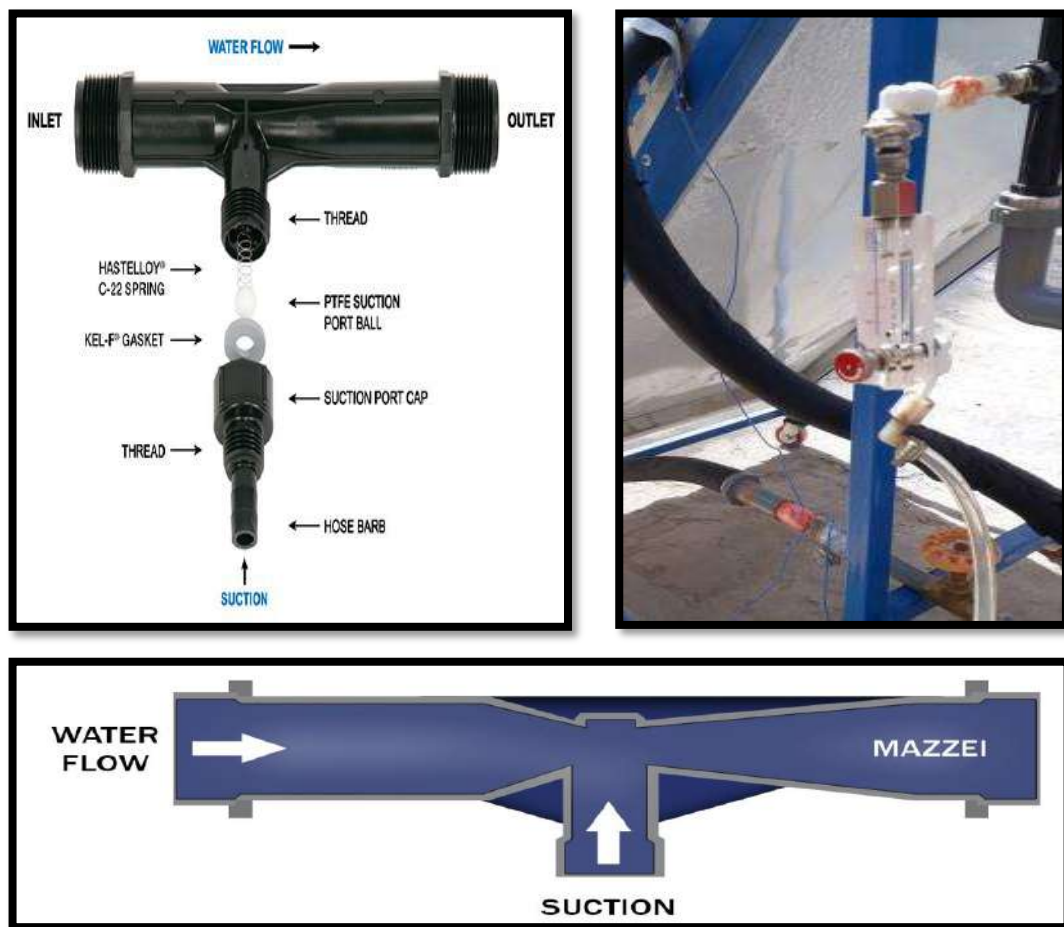
Figure 4-7: The Components and Schematic View for the Venturi Tube.

4.3.6 Air Compressor

A refrigerator motor (type C-BZN200L) was used as an air bubble injector to provide the amount of air that was needed for the system, which is shown in figure (4.8). The characteristics of the air compressor are illustrated in table (4.4). An air flowmeter was used to control and compute the quantity of airflow entering the system by attaching a tube to one end of the compressor and the other to the air flowmeter.

Table 4-4: The Specification of the Air Compressor.

Parameter	Comment
Model	C-BZN200L
Type	CSIR
power	1/3 HP
Frequency	50 Hz
Voltage	220 V

Figure 4-8: Air Compressor

4.4 Measurements

There are several measurement devices utilized in the experimental work, which they are:

1. Water flowmeter.
2. Air flowmeter.
3. Solar power meter.
4. Temperature recorder and Thermocouple.
5. Manometer.

4.4.1 Water Flowmeter

The water flowmeter type (ZYIA) was used in this experiment, with a flow rate range of (0.8-8) LPM, high-specification materials and a $\pm$ 4 % accuracy, which has been calibrated manually by using a bucket of known volume and stopwatch. The flowmeter was installed between the water pump and the inlet section of the collector, to control the amount of water that enters the system from the reservoir, as shown in figure (4.9).

Figure 4-9: Water Flowmeter

4.4.2 Air Flowmeter

The air flowmeter is used to control the amount of air entering to the system, which placed in between the air compressor and the venturi that inject air bubbles into the solar collector, the flow range of (0.2-4) LPM, as in figure (4.10).

Figure 4-10: Air Flowmeter

4.4.3 Solar Power Meter

The TES132 data logging solar power meter, which has an accuracy of $\pm$ 10% and range of (200–2000) w/m^2, was used in the experiment to measure the amount of solar radiation, as depicted in figure (4.11). The device was calibrated by the central organization for standardization and quality control as shown in appendix B.

Figure 4-11: Solar Power Meter

4.4.4 Temperature Recorder and Thermocouple Nodes

The temperature measurements instrument is a digital thermometer reader type (Lutron BTM-4208SD Temperature Recorder Data Logger Meter) that shown in figure (4.12).

As numbered in table (4.5) and illustrated in figures (4.13) and (4.14), six thermocouples are used to measure the temperature of the system, they distribute as one in the center of the inlet pipe and other in the center of outlet pipe. While three thermocouples for the absorber plate's (top, center and bottom) fixed inside the plate by using an insulating adhesive tape, allowing it to measure the plate's temperature alone, independently of its surroundings. Also, there was one thermocouple to measure the ambient temperature.

The device was calibrated by the central organization for standardization and quality control as shown in appendix B.

Figure 4- 12: Temperature Recorder   *Figure 4-13: Thermocouple Type K*
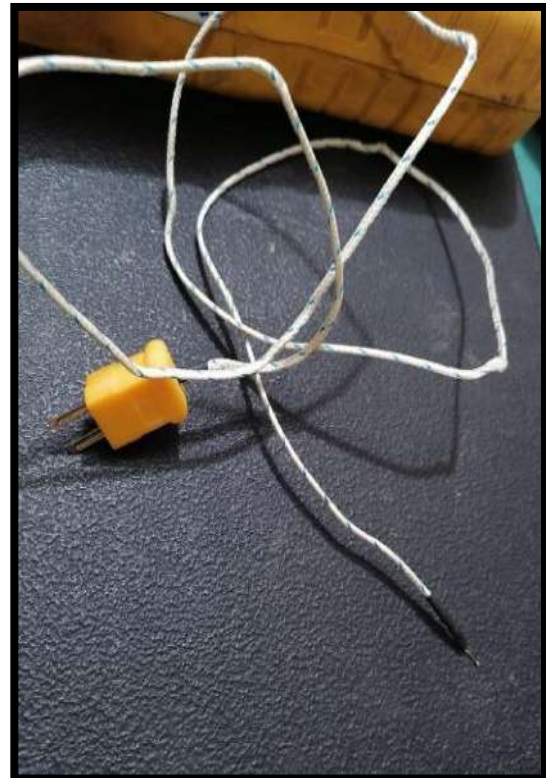
Table 4-5: Location of the Thermocouples

Thermocouple No.	Location
1	Tube inlet
2	Tube outlet
3, 4 and 5	Absorber plate
6	ambient
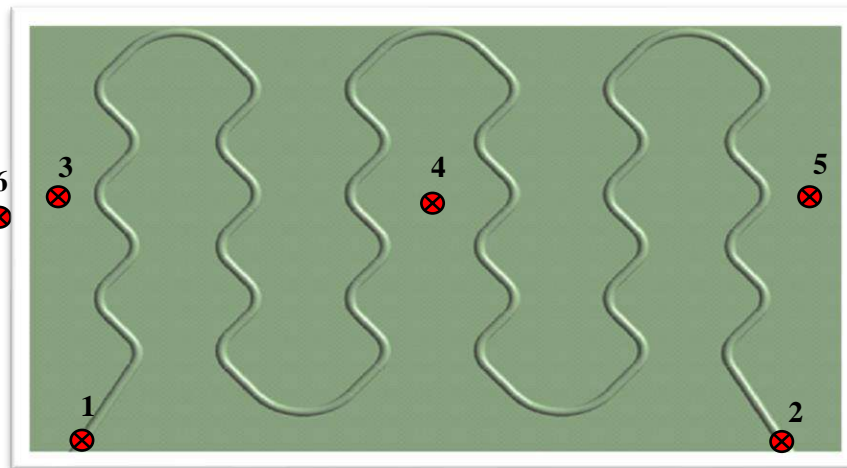
Figure 4-14: Thermocouples Location

4.4.5 Manometer

With twin inputs for differential pressure measurement, the Comark C9555 pressure meter combines high accuracy with speed response with range of pressure measurement of (0 ± 140) mbar. It measures the pressure difference between a point on the pipe entering the solar collector and a point on the tube leaving it, as shown in figure (4.15).

Figure 4-15: Digital Pressure Meter.

4.5 Experimental Procedures

The rig was established in Karbala city with latitude and longitude equal 32.616 ° N and 44.0249 ° E respectively with a 45° collector tilt angle as showed in figure (4.16). Fourteen experiments were carried out in this study, every experiment was carried out in outside on a cleared day, and readings were recorded once the system had stabilized.

The tests were classified in to two types of system, opened and closed type. Four water flowrates were taking (0.5, 1, 1.5 and 2) L/min for both opened and closed systems, while air flow rates of (0.15, 0.25, and 0.35) L/min were employed for the most efficient case in both systems. All of above classifications were illustrated in the table (4.6).

Figure 4-16: Photos for The Experimental Rig

Table 4-6: The Experiment Procedure for opened and closed System

Type of System	Type of working fluid	Flowrate
Opened system	Water	(0.5,1,1.5,2) L/min
	Air	(0.15,0.25,0.35) L/min
	Water + Air	1 L/min water (0.15,0.25,0.35) L/min Air
Closed system	Water	(0.5,1,1.5,2) L/min
	Air	(0.15,0.25,0.35) L/min
	Water + Air	2 L/min water (0.15,0.25,0.35) L/min Air

4.6 Uncertainty of Measurements

For accurate findings, each experiment was carried out three times under identical operating circumstances. The calculation of uncertainty due to systematic error and random error was evaluated using the following equation was used to quantify the variance of the experimental results and the estimated uncertainties. The variables which are measured their Uncertainty are the solar intensity, ambient temperature, inlet temperature, outlet temperature, temperature difference.as shown in the table (4.7).

The mean value of the variable x calculated as:

$$\bar{X}_{mean} = X_{average} = \frac{\sum_1^n xi}{n} \tag{4-1}$$

The standard deviation of x given by: $\quad\quad \sigma = \sqrt{\frac{\sum_1^n (xi-x)2}{n-1}} \quad$ (4-2)

The standard error is given by: $\quad\quad\quad \sigma_{m} = \frac{\sigma}{\sqrt{n}} \quad\quad$ (4-3)

The uncertainty of the variable x is given by: $x = \bar{X} \pm \sigma_m = \bar{X} \pm \frac{\sigma}{\sqrt{n}}$ (4-5)

Table (4.7) The Uncertainty calculations

No	The Variable	Number of values	The tested value	$\bar{X}_{mean}$	σ	σ $_m$	x	Uncertainty Percentage
1	Solar Intensity	X1	900	880	55.88	27.94	907.94	0.0015929
		X2	950					
		X3	832				852.06	
		X4	838					
2	Ambient Temperature	X1	18	17.375	0.6849	0.342	17.717	0.1299
		X2	16.4					
		X3	17.6				17.033	
		X4	17.5					
3	Inlet Temperature	X1	20.5	19.475	1.04	0.25	19.995	0.0854
		X2	19.3					
		X3	20				18.955	
		X4	18.1					
4	Outlet Temperature	X1	25	21.65	2.49	1.245	22.895	0.0357
		X2	20.5					
		X3	21.9				20.405	
		X4	19.2					
5	Temperature Difference	X1	4.5	2.175	1.59	0.795	2.97	0.0559
		X2	1.2					
		X3	1.9				1.38	
		X4	1.1					

Chapter Five

Results and Discussions

5

Chapter Five

Results and Discussions

Introduction

Discussions of the numerical and experimental results are presented in this chapter. In Holly Karbala City in (January, February, March, and April) 2022, the study employed a solar water heater collector model with various water and air flowrates. The effect of the following parameters on the model was studied:

1. Solar intensity (w/m^2).
2. Ambient Temperature (^{o}C).
3. Inlet and outlet temperature (^{o}C).
4. Pressure drops (kpa).
5. Temperature difference (^{o}C).
6. Solar collector efficiency.

All these variables were studied and investigated for different weather conditions of incident solar radiation and ambient temperature to show their effect on the collector's performance.

5.1 Validation

The results of the experimental parts of the current work were compared with other experimental research in the same area of competence in order to validate the findings. An opened system examination at a flow rate of 1.5 L/min was compared with Khwayyir [40] as illustrated in figure (5.1) for outlet temperature with time. Another research project in the same field of study will investigate the flow rate of 0.5 L/min in closed systems. The efficiency with time was validated with Mohammad [23] as shown in figure (5.2). A good agreement was achieved with the experimental results of the two studies and not exceed 10%.
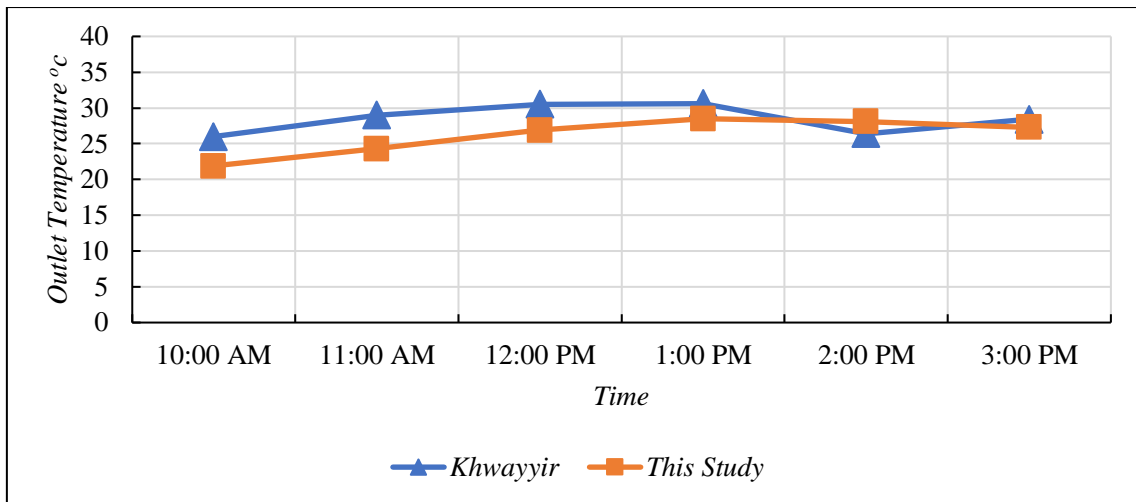
Figure 5-1: Variation in Outlet Temperature with Time Compared with Khwayyir [40]
Study for Open System With 1.5 L/min
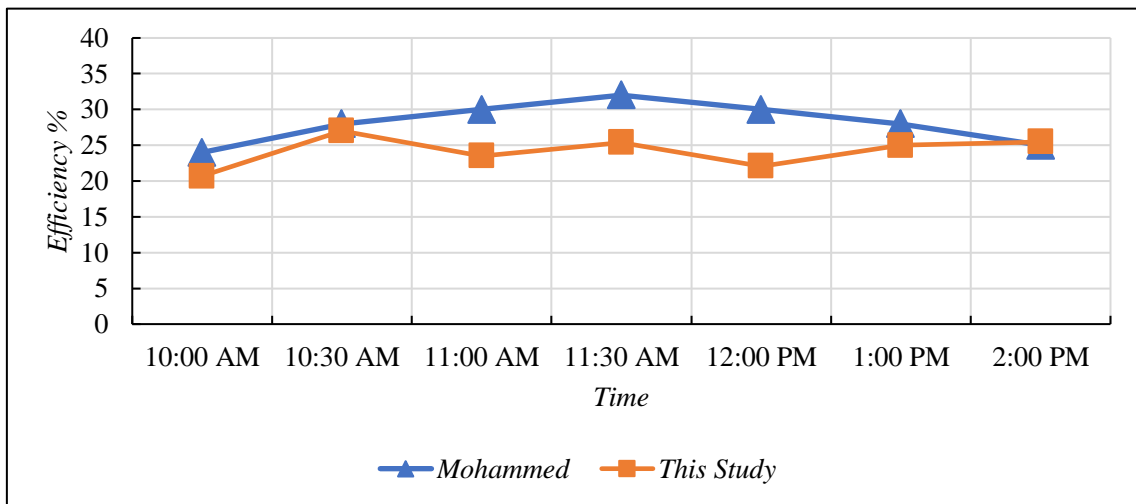
Figure 5-2: Variation in Efficiency with Time Compared with Mohammad [23] *Study for*
Closed System With 0.5 L/min

5.2 Part I: Numerical Results

Under the effect of various amounts of water flowrates, the performance of the solar water collector was tested using ANSYS R1 2021. The work was done by taking into account different time work to simulate the FPSC(Flat plate solar collector) on different days throughout the months (January, February, March and April) under nearly identical conditions in terms of solar radiation, air temperature and wind speed, all

of which had a clear impact on the performance of the solar water collection device.

The work done in the program on multi parts, which first divided to two working systems (opened and closed). These systems were simulated and tested in four selective times with only water as working fluid. After that, the efficiency was calculated to obtain the most efficient case to inject air bubble to it.

5.3 Opened System without Air Bubble Injection

In this part, four water flowrate (0.5, 1, 1.5 and 2) L/min were simulated for the opened system as shown in the contours figures from (5.3) to (5.7), which is illustrate the temperature and pressure contours in four different selective hours. Based on previous research, working hours were adopted from (10 am to 3 pm) because the intensity of solar radiation before 10 pm is low, as well as after 3 pm in the winter season and by taking into account the weather boundary condition of Holly Karbala city for the first four months of the year.

5.3.1 Temperature Contour for Opened System

The numerical study reveals that the best results are obtained in four period time between (10:00 AM to 3:00 PM), the average range of solar intensity for the solar collector area of (0.96) m^2 with title angle of 45 degree was (520 -1050) W/m^2 which can be calculated from solar equations as in [35]. When the water flow rate (0.5 L/min) due to the sluggish water flow through the copper tubes in the solar collector, which offers the absorber plate more time to transfer the needed heat to the water. At this flow rate, the resulting water is as hot as it can be, with the greatest water outlet temperature in the opened system being (37.1°C), as shown in figure (5.3). Figure (5.4) shows the effect of the water flowrate of (1 L/min) on the temperature difference between inlet and outlet water during

working hours (10 am - 3 pm) and shows the highest amount of water outlet temperature is (30.1 °C). While figure (5.5) shows the effect of the water flowrate of (1.5 L/min) on inlet and outlet water temperature difference during working hours (10 am - 3 pm) and shows the highest amount of water outlet temperature is (29.5 °C). Figure (5.6) shows the effect of the water flowrate of (2 L/min) on the temperature difference during working hours (10 am - 3 pm) and shows the highest amount of water outlet temperature is (28.8 °C).

It was observed that lowering the mass flow rate (0.5, 1, 1.5, and 2) produces an increase in the water output temperature, and thus an increase in the difference between the outlet and inlet water temperature in the two systems of closed and opened. This is because the heat transfer time between the working fluid and the absorption plate has increased, so the fluid exposed to solar radiation for a longer period, thus increasing the heating of the fluid and obtaining a higher outside temperature
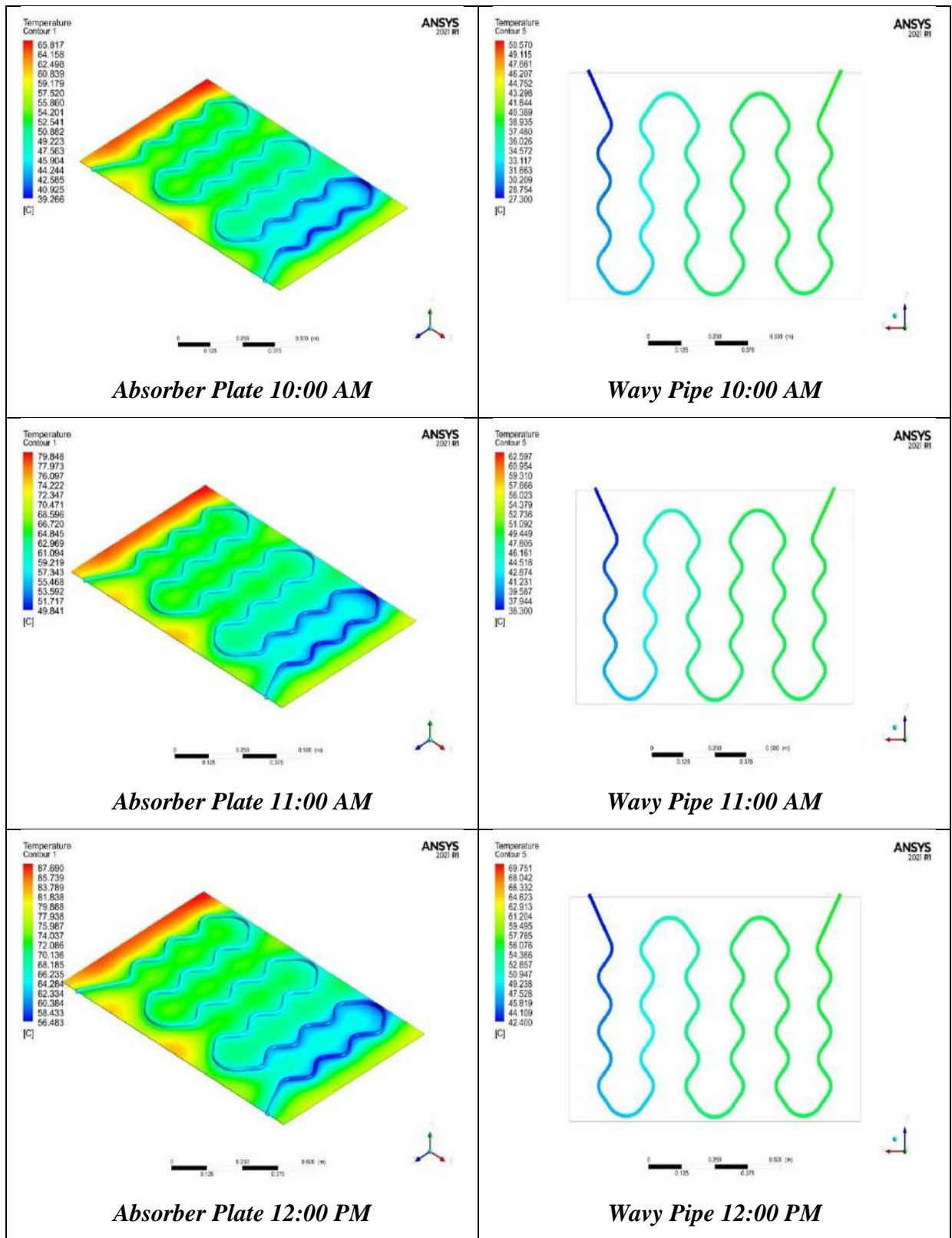

Absorber Plate 10:00 AM   *Wavy Pipe 10:00 AM*
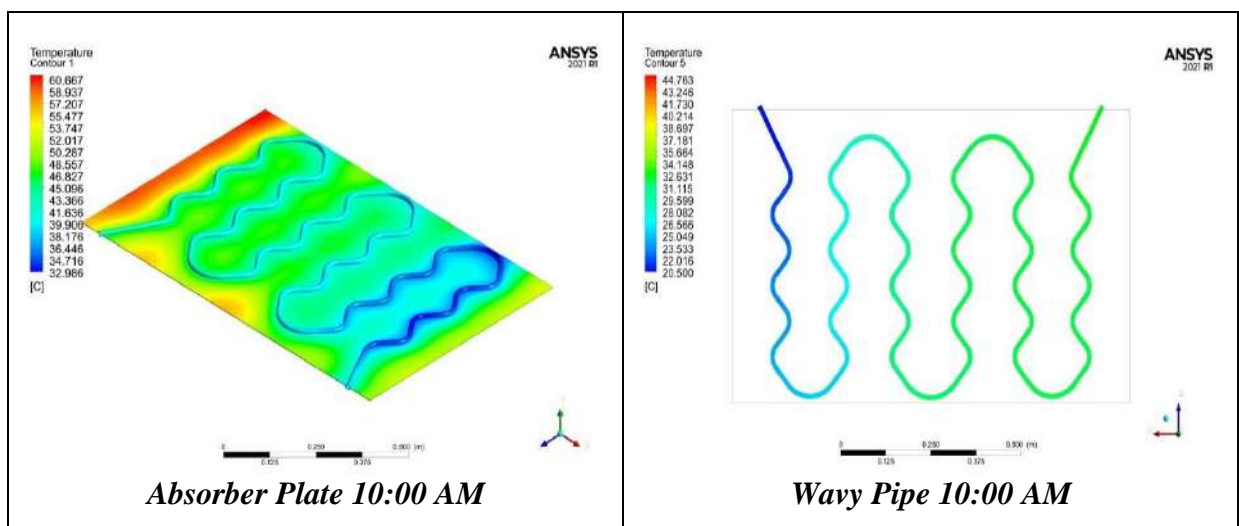
Figure 5-3: Temperature Distribution Contours (°C) for the Time Period from 10:00 Am to 03:00 Pm for Opened System with 0.5 L/min Water Flowrate Without Air Injection.

Absorber Plate 11:00 AM

Wavy Pipe 11:00 AM

Absorber Plate 12:00 PM

Wavy Pipe 12:00 PM

Absorber Plate 03:00 PM

Wavy Pipe 03:00 PM

Figure 5-3: Contd.

Absorber Plate 10:00 AM	Wavy Pipe 10:00 AM
Absorber Plate 11:00 AM	Wavy Pipe 11:00 AM
Absorber Plate 12:00 PM	Wavy Pipe 12:00 PM
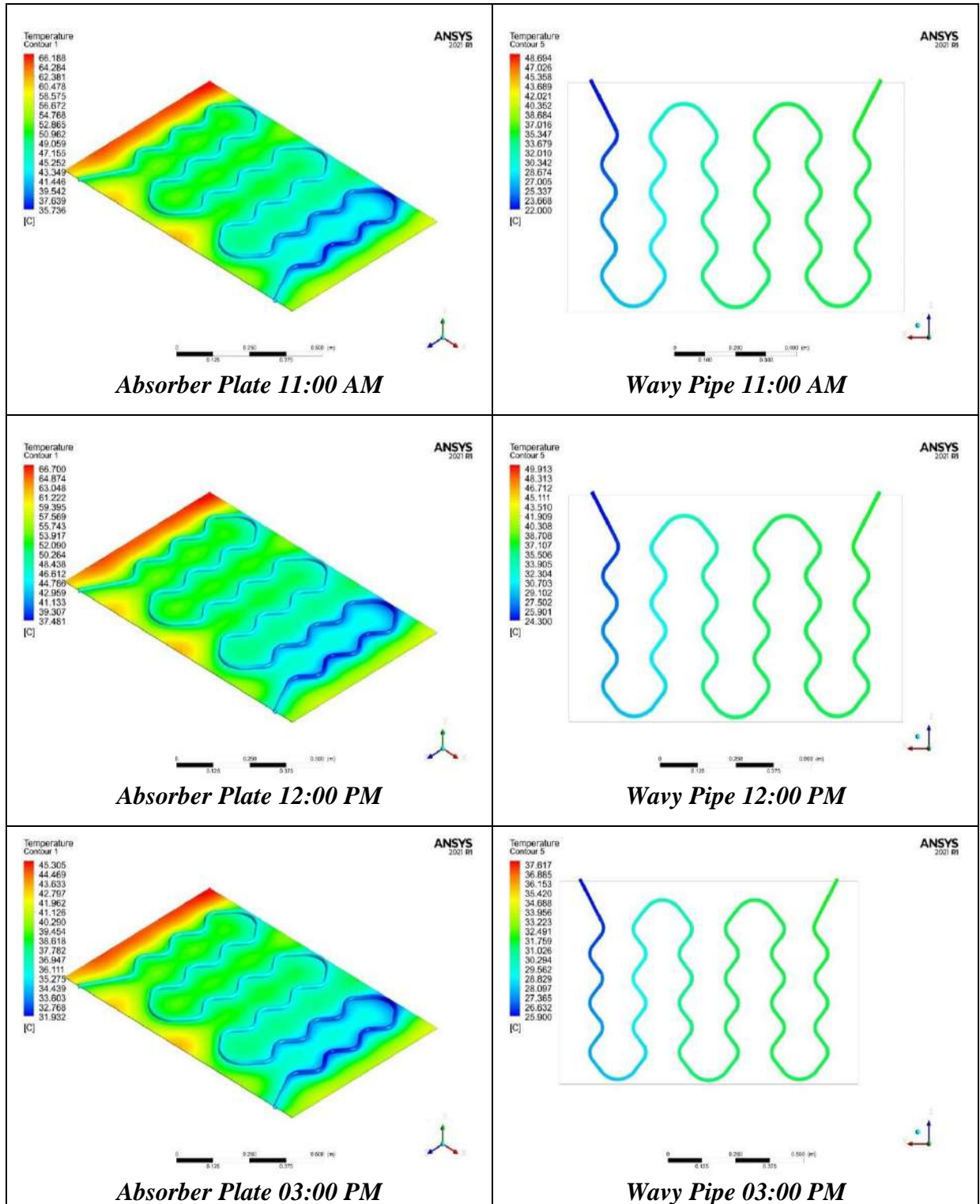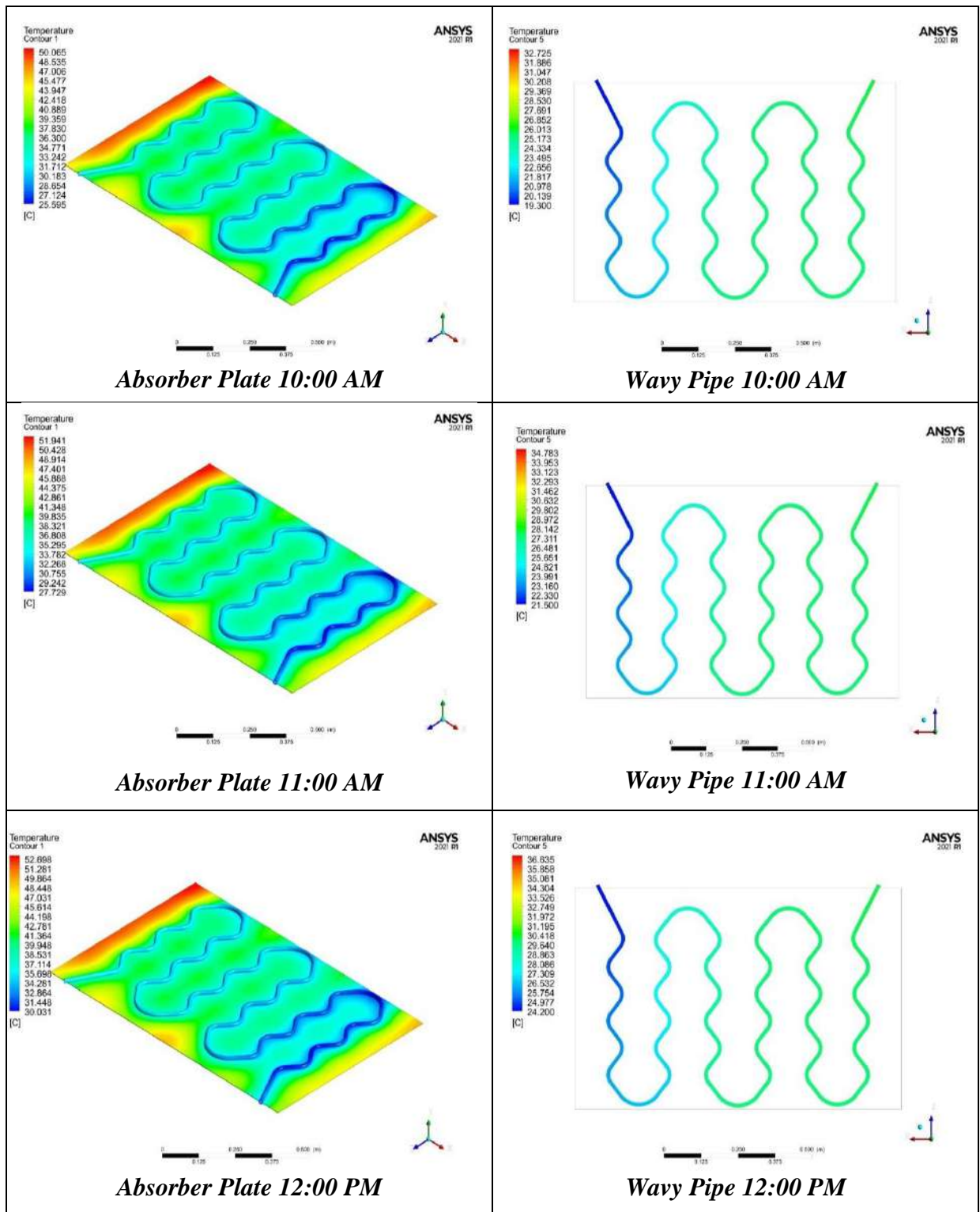
Figure 5-4: Temperature Distribution Contours (°C) for the Time Period from 10:00 Am to 03:00 Pm for Opened System with 1 L/min Water Flowrate Without Air Injection
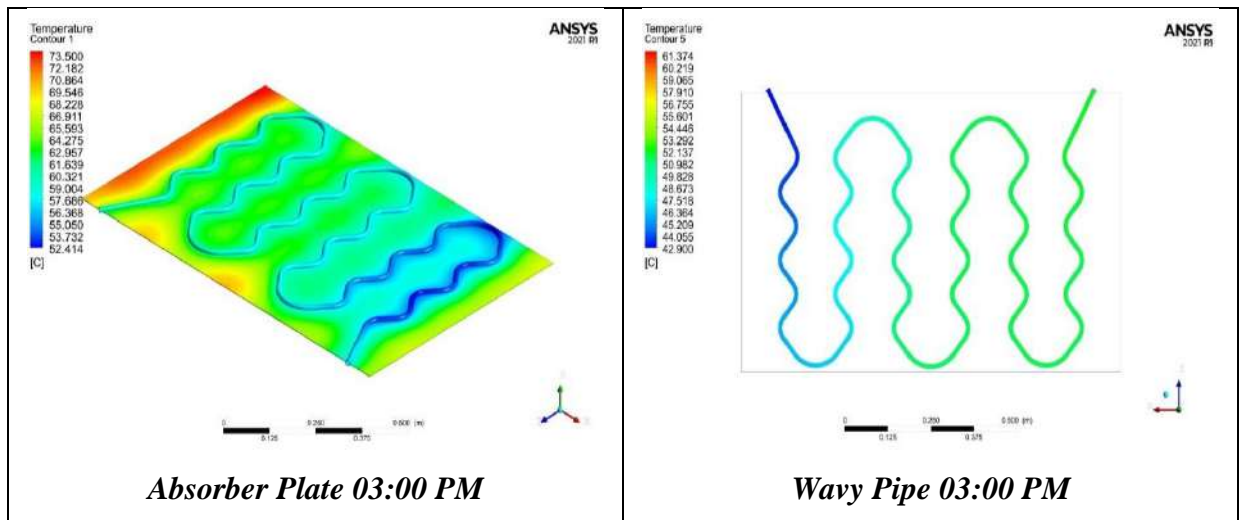
| Absorber Plate 03:00 PM | Wavy Pipe 03:00 PM |

Figure 5-4: Contd.

| Absorber Plate 10:00 AM | Wavy Pipe 10:00 AM |

| Absorber Plate 11:00 AM | Wavy Pipe 11:00 AM |
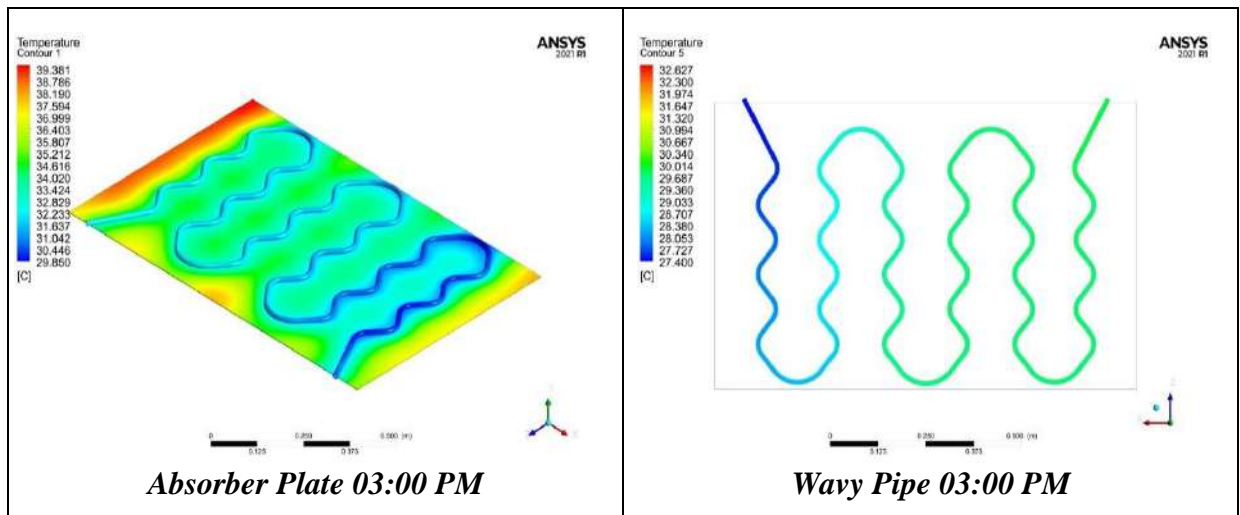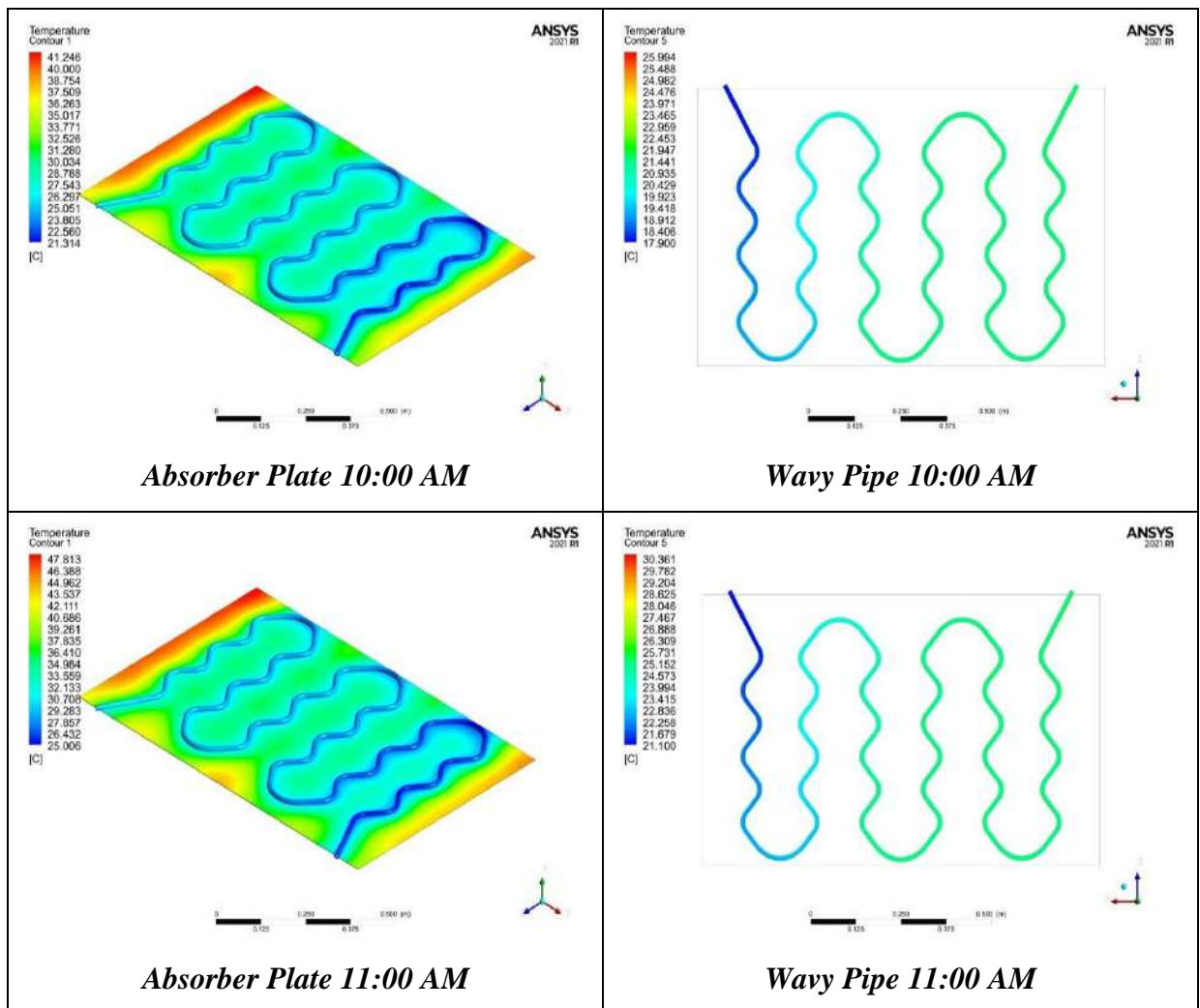
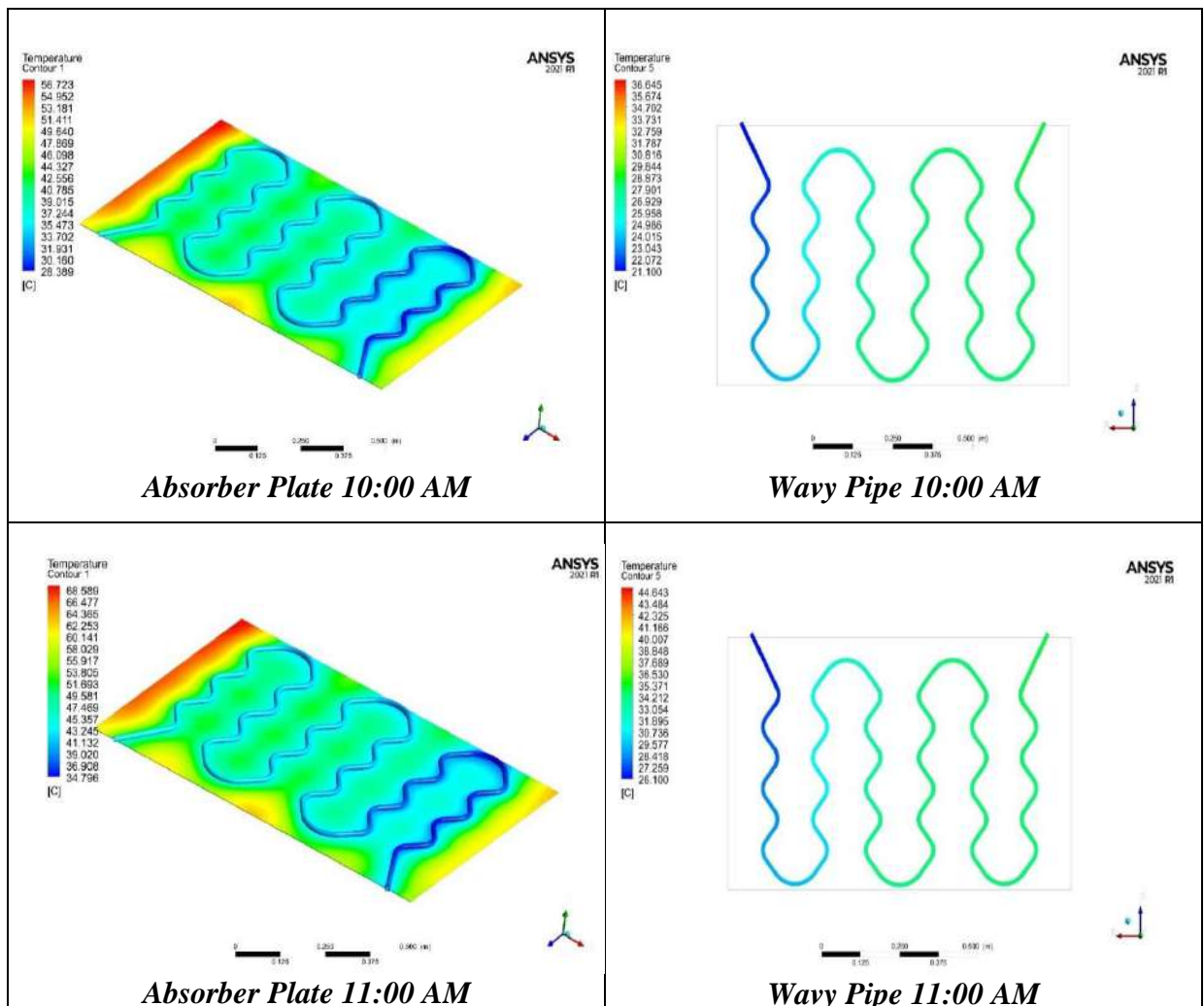*Figure 5-5: Temperature Distribution Contours (°C) for the Time Period from 10:00 Am to 03:00 Pm for Opened System with 1.5 L/min Water Flowrate Without Air Injection.*

Absorber Plate 12:00 PM	*Wavy Pipe 12:00 PM*
Absorber Plate 03:00 PM	*Wavy Pipe 03:00 PM*

Figure 5-5: Contd.

Absorber Plate 10:00 AM	*Wavy Pipe 10:00 AM*
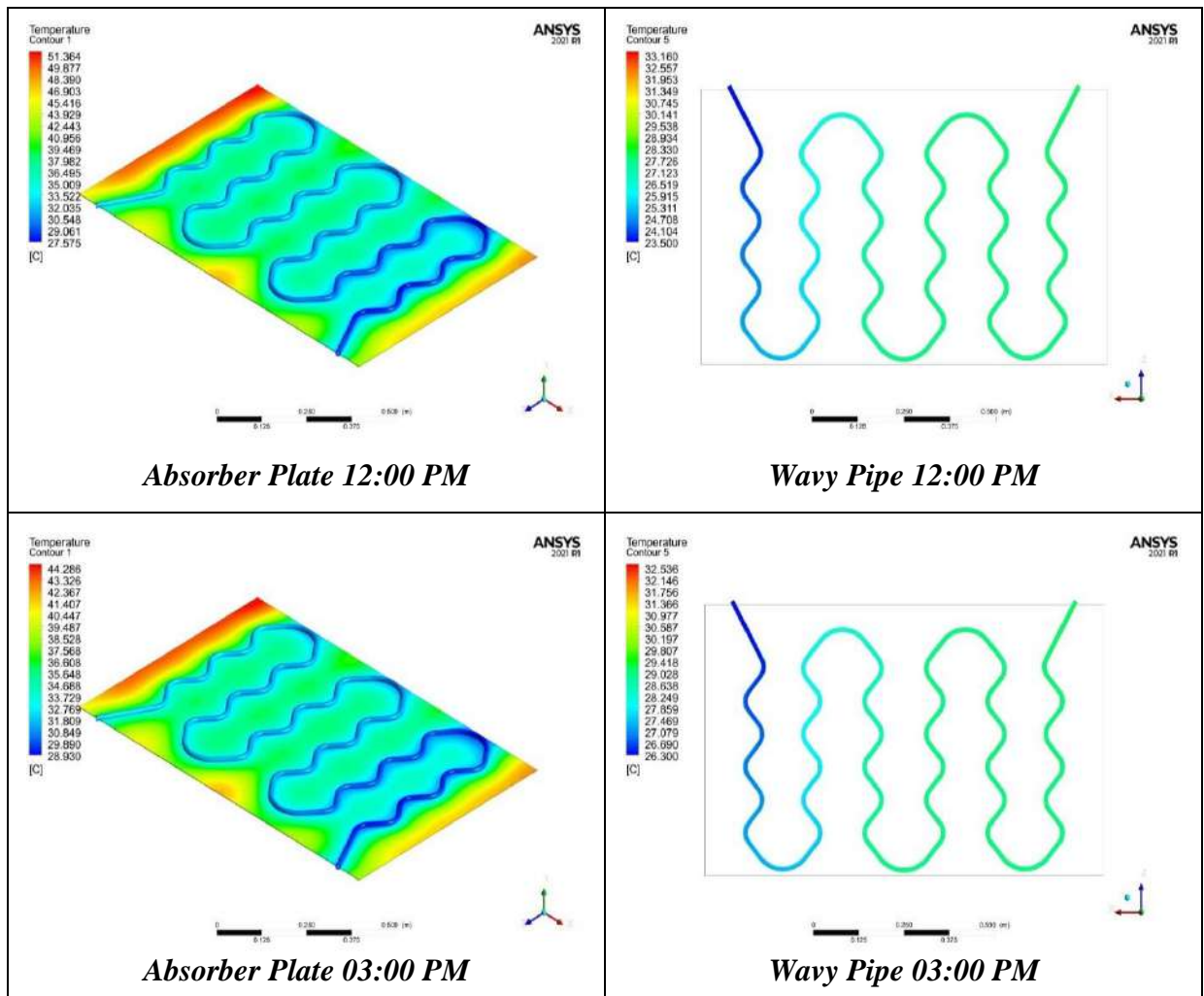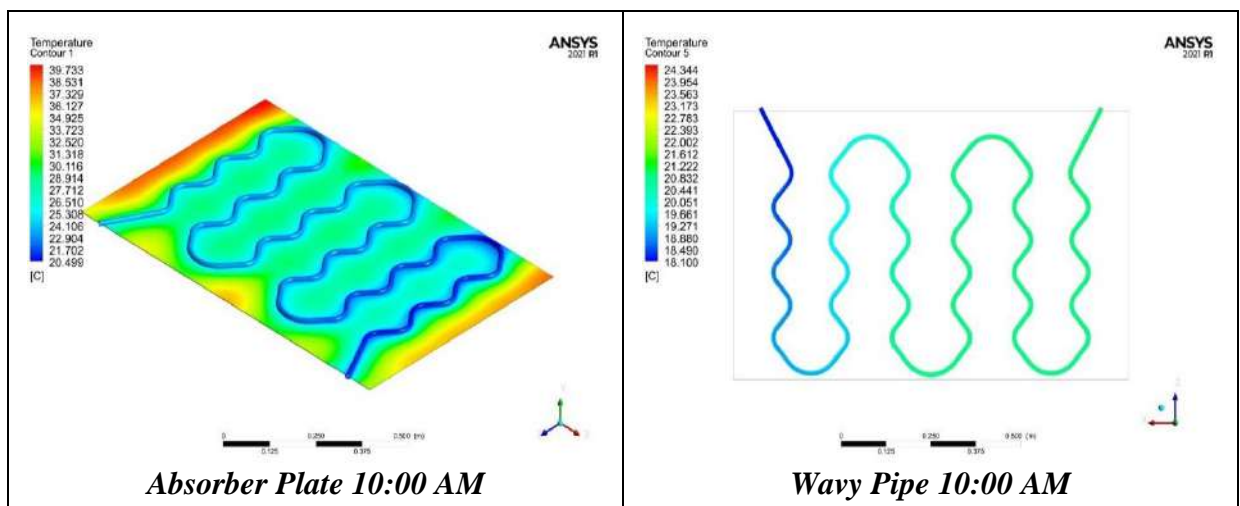
Figure 5-6: Temperature Distribution Contours (°C) for the Time Period from 10:00 Am to

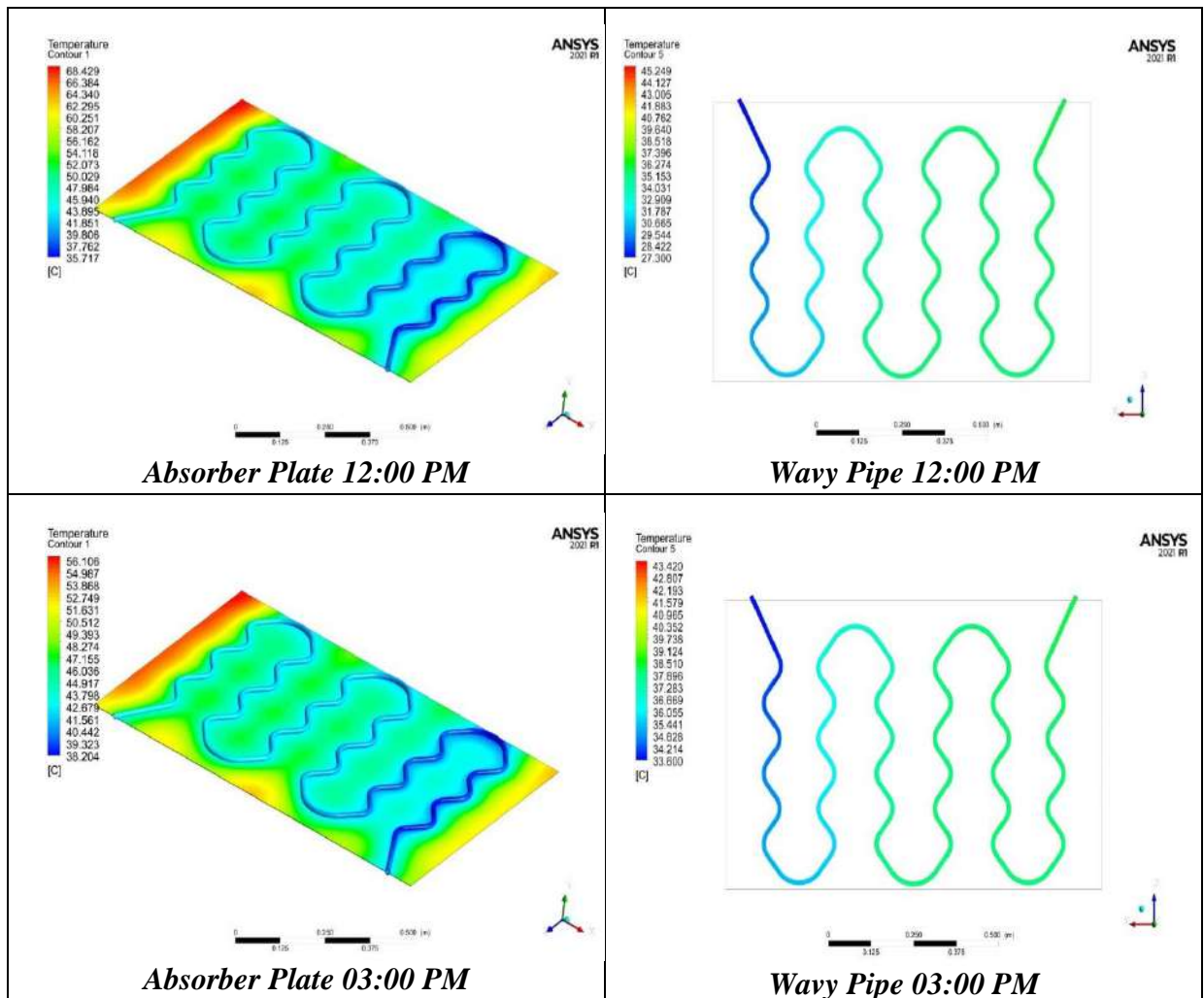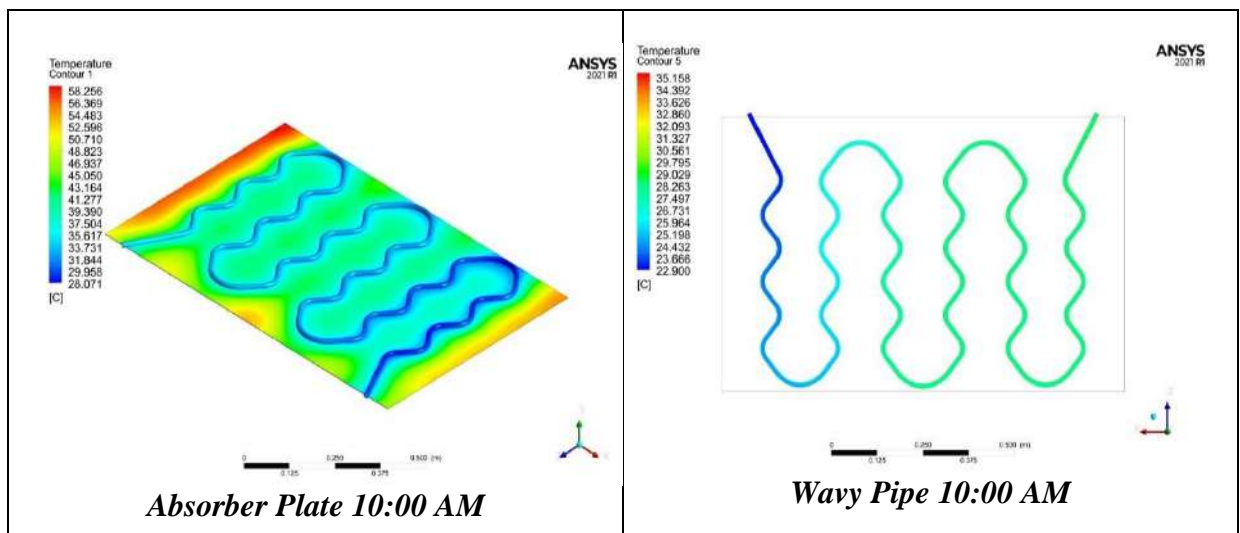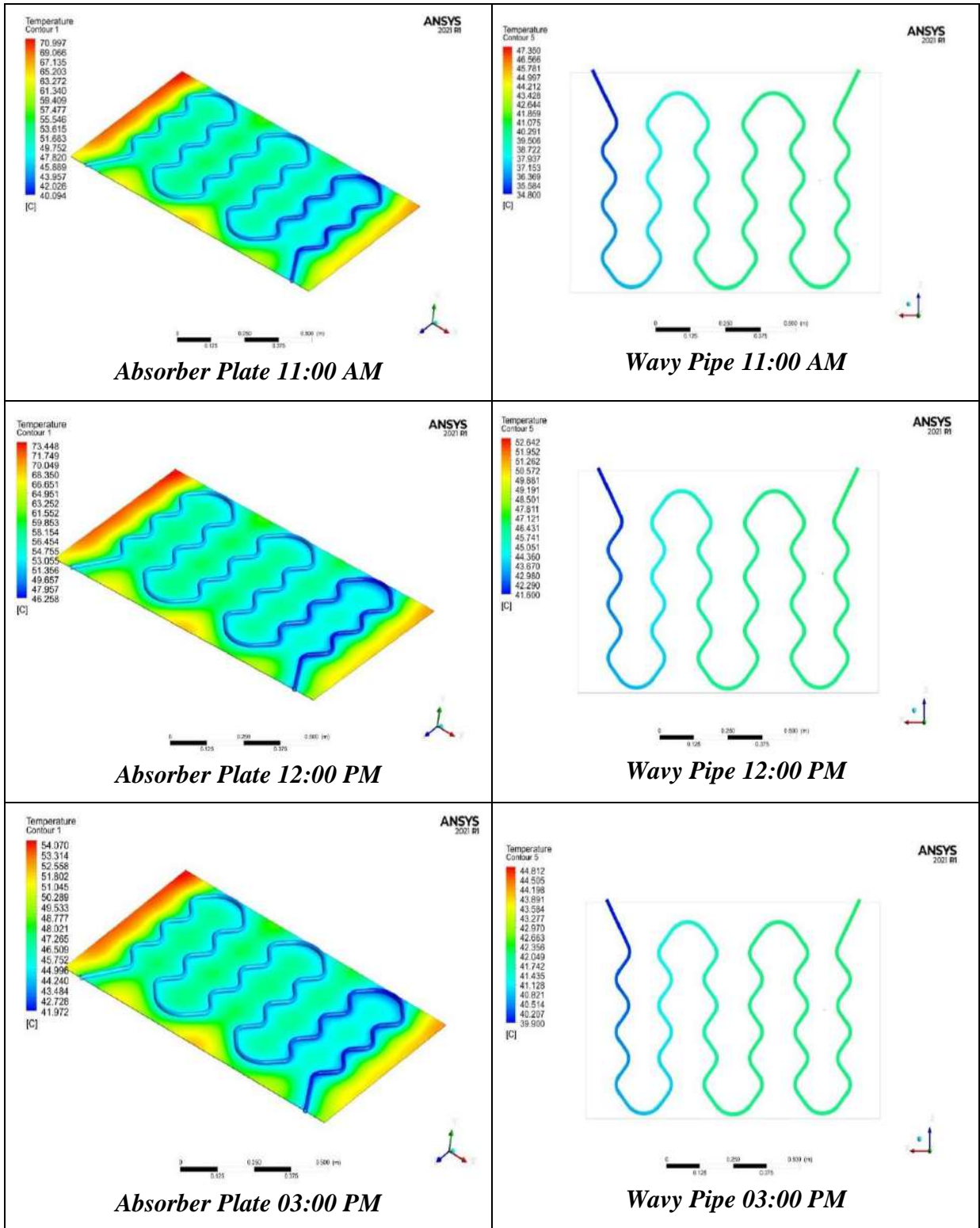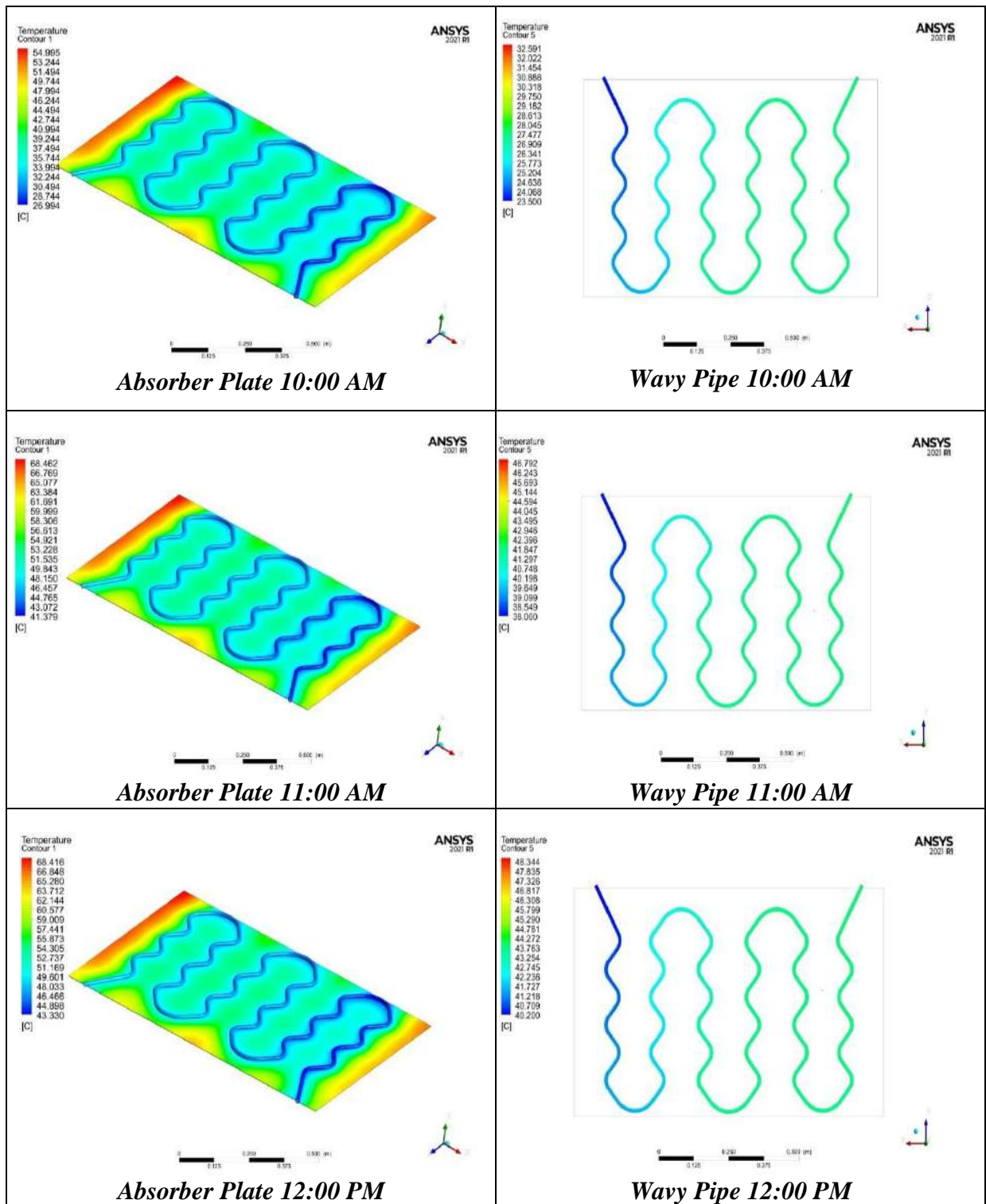*03:00 Pm for Opened System with 2 L/min Water Flowrate Without Air Injection.*

Absorber Plate 11:00 AM	*Wavy Pipe 11:00 AM*
Absorber Plate 12:00 PM	*Wavy Pipe 12:00 PM*
Absorber Plate 03:00 PM	*Wavy Pipe 03:00 PM*
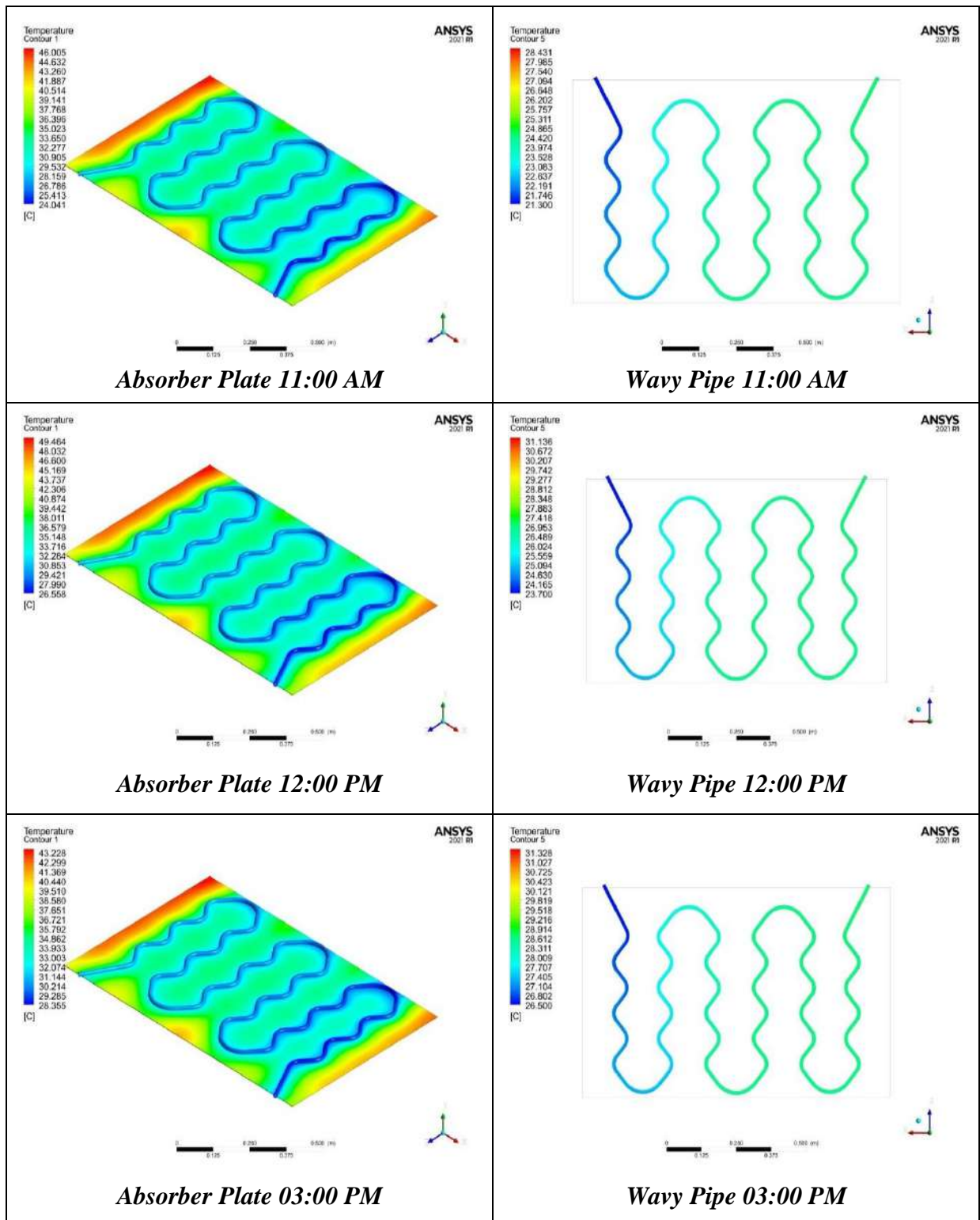
Figure 5-6: Contd.

5.3.2 Pressure Contour for Opened System

In a solar collector, the total pressure drop is given by the sum of two types of pressure losses: friction (or major) losses and local (or minor) losses. The friction loss along a straight pipe of constant cross section is a

function of the flow velocity, pipe length, pipe diameter and a friction factor which strongly depends on whether the fluid flow is turbulent or laminar. Figure (5.7) illustrates the values of pressure drops that almost constant for each various water discharge (0.5, 1, 1.5 and 2) L/min, which show the highest values are (5.09, 5.78, 6.5 and 6.9) kpa respectively. As friction results between the fluid and the inner surface of the pipe Pressure drop occurs. also, the higher the flow rate, the greater pressure drop that because the relationship is direct depending on Darcy's equation.

Water Flowrate 0.5 L/min

Water Flowrate 1 L/min

Water Flowrate 1.5 L/min

Water Flowrate 2 L/min
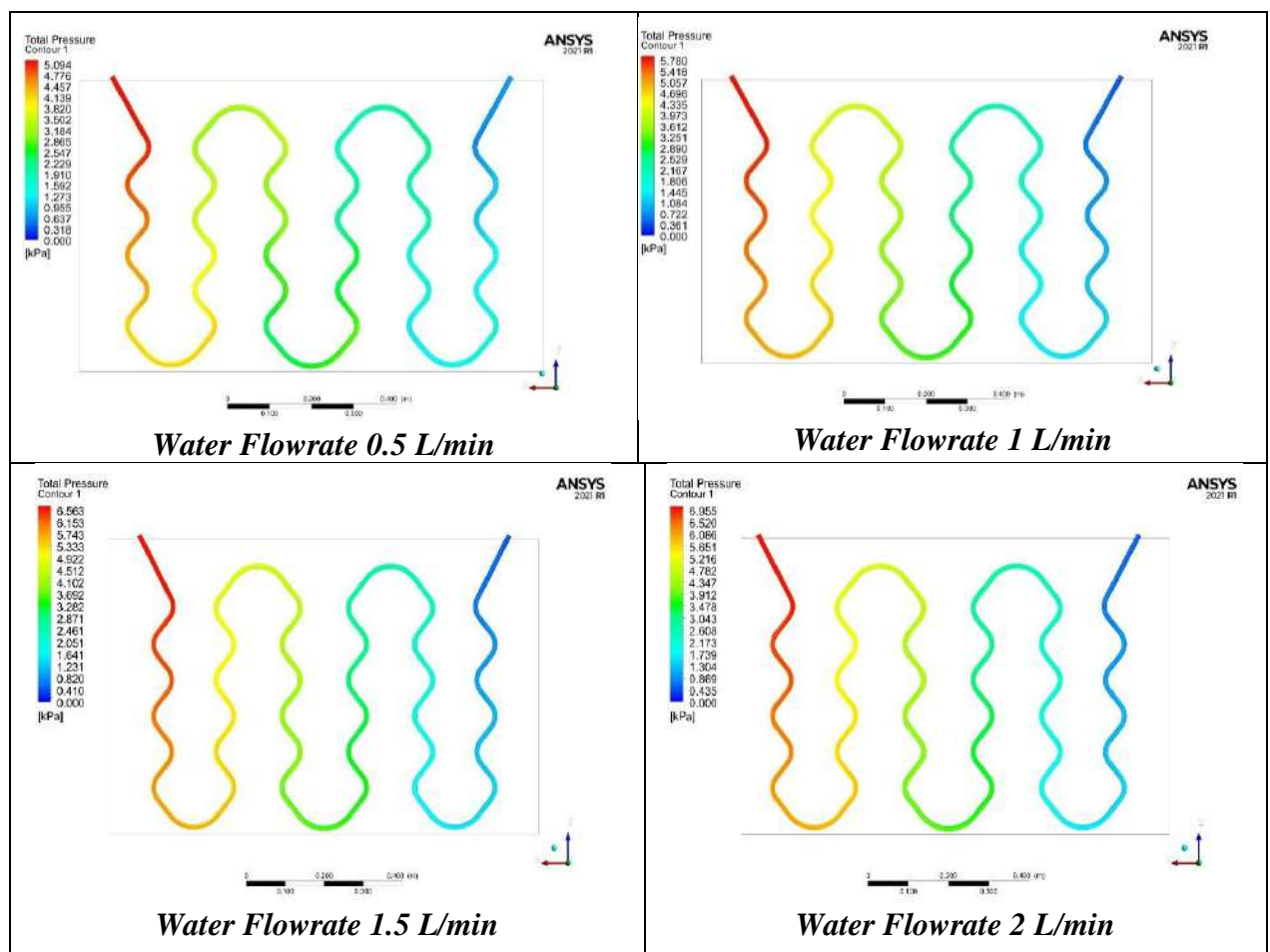
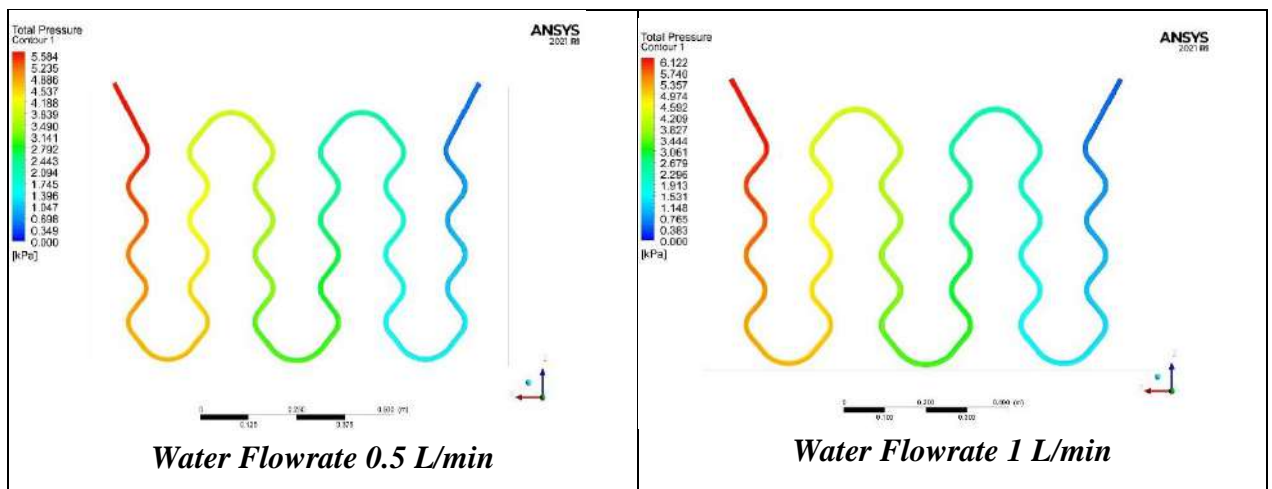*Figure 5-7: Pressure Distribution Contours (kpa) for Open System with (0.5, 1, 1.5 and 2) L/min Water Flowrate Without Air Injection.*

## 5.4 Closed System without Air Bubble Injection

As shown in the contours in figures (5.8) to (5.12), four flowrates (0.5, 1, 1.5, and 2) L/min were simulated for closed systems. To simulate the temperature and pressure contours for the first four months of the year,

the weather boundary conditions of Holly Karbala city were taken into consideration during four separate chosen hours from 10 AM to 3 PM.

5.4.1 Temperature Contour for Closed System

The numerical analysis reveals that the optimal results are obtained during the four-hour period between (10 AM to 3 PM), according to solar equations that can be seen in [35], the average range of solar radiation for the solar collector area of (0.96) m^2 with a title angle of 45 degrees was (520 -1050) W/m^2. When the water flow rate is (0.5 L/min), which gives the absorber plate more time to transfer the required heat to the water. The resultant water is as hot as it can possibly be at this flow rate, with the highest water outlet temperature in the closed system being (56.1°C), as represented in figure (5.8). Figure (5.9) shows the effect of the flow (1 L/min) on the water temperature difference during working hours (10 am - 3 pm) and shows the highest amount of water outlet temperature is (38.3 °C). In the figure (5.10) shows the effect of the flow (1.5 L/min) on the water temperature difference during working hours (10 am - 3 pm) and the highest amount of water outlet temperature is (46.7 °C). In the figure (5.11) shows the effect of the flow (2 L/min) on the water temperature difference during working hours (10 am - 3 pm) and shown, as is the highest amount of water outlet temperature is (43.8 °C). It was discovered that lowering the mass flow rate (0.5, 1, 1.5, and 2) produces an increase in the water output temperature, and thus an increase in the difference between the outlet and inlet water temperature in the two systems of closed and opened. This is because the heat transfer time between the working fluid and the absorption plate has increased, so the fluid exposed to solar radiation for a longer period, thus increasing the heating of the fluid and obtaining a higher outside temperature
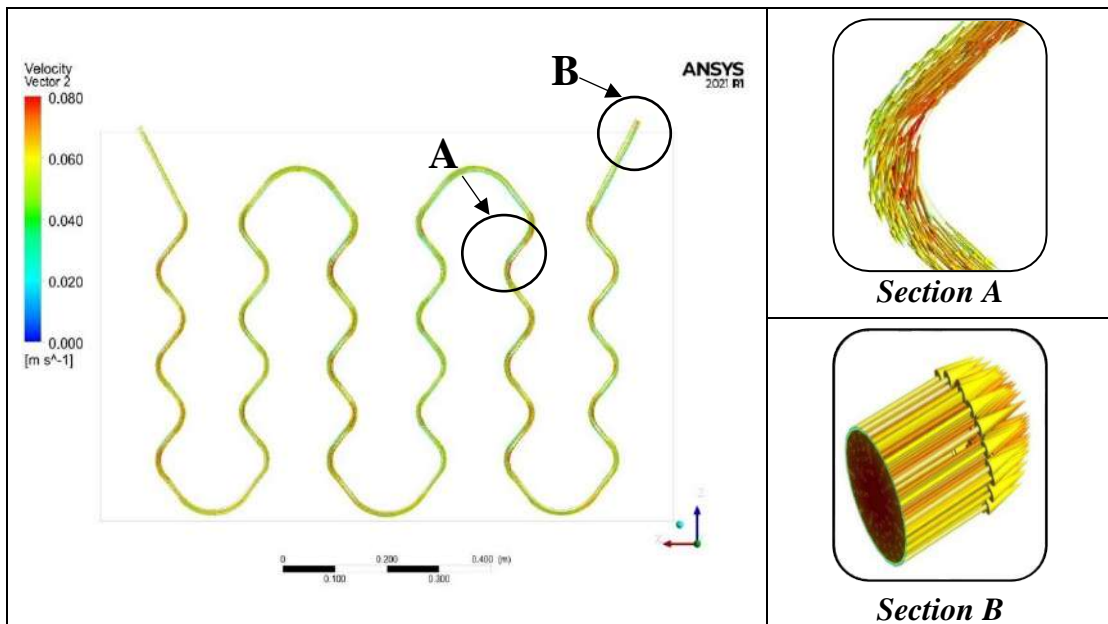
Figure 5-8: Temperature Distribution Contours (°C) for the Time Period from 10:00 Am to 03:00 Pm for Closed System with 0.5 L/min Water Flowrate Without Air Injection.

Absorber Plate 03:00 PM	*Wavy Pipe 03:00 PM*

Figure 5-8: Contd.

Absorber Plate 10:00 AM	*Wavy Pipe 10:00 AM*
Absorber Plate 11:00 AM	*Wavy Pipe 11:00 AM*

Figure 5-9: Temperature Distribution Contours (°C) for the Time Period from 10:00 Am to

*03:00 Pm for Closed System with 1 L/min Water Flowrate Without Air Injection.*

| Absorber Plate 12:00 PM | Wavy Pipe 12:00 PM |
| Absorber Plate 03:00 PM | Wavy Pipe 03:00 PM |

Figure 5-9: Contd.

| Absorber Plate 10:00 AM | Wavy Pipe 10:00 AM |

Figure 5-10: Temperature Distribution Contours (°C) for the Time Period from 10:00 Am to 03:00 Pm for Closed System with 1.5 L/min Water Flowrate Without Air Injection.

Figure 5-10: Contd.

Absorber Plate 10:00 AM	Wavy Pipe 10:00 AM
Absorber Plate 11:00 AM	Wavy Pipe 11:00 AM
Absorber Plate 12:00 PM	Wavy Pipe 12:00 PM

Figure 5-11: Temperature Distribution Contours (°C) for the Time Period from 10:00 Am to 03:00 Pm for Closed System with 2 L/min Water Flowrate Without Air Injection.

Absorber Plate 03:00 PM	***Wavy Pipe 03:00 PM***
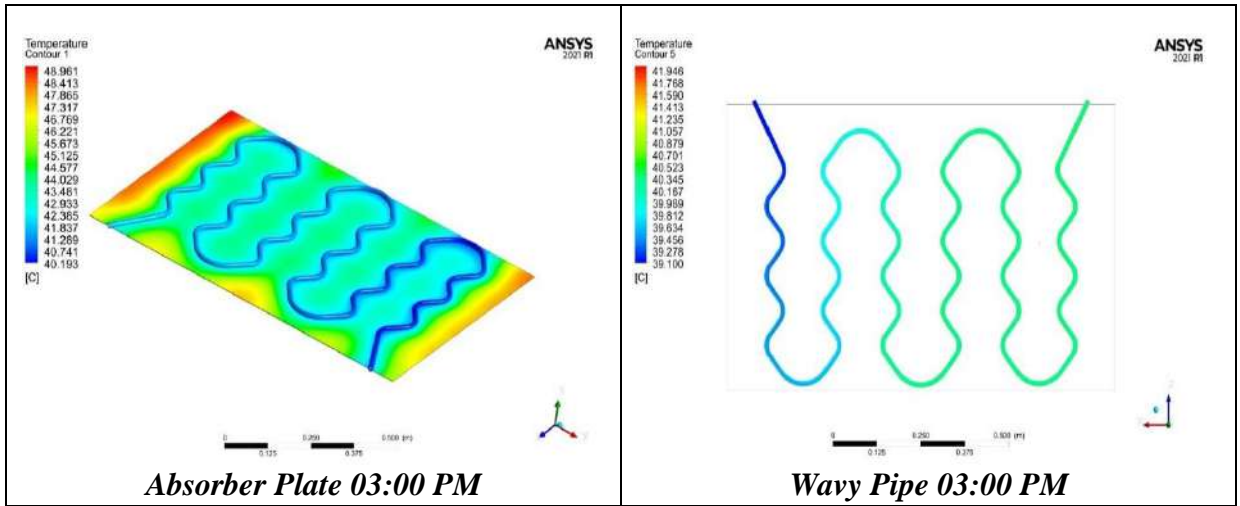
Figure 5-11: Contd.

5.4.2 Pressure Contour for Closed System

The pressure drop for the various water discharges is shown in Figure (5.12). The contours demonstrate that as water flowrate increases, the pressure difference also rises as a result of the direct relationship between pressure drop and fluid velocity. The values of pressure drop that almost constant for each various water discharge (0.5, 1, 1.5 and 2) L/min, which show the highest values are (5.58, 6.12, 6.66 and 7) kpa respectively. As a result of friction between the fluid and the pipe's inner surface There is a pressure drop. Furthermore, because the relation is direct according to Darcy's equation, the higher the flow rate, the larger pressure drop.

Water Flowrate 0.5 L/min	***Water Flowrate 1 L/min***

Figure 5-12: Pressure Distribution Contours (kpa) for Closed System with (0.5, 1, 1.5 and 2) L/min Water Flowrate Without Air Injection.

| Water Flowrate 1.5 L/min | Water Flowrate 2 L/min |
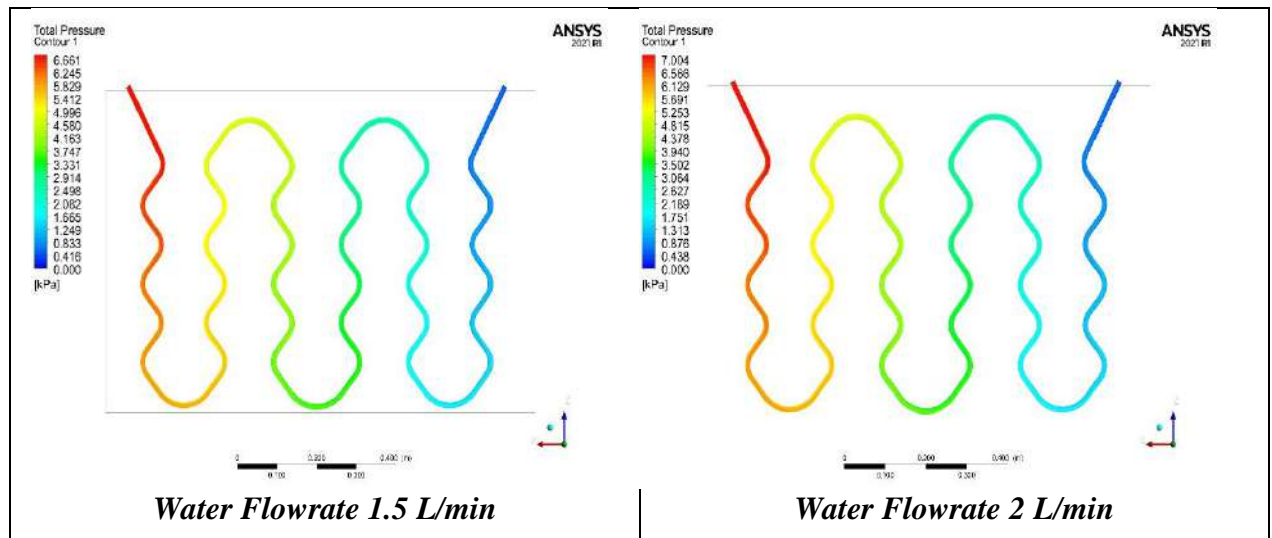
Figure 5-12: Contd.

5.4.3 Velocity Contour for Opened and Closed System

During the simulation process, it was observed that there is a matching in the velocity contours for both closed and opened systems to the same discharge, due to the cross-sectional area of the tube is constant. Figures (5.13) to (5.16) show the velocity contours for the case when the system work at (0.5, 1, 1.5 and 2) L/min only in the present work for both opened and closed systems, by taking into account the timework from (10:00 AM to 03:00 PM) to simulate the flat plate water solar collector. When 0.5 L/min of water flows, the average velocity is (0.067 m/s), while at 1 L/min of water flows, the average velocity is (0.135 m/s), the results show at 1.5 L/min of water flows, the average velocity is (0.19 m/s), but at 2 L/min of water flows, the average velocity is (0.25 m/s). The contour sections for all cases show a water steady stream through the pipes with increasing water velocity in the bending of the pipes. This was due to the fact that the flowrate was constant along the pipe cross section area, resulting in constant fluid velocity according to the discharge formula.

Figure 5-13: Velocity Distribution Contours (m/s) for the Time Period from 10:00 Am to 03:00 Pm for Both Systems with 0.5 L/min Water Flowrate Without Air Injection.
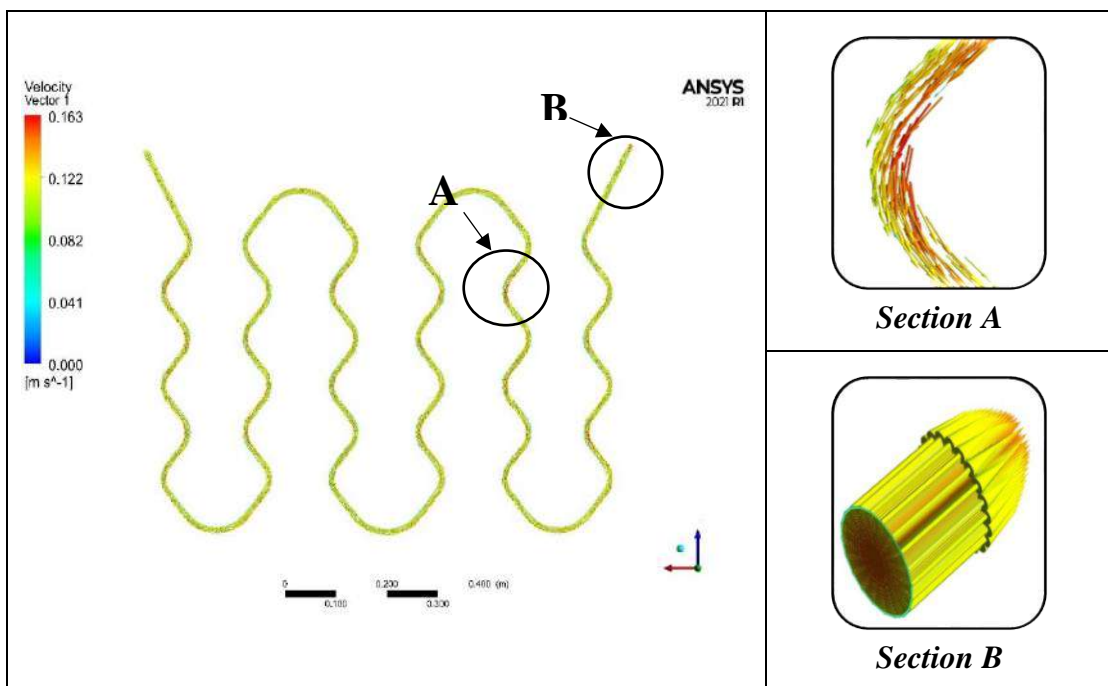
Figure 5-14: Velocity Distribution Contours (m/s) for the Time Period from 10:00 Am to 03:00 Pm for Both Systems with 1 L/min Water Flowrate Without Air Injection.
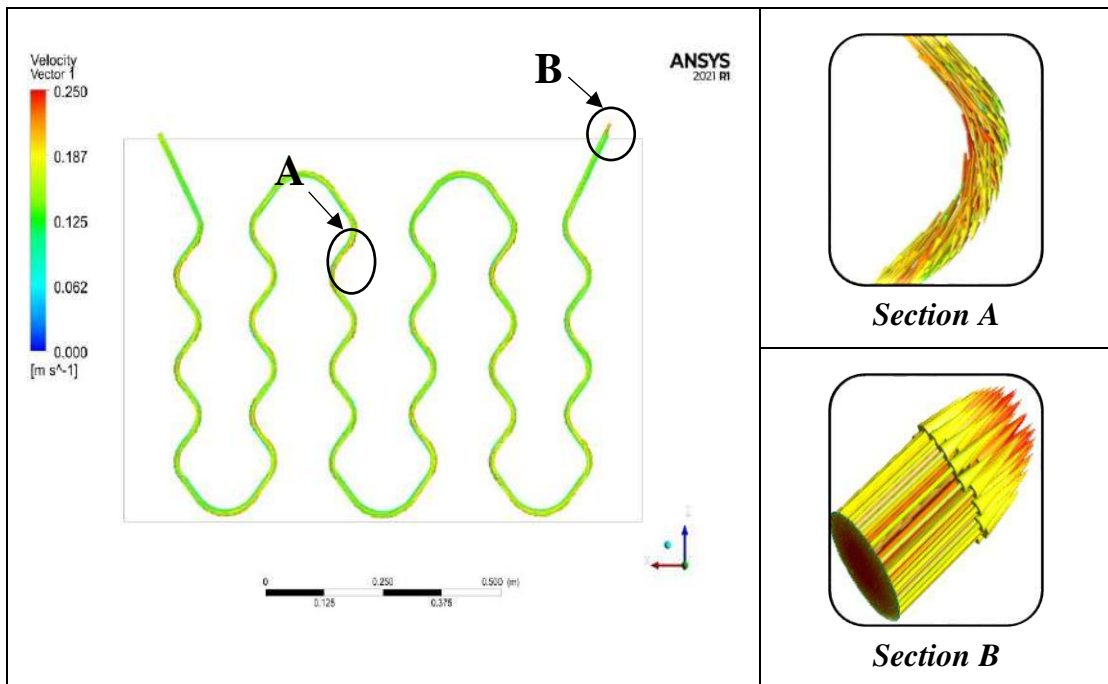
Figure 5-15: Velocity Distribution Contours (m/s) for the Time Period from 10:00 Am to 03:00 Pm for Both Systems with 1.5 L/min Water Flowrate Without Air Injection.
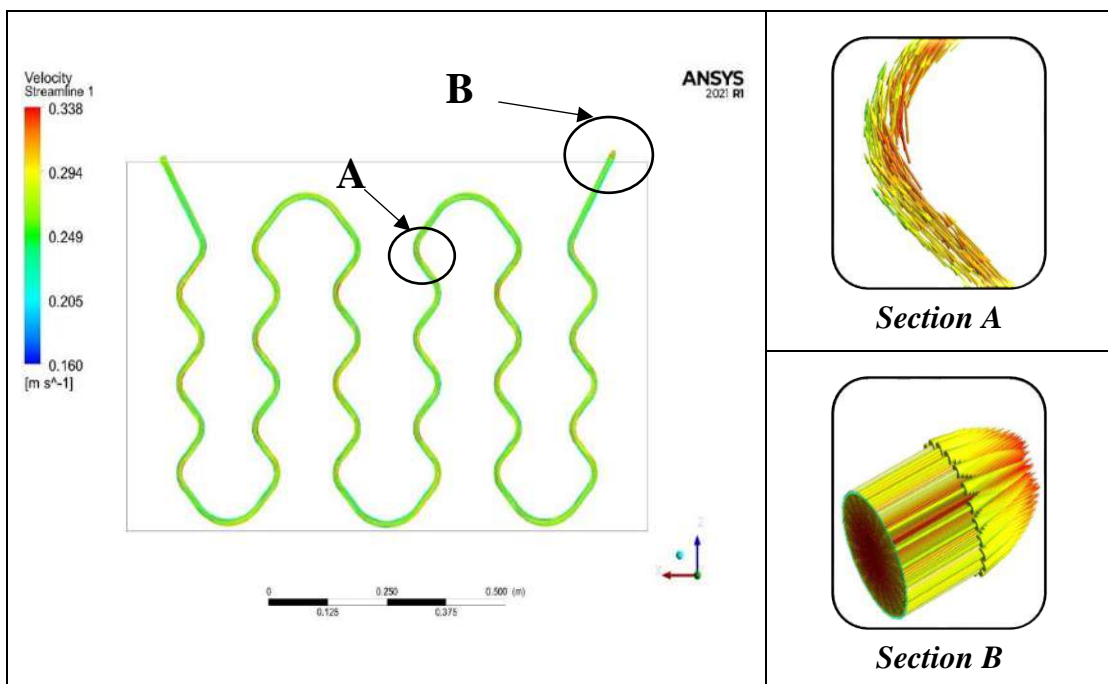
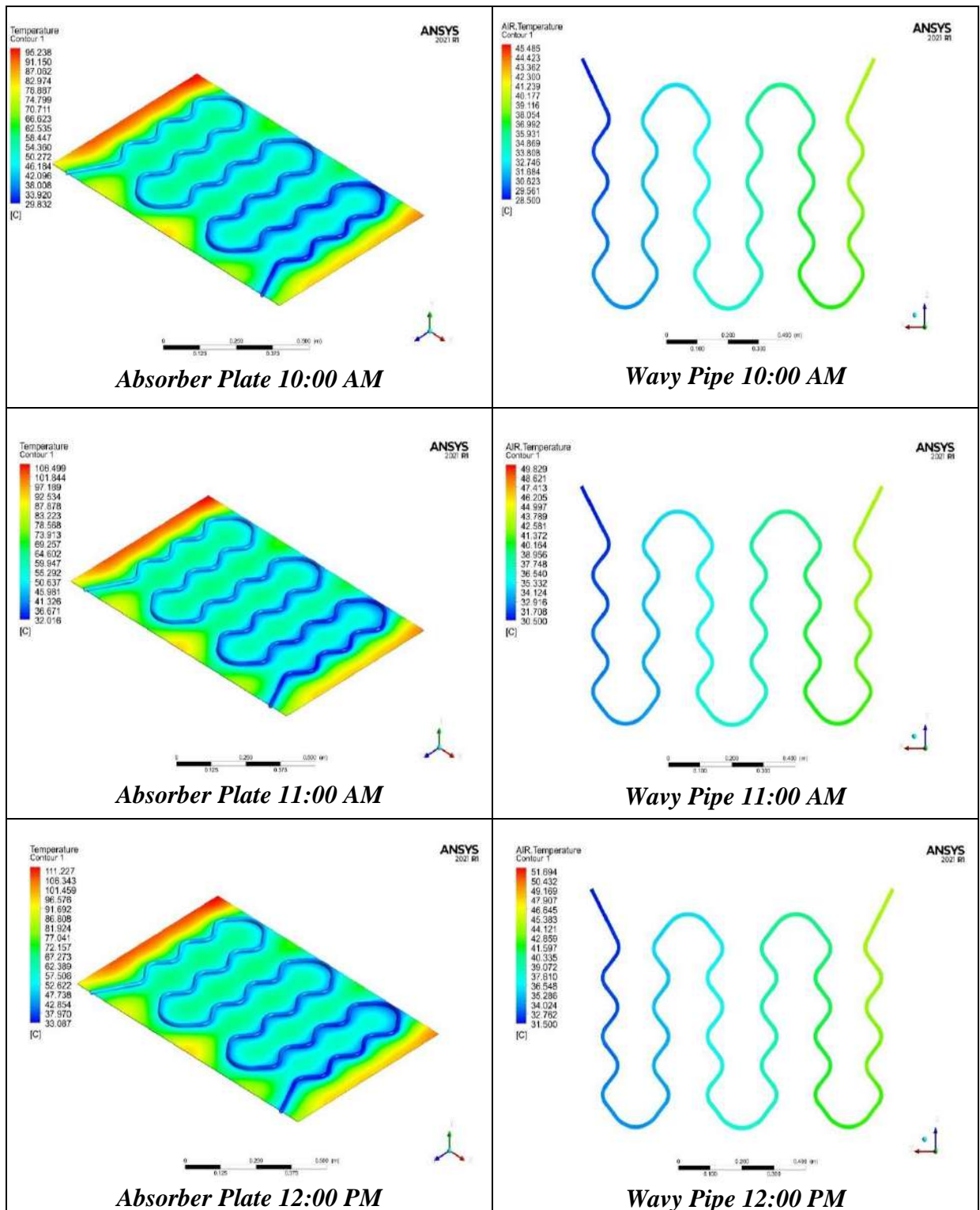*Figure 5-16: Velocity Distribution Contours (m/s) for the Time Period from 10:00 Am to 03:00 Pm for Both Systems with 2 L/min Water Flowrate Without Air Injection.*
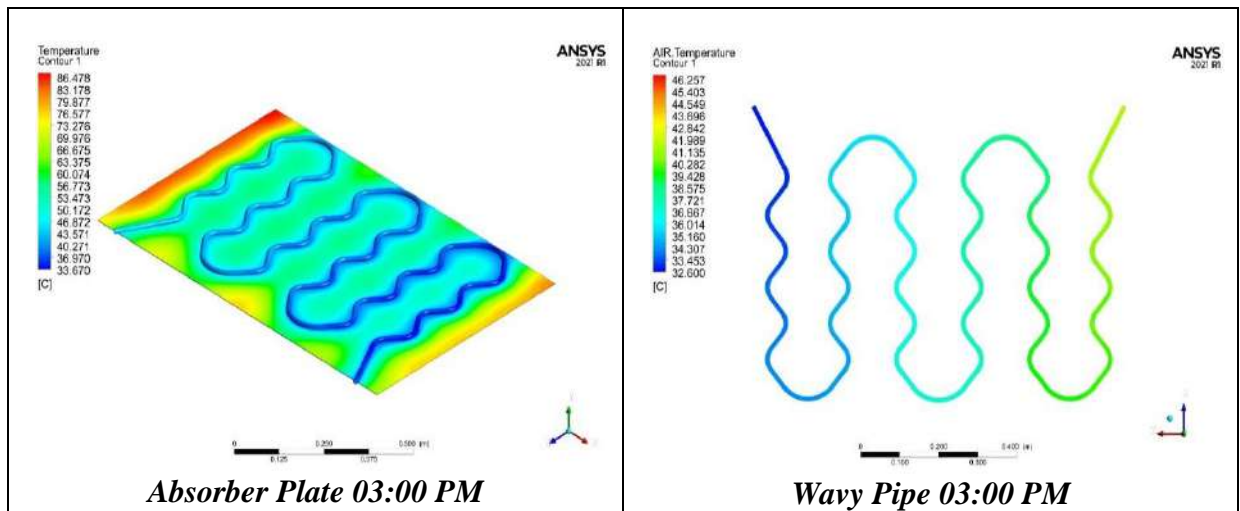
5.4.4 Optimum Case for the Water Flowrates

After completing the simulation to the two-type system (Opened and Closed) for the four flowrate categories (0.5, 1, 1.5 and 2) L/min, the

efficiencies were calculated to each flow rate to find the most efficient case to inject the air bubble. By using equation (3-15), the useful energy was calculated and applied to the efficiency equation (3-19), it was observed that the useful energy reached its maximum value when the water flowrate for the opened system was 1 L/min and 2 L/min for the closed system comparing with the other flowrates. These results led to conclude that 1 L/min was the most efficient flow rate for the opened system and the closed system was 2 L/min water flow rates shown in the figures (5.17) and (5.18).
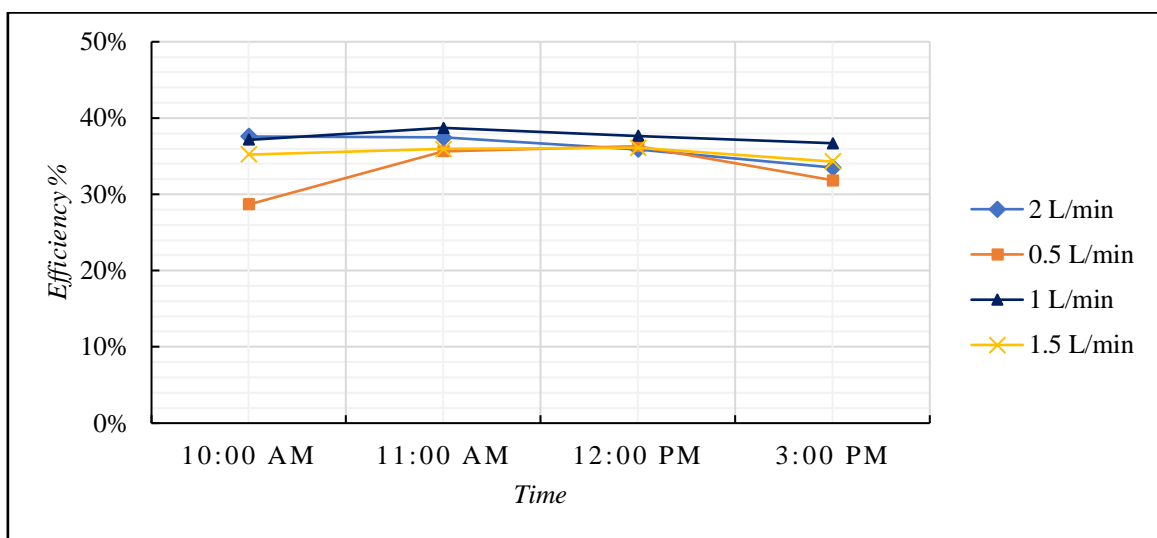
Figure 5-17: The System Efficiency for All Cases of the Opened System Without Air Injection for (0.5, 1, 1.5 and 2) L/min
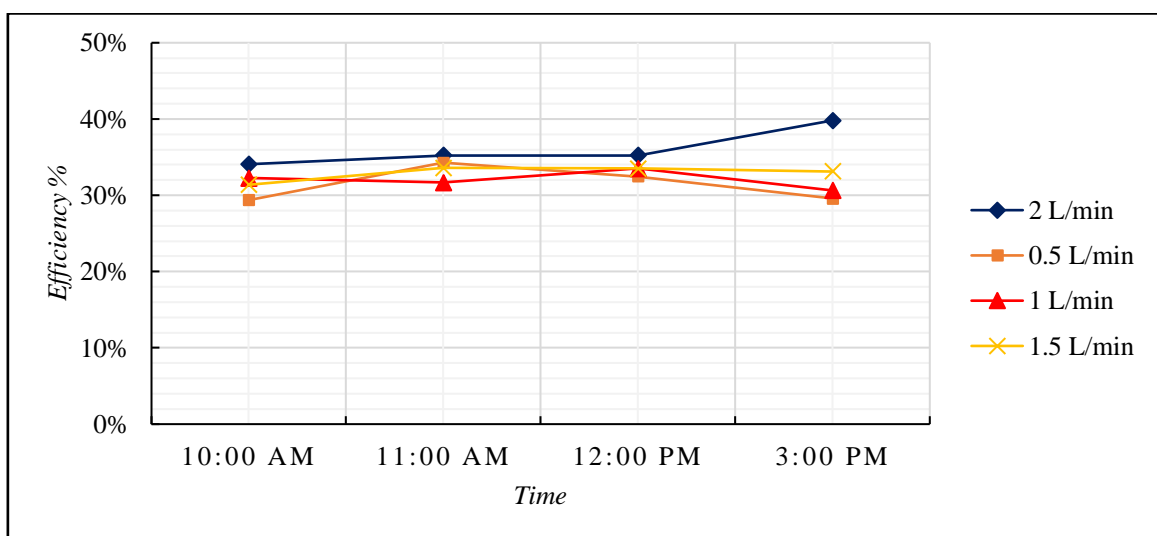
Figure 5-18: The System Efficiency for All Cases of the Closed System Without Air Injection for (0.5, 1, 1.5 and 2) L/min

5.5 The System with Air Bubble Injection

Due to the air bubbles' buoyant force and movement, there is significant mixing occurring inside the heat exchanger pipe. The random motion of bubbles will mix the liquid bulk and break down the hydrodynamic and thermal boundary layers, enhancing heat exchange in thermal systems. In order to choose the suitable air flowrates to mixed with the most efficient water flowrate of (1 and 2) L/min for both opened and closed system respectively, a simulation was carried out for several discharges of the air flowrates, three discharges were chosen which are (0.15, 0.25 and 0.35) L/min. It was observed that when the amount of air flowrate is greater than 0.35 L/min, choking occurs in the fluid stream due to the large amount of air compared to the specifications of this system cause a stop in the flow stream and the occurrence of high pressure drops. As for pumping air flowrate less than 0.15 L/min, it was observed that there was no significant effect of the added air to improve the thermal performance of the system.

5.5.1 Opened System with Air Bubble Injection

After finding the most efficient case in opened system without air bubble injection, which was (1 L/min water). The air bubbles were injected to the system at three different air flowrates of (0.15, 0.25 and 0.35) L/min and simulated by using Ansys program to find the most efficient case in four period time between 10:00 a.m. to 3:00 p.m.

5.5.1.1 Temperature Contour for Opened System

Simulation is carried out using ANSYS R21 program the performance of the solar water collector was tested numerically. The work was done in four period time form (10 Am to 3 Pm) with average solar calculated range of (600-1200) w/m^2, which injected three different air flowrates of (0.15, 0.25 and 0.35) L/min to the most efficient case in the

opened system, which was 1 L/min. The simulation results in figure (5.19) shows the temperature contours of flowrate (1 L/min water and 0.15 L/min air) during working hours (10 am - 3 pm) and shows the highest value of water outlet temperature is (42.2 C). While the figure (5.20) shows the temperature contours of flowrate (1 L/min water and 0.25 L/min air) during working hours (10 am - 3 pm) and illustrated that the highest value was (41.5 C) for the outlet water temperature. Finally, the figure (5.21) illustrated that (37.7 C) was the highest degree for the flowrate (1 L/min water and 0.35 L/min air) during working hours (10 am - 3 pm). The results show that air flowrate at 0.15 L/min gives a small enhancement comparing with 0.25 L/min. when the flowrate was 0.25 L/min, the enhancement being much better because the relation between the water and air reach to it perfect value. After adding 0.35 air with the 1 l/min water, the mixture being not satisfied to the system and gives less enhancement which can observe in the results below.

| Absorber Plate 10:00 AM | Wavy Pipe 10:00 AM |
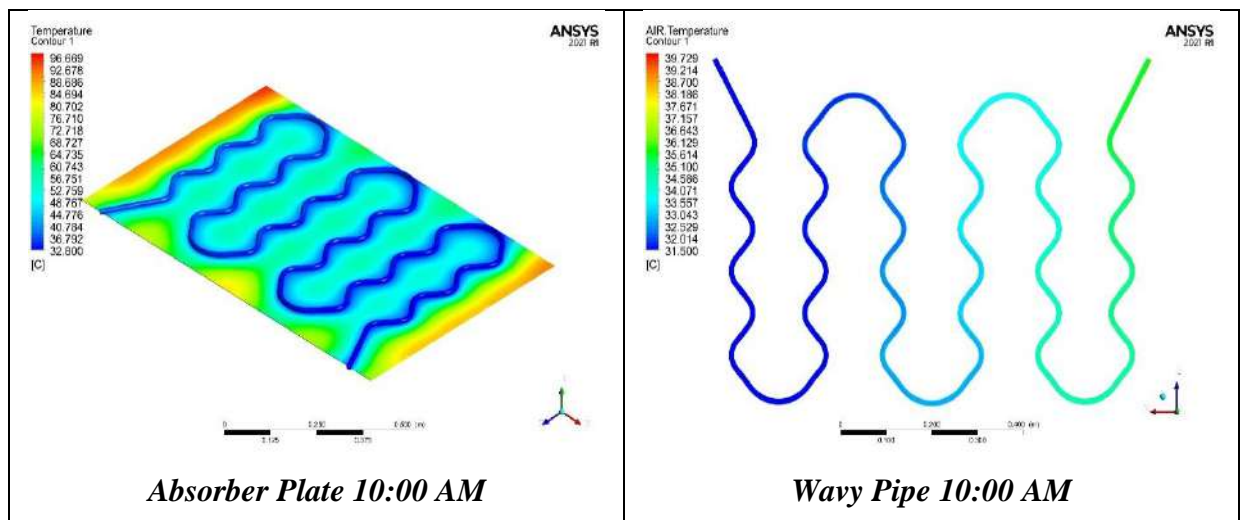
Figure 5-19: Temperature Distribution Contours (°C) for the Time Period from 10:00 Am to 03:00 Pm for Opened System with 1 L/min Water Flowrate with 0.15 L/min Air Bubble Injection.

Absorber Plate 11:00 AM	*Wavy Pipe 11:00 AM*
Absorber Plate 12:00 PM	*Wavy Pipe 12:00 PM*
Absorber Plate 03:00 PM	*Wavy Pipe 03:00 PM*
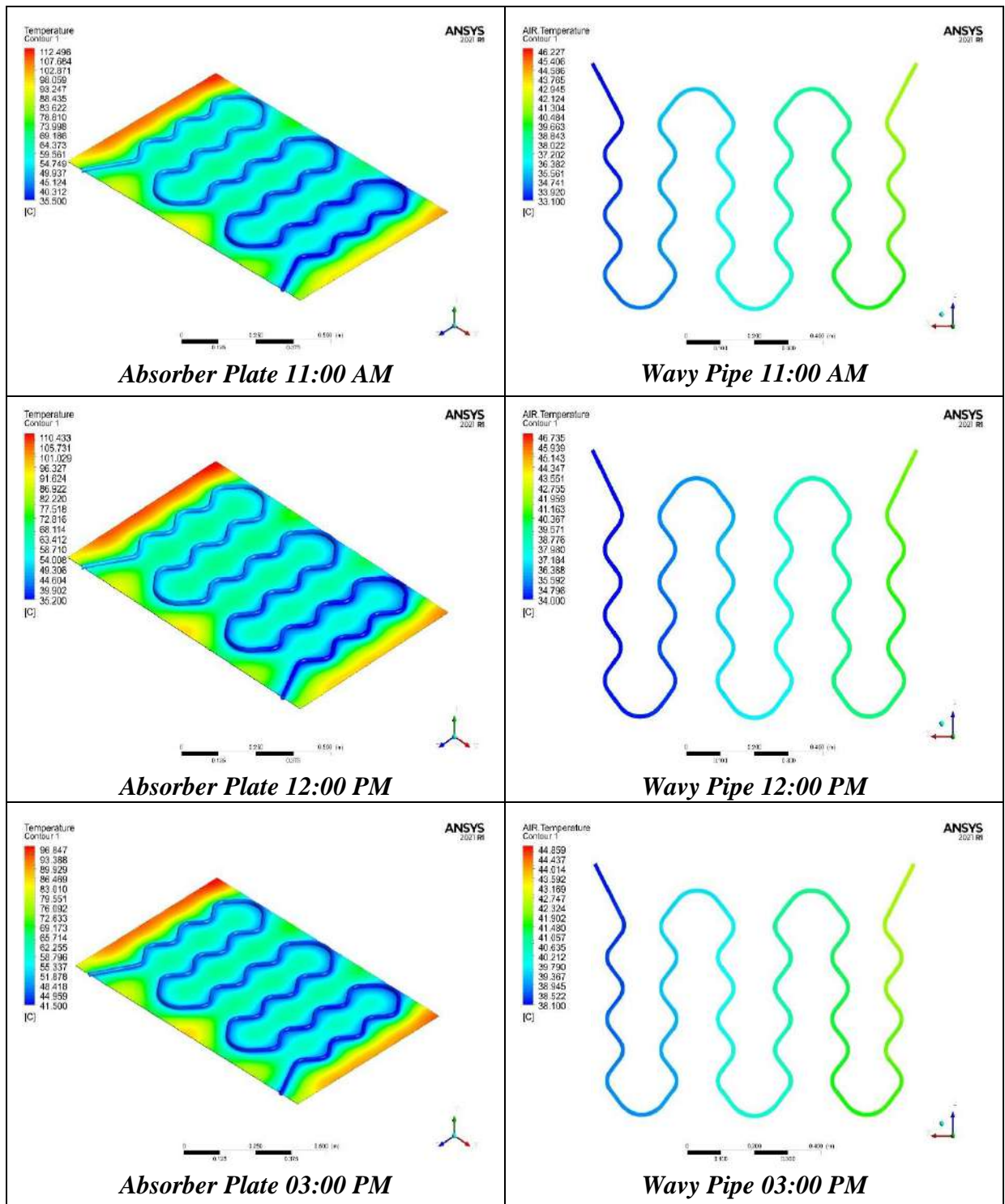
Figure 5-19: Contd.

Figure 5-20: Temperature Distribution Contours (°C) for the Time Period from 10:00 Am to 03:00 Pm for Opened System with 1 L/min Water Flowrate With 0.25 L/min Air Bubble Injection.

Absorber Plate 03:00 PM | *Wavy Pipe 03:00 PM*

Figure 5-20: Contd.

Absorber Plate 10:00 AM | *Wavy Pipe 10:00 AM*

Absorber Plate 11:00 AM | *Wavy Pipe 11:00 AM*
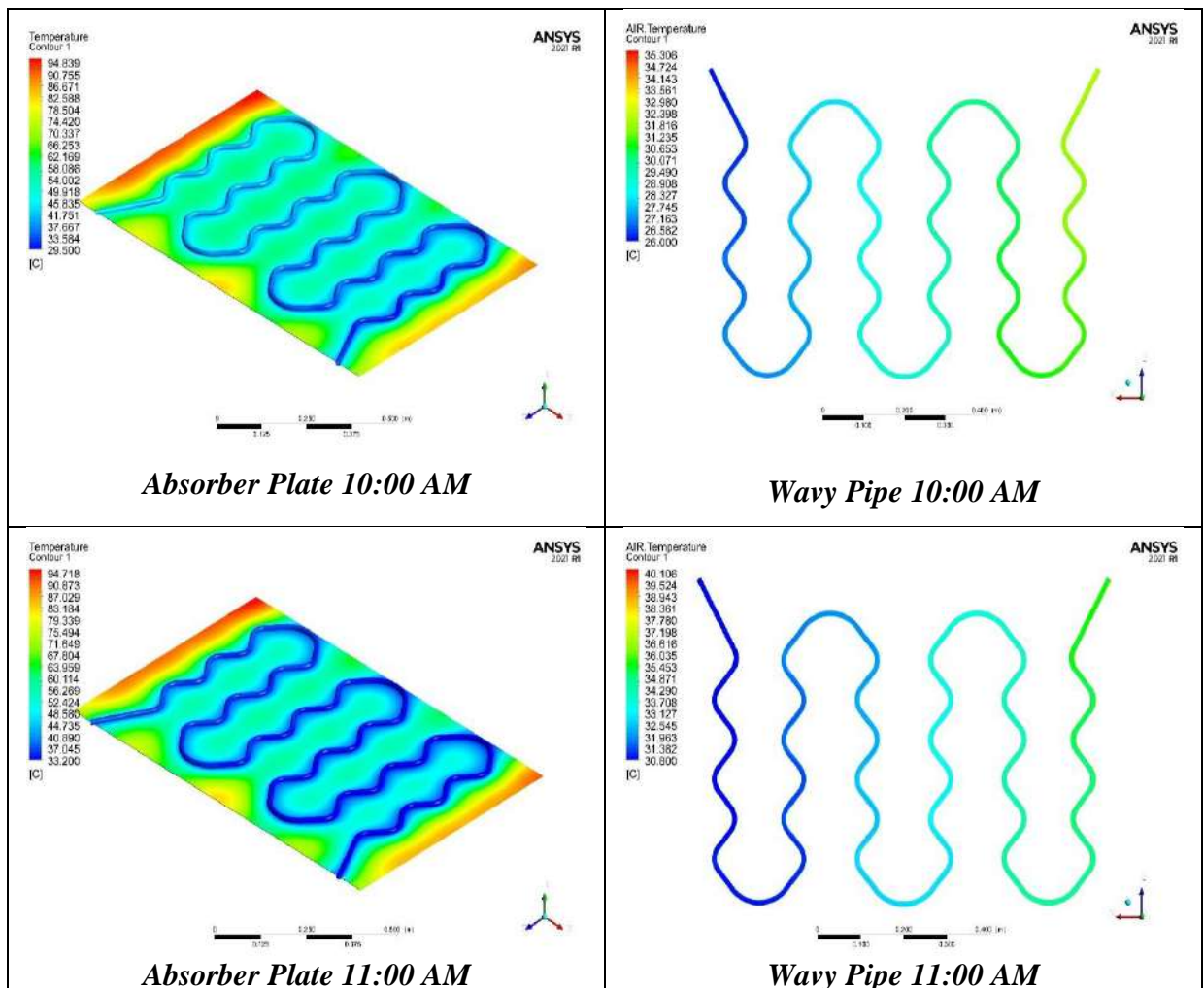
Figure 5-21: Temperature Distribution Contours (°C) for the Time Period from 10:00 Am to 03:00 Pm for Opened System with 1 L/min Water Flowrate with 0.35 L/min Air Bubble Injection.

Absorber Plate 12:00 PM   *Wavy Pipe 12:00 PM*

Absorber Plate 03:00 PM   *Wavy Pipe 03:00 PM*
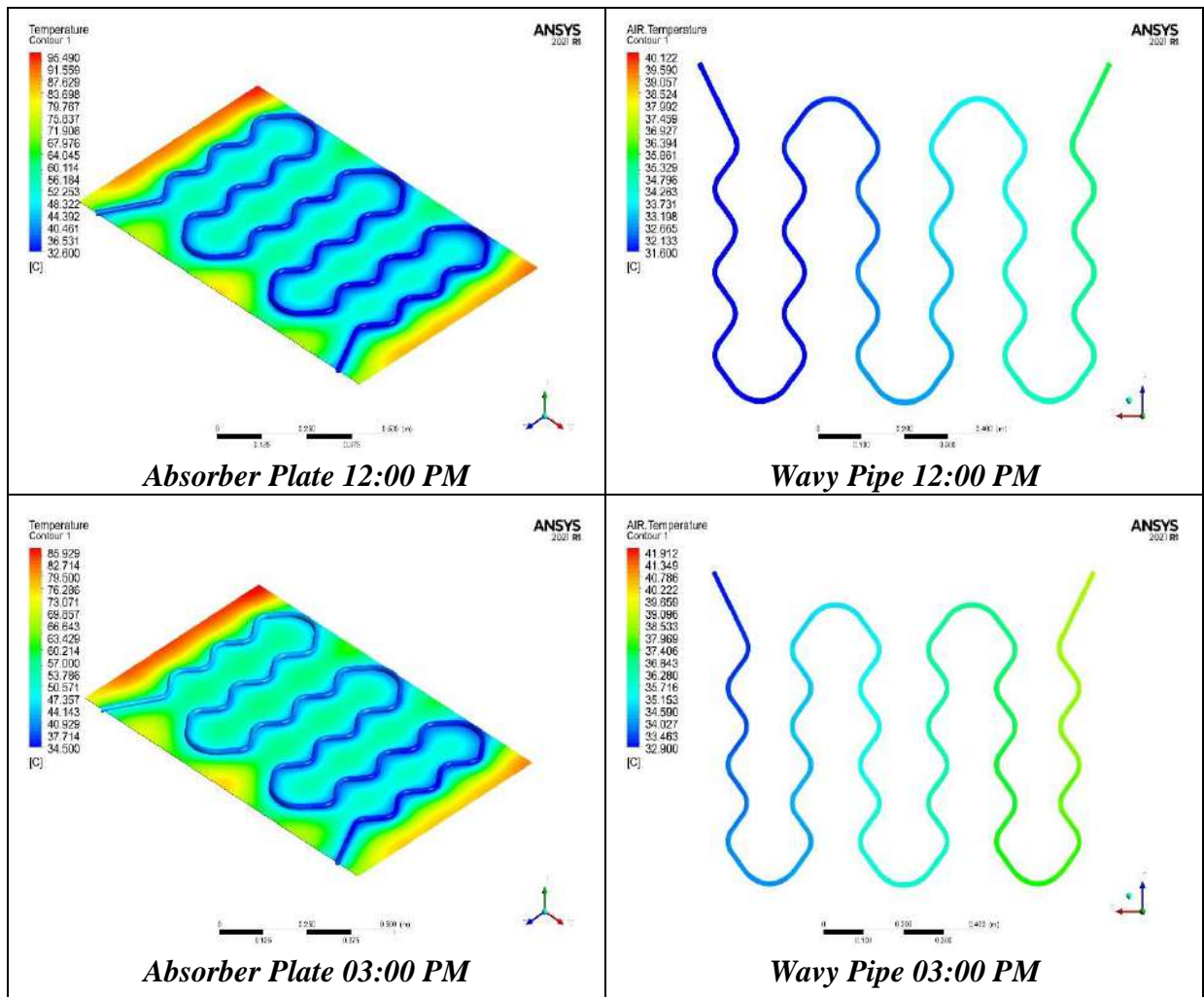
Figure 5-21: Contd.

5.5.1.2 Pressure Contour for Opened System

For air bubbles that were injected by the air flowrates of (0.15, 0.25 and 0.35) L/min, the pressure drop was simulated and shown in figure (5.22). As expected, given the same conditions and flow rate, the pressure drop for the air/water mixture was larger than that of water. The values of pressure drop for each various air flowrates (0.15, 0.25 and 0.35) L/min, which show the highest values are (12.04, 9.6 and 10.48) kpa respectively.

(1 L/min water and 0.15 L/min air)

(1 L/min water and 0.25 L/min air)

(1 L/min water and 0.35 L/min air)
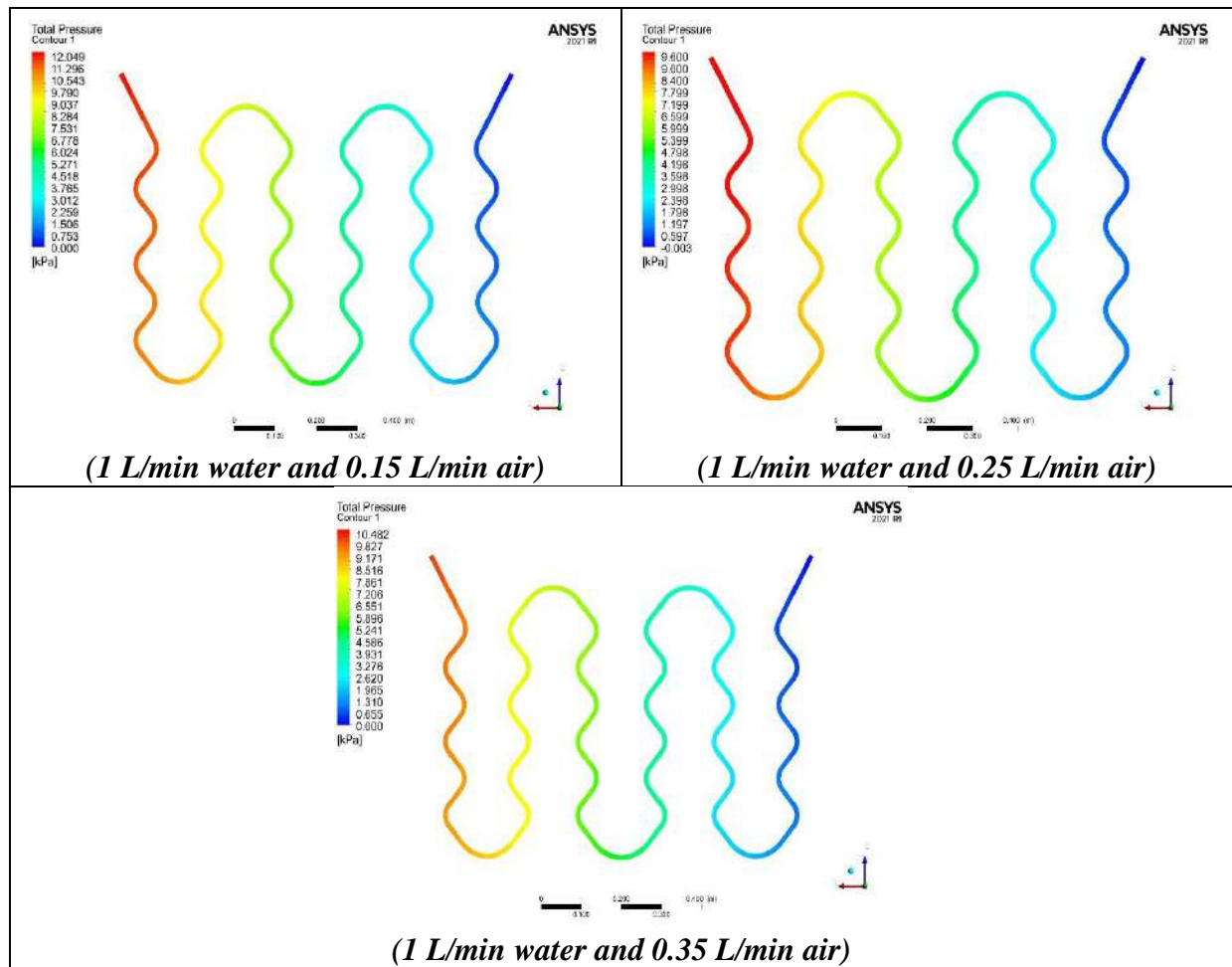
Figure 5-22: Pressure Distribution Contours (kpa) for Opened System with Air Injection at (0.15, 0.25 and 0.35 L/min) for 1 L/min Water Flowrate.

The lower the pressure drop led to less additional power is required to transport the fluid in the pipeline and lower energy consumption. so that, according to the figure (5.22), the injection of 0.25 L/min air flowrate is lowest pressure drops for the opened system.

By taking into the account the efficiencies of the three air bubble injection cases (0.15, 0.25 and 0.35) L/min, which they simulated by the Ansys program. It found that injected 0.25 L/min air into 1 L/min water was the most efficient case according to the schematic figure (5.23). When mixing 0.35 L/min air with 1 l/min water, the results show that the mixture does not satisfy the system's requirements and gives less improvement, as shown in the results below. When compared to air at flowrate of 0.25

L/min, air flowrate at 0.15 L/min provides a slight improvement. The enhancement was significantly better when the flowrate was 0.25 L/min because the mixing between the water and air reached its perfect value.
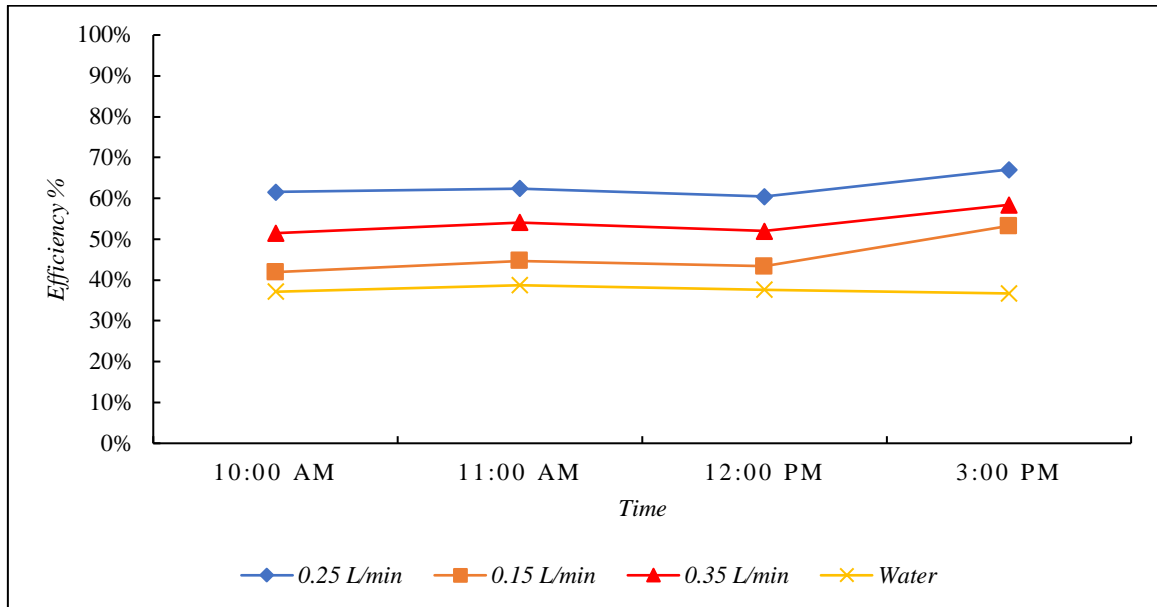
Figure 5-23: The System Efficiency for the Opened System with Air Injection flowrates of (0.15, 0.25 and 0.35 L/min) for 1 L/min Water Flowrate

5.5.1.3 Velocity Contour for Opened System

Figure (5.24) show the velocity contours for the most efficient case when the system works at water flow rate 1 L/min mixed with 0.25 L/min air flowrate by taking into account the time period from (10:00 AM to 03:00 PM). The air flow creates better turbulence in the flow and thus enhances the heat transfer coefficients of the tube surfaces in contact with the air-water mixture. Section (A and B) were taken from the air contour at the elbows, showing the flow vortex that mixed the flow.
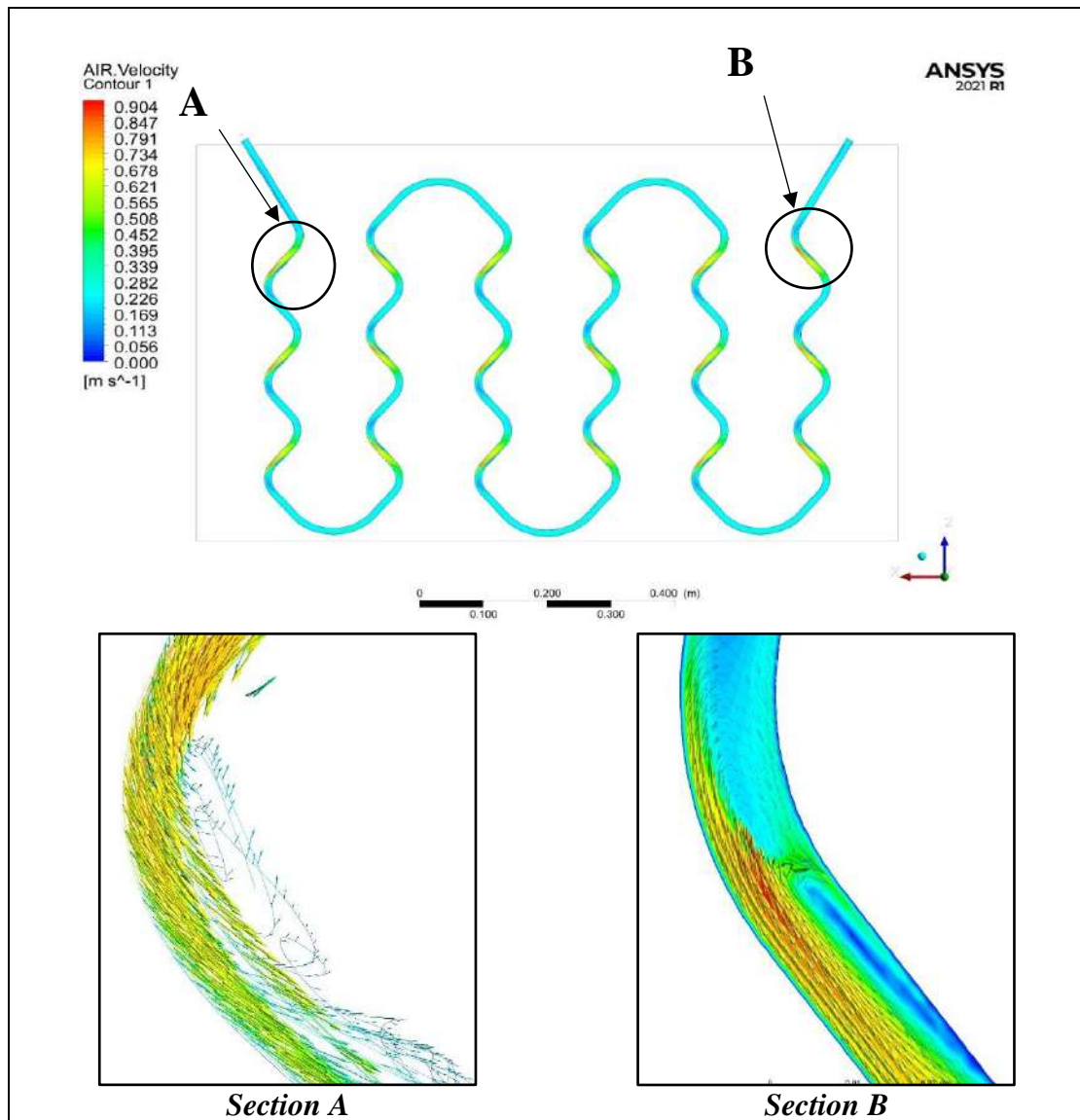
Figure 5-24: Velocity Distribution Contours for the Time from 10:00 Am to 03:00 Pm for Open System with 1 L/min Water Flowrate with 0.25 L/min Air Injection.

5.5.1.4 Volume Fraction for Opened System

Volume fractions represent the space occupied by each phase, and the laws of conservation of mass and momentum are satisfied by each phase individually. The volume fraction is defined as the ratio of the volume of one phase divided by the total volume of the mixture passing through the cross-section per unit of time. The volume fraction for the air water mixture is shown in the figure below (5.25), and the flow type of the mixture was stratified.
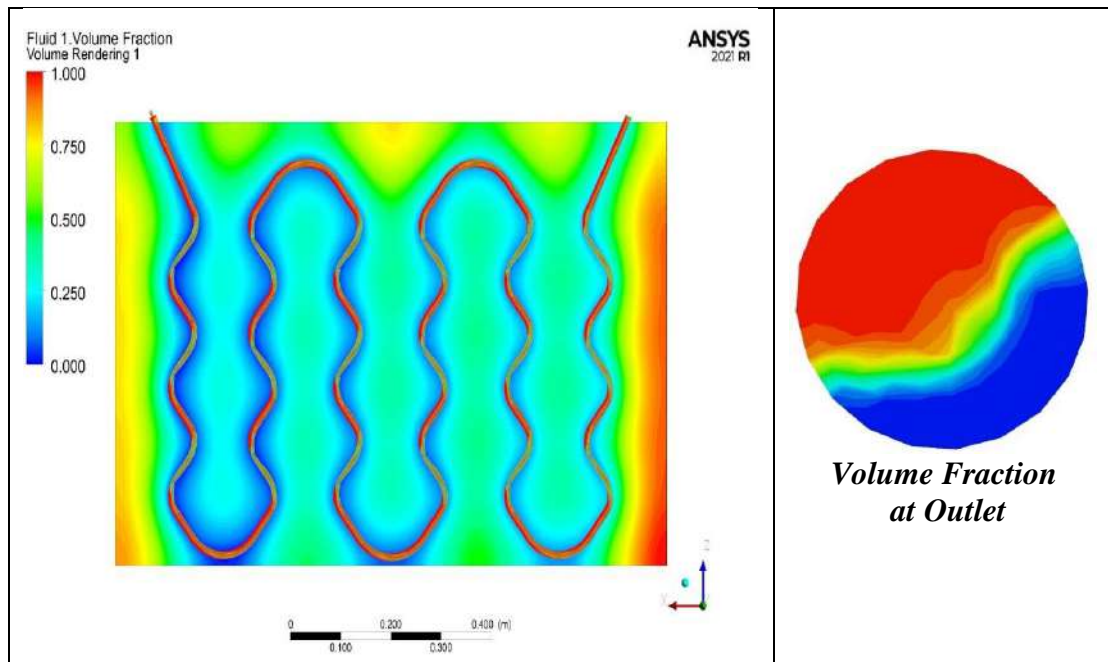
Figure 5-25: Volume Fraction Contours for the Time from 10:00 Am to 03:00 Pm

for Open System with 1 L/min Water Flowrate with 0.25 L/min Air Injection.

5.5.2 Closed System with Air Bubble Injection

After determining that the closed system with water flowing at the rate of (2 L/min) was the most effective water flowrate. Meanwhile to obtain the most effective case for the air-water mixture, the air bubbles were injected into the system over a four-hour period between 10:00 a.m. and 3:00 p.m. at three different air flowrates of (0.15, 0.25, and 0.35 L/min).

5.5.2.1 Temperature Contour for Closed System

The performance of the solar water collector was investigated numerically by using the ANSYS R21 program. The work was carried out during a four-hour period (10 Am to 3 PM) with average solar calculated range of (600-1200) w/m^2, with three different air flowrates of (0.15, 0.25, and 0.35) L/min being injected into the closed system's most efficient case, which was 2 L/min.

The simulation's results, shown in figure (5.26), illustrates the temperature contours of a flowrate of (2 L/min of water and 0.15 L/min of

air) during working hours (10 am to 3 pm). It reveals that the water outlet temperature reached its greatest value of (51.5 ℃). While the figure (5.27), which shows the temperature contours of the flowrate (2 L/min water and 0.25 L/min air) during working hours (10 am to 3 pm), shows that the outlet water temperature reached its highest value of (51 ℃). Finally, the figure (5.28) showed that the flow rate (2 L/min water and 0.35 L/min air) during working hours reached a maximum temperature of (53.8 ℃). (10 am - 3 pm). This is because the heat transfer time between the working fluid and the absorption plate has increased, so the fluid exposed to solar radiation for a longer period, thus increasing the heating of the fluid and obtaining a higher outside temperature. so that, Lowering the mass flow rate (0.5, 1, 1.5, and 2) causes a rise in the water output temperature, and consequently an increase in the difference between the outlet and inlet water temperature in both closed and opened systems.

| **Absorber Plate 10:00 AM** | **Wavy Pipe 10:00 AM** |
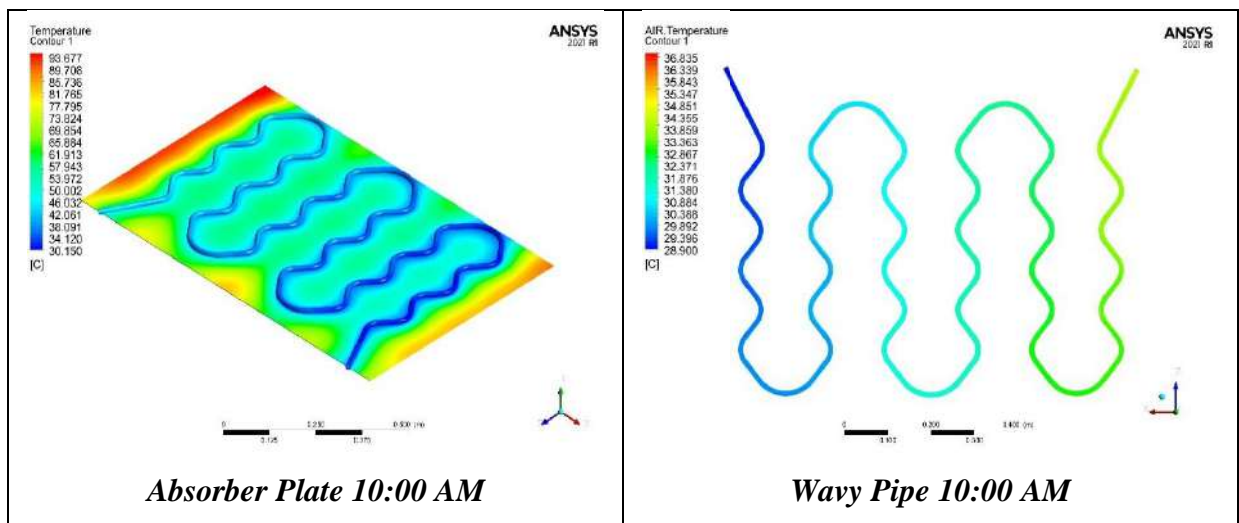
Figure 5-26: Temperature Distribution Contours (°C) for the Time Period from 10:00 Am to 03:00 Pm for Closed System with 2 L/min Water Flowrate with 0.15 L/min Air Bubble Injection.
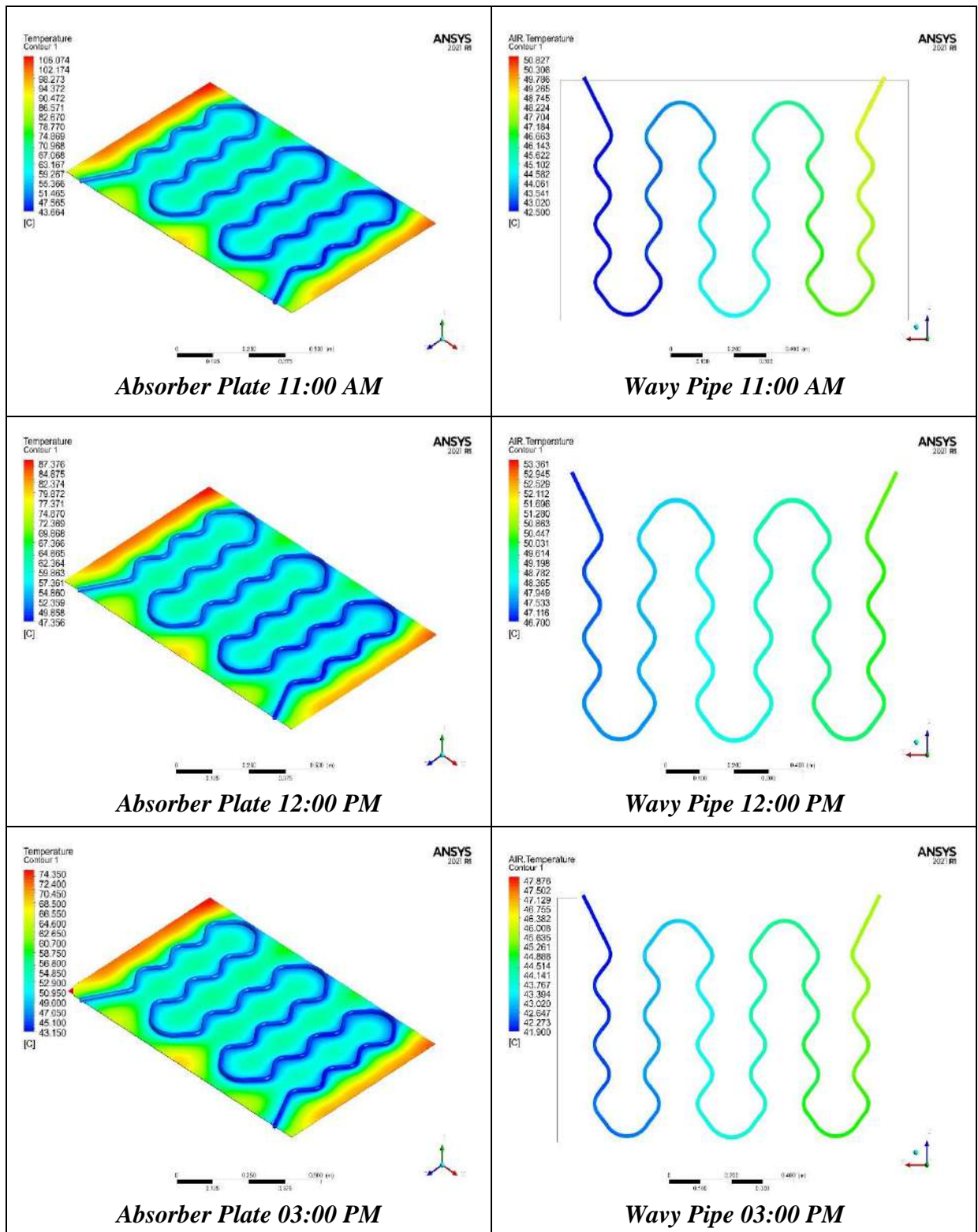
Figure 5-26: Contd.
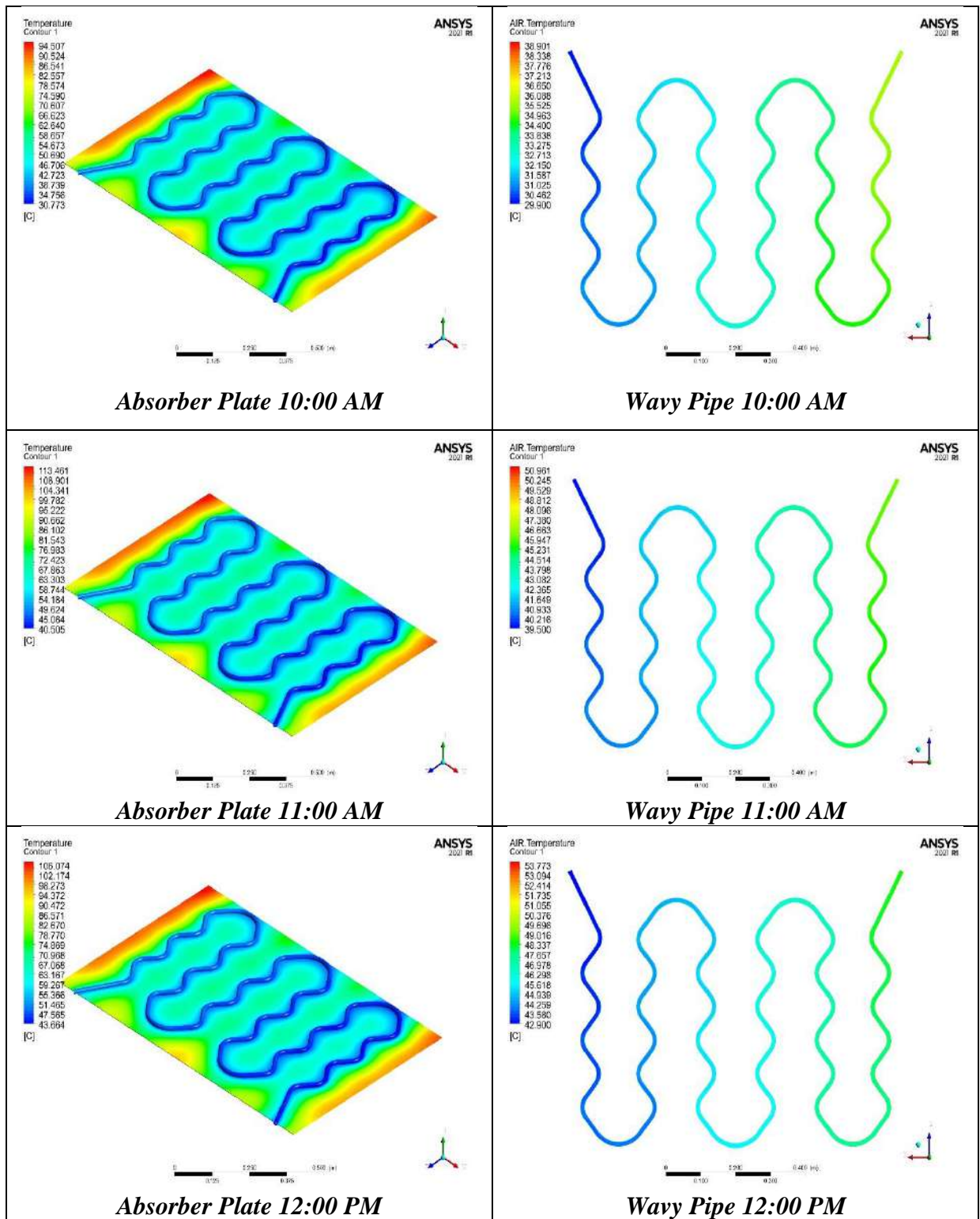
Figure 5-27: Temperature Distribution Contours (°C) for the Time Period from 10:00 Am to 03:00 Pm for Closed System with 2 L/min Water Flowrate with 0.25 L/min Air Bubble Injection.

Absorber Plate 03:00 PM   *Wavy Pipe 03:00 PM*

Figure 5-27: Contd.

Absorber Plate 10:00 AM   *Wavy Pipe 10:00 AM*

*Absorber Plate 11:00 AM*   *Wavy Pipe 11:00 AM*
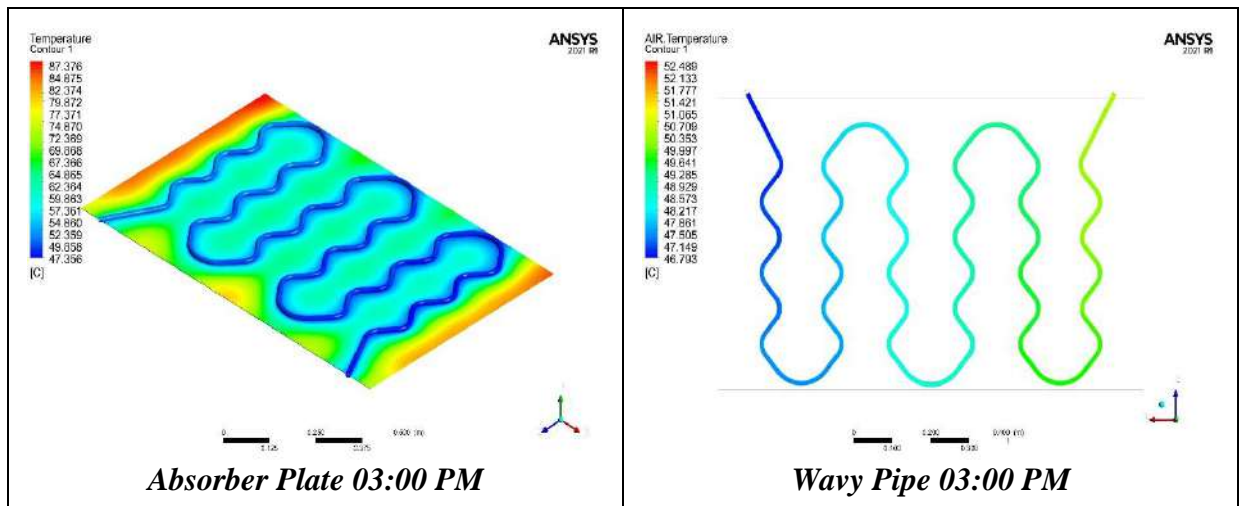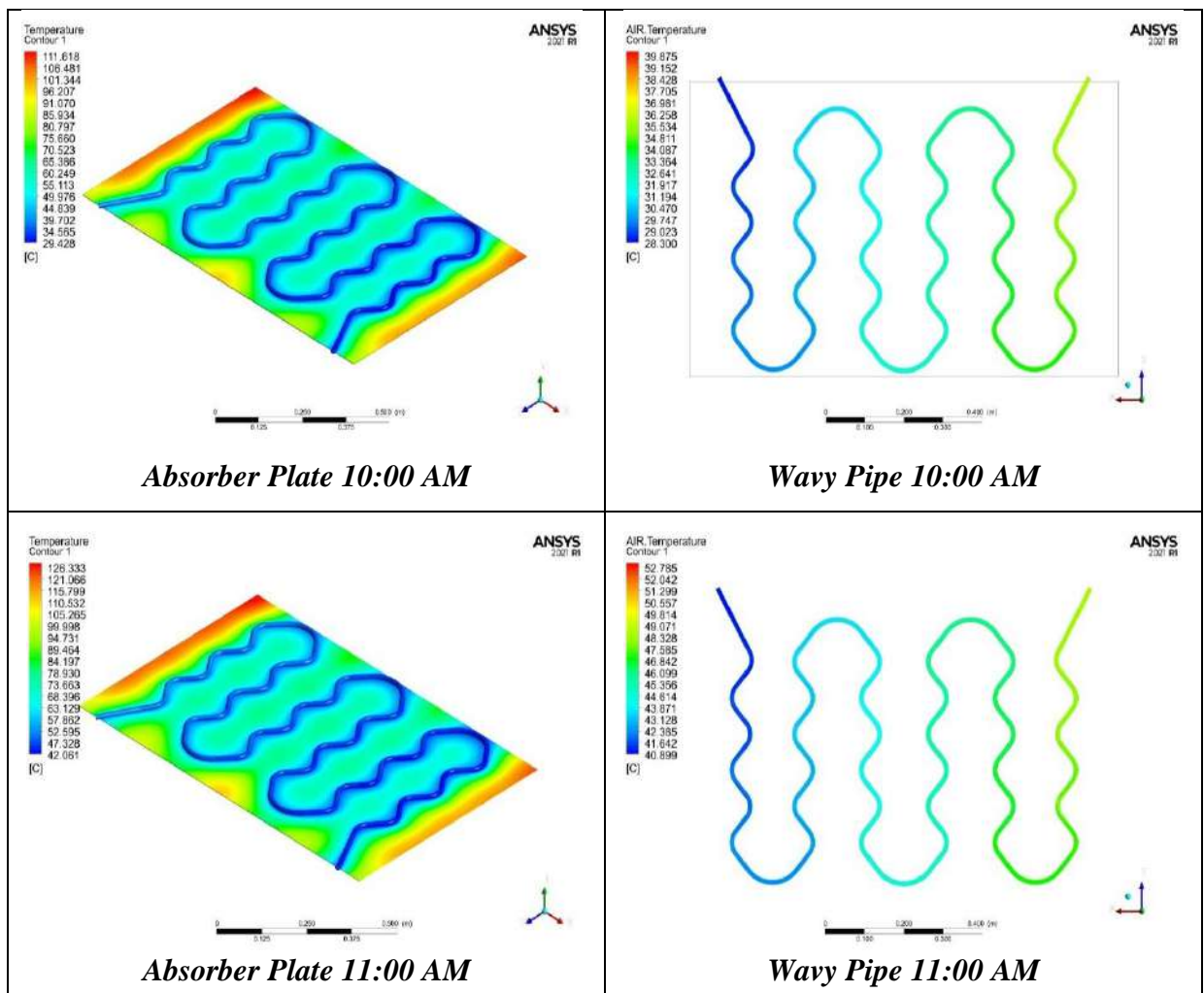
Figure 5-28: Temperature Distribution Contours (°C) for the Time Period from 10:00 Am to 03:00 Pm for Closed System with 2 L/min Water Flowrate with 0.35 L/min Air Bubble Injection.

Absorber Plate 12:00 PM   *Wavy Pipe 12:00 PM*

Absorber Plate 03:00 PM   *Wavy Pipe 03:00 PM*
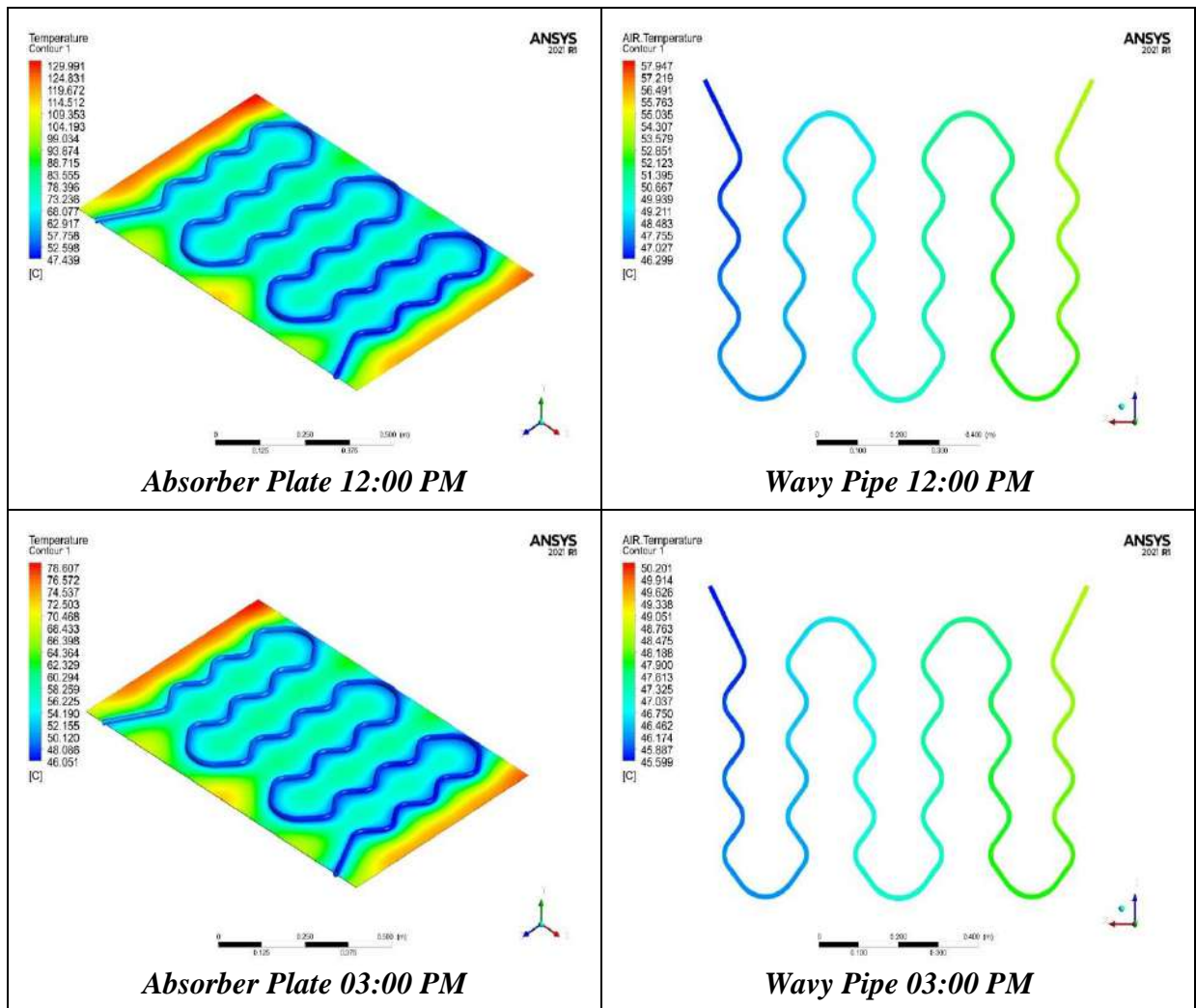
Figure 5-28: Contd.

5.5.2.2 Pressure Contour for Closed System

The pressure drops for air bubbles injected at air flowrates of (0.15, 0.25, and 0.35) L/min was simulated and illustrated in the figure (5.29). Given the same environment and flowrate, it was showed that the pressure drop for the mixture of air and water would be greater than for only water. The maximum values for pressure drop for the different air flowrates (0.15, 0.25, and 0.35) L/min are (10.38, 10.125, and 10.09) kpa respectively. So that, according to the figure (5.29), the injection of 0.35 L/min air flowrate is lowest pressure drops for the closed system.

(2 L/min water and 0.15 L/min air)   *(2 L/min water and 0.25 L/min air)*

(2 L/min water and 0.35 L/min air)
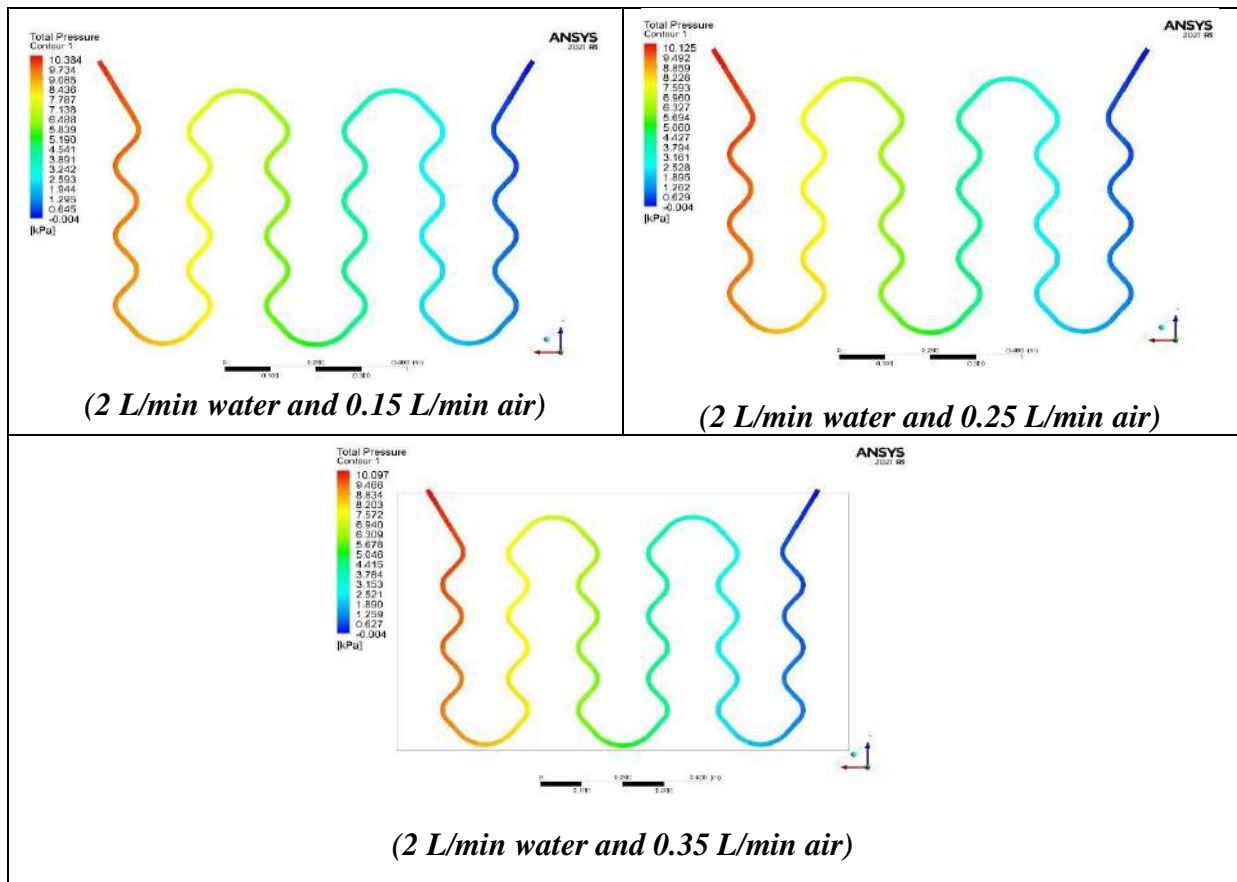
Figure 5-29: Pressure Distribution Contours (Kpa) for Closed System with Air Injection at (0.15, 0.25 and 0.35 L/min) for 2 L/min Water Flowrate.

Based on the simulation by using Ansys program for the closed system to the three air flowrates injection (0.15, 0.25, and 0.35 L/min), which they took into account. It was discovered that the most effective case, as shown in the schematic (5.30) was injecting 0.35 L/min of air into 2 L/min of water. The enhancement was significantly better when the air flowrate was 0.35 L/min with water flowrate of 2 L/min because the mixing between the water and air reached its perfect value comparing with the other air flowrates 0.15 and 0.25 L/min.
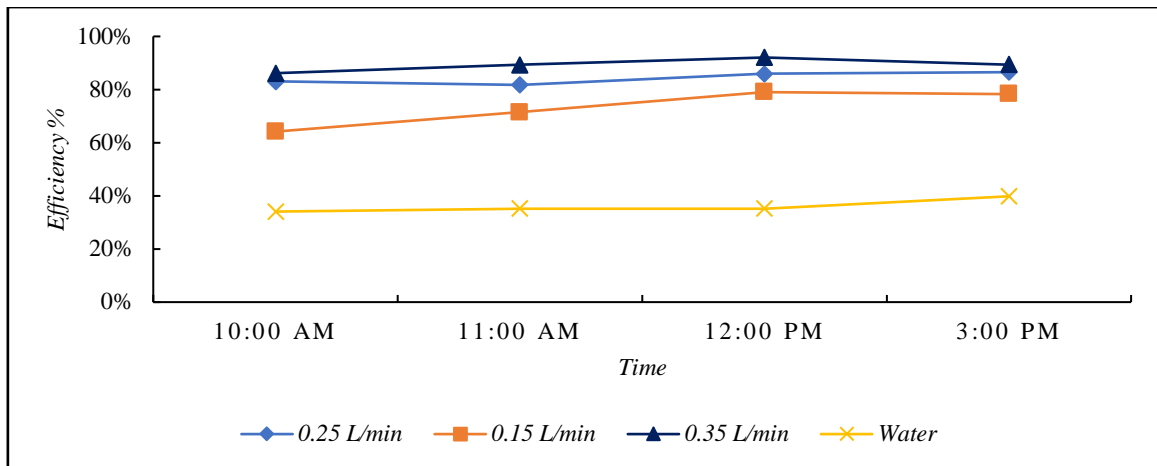
Figure 5-30: The System Efficiency for the Closed System with Air Injection flowrates of (0.15, 0.25 and 0.35 L/min) for 2 L/min Water Flowrate

5.5.2.3 Velocity Contour for Closed System

When the closed system operates at a water flowrate of 2 L/min mixed with an air flowrate of 0.35 L/min, Figure (5.31) illustrates the velocity contours for the time period of (10:00 AM to 03:00 PM). The heat transfer coefficients of the tube surfaces in contact with the air-water mixture are improved by the air flow because it increases turbulence in the flow. The flow vortex that was mixing the flow appeared in sections (A and B) taken from the air contour at the elbows.
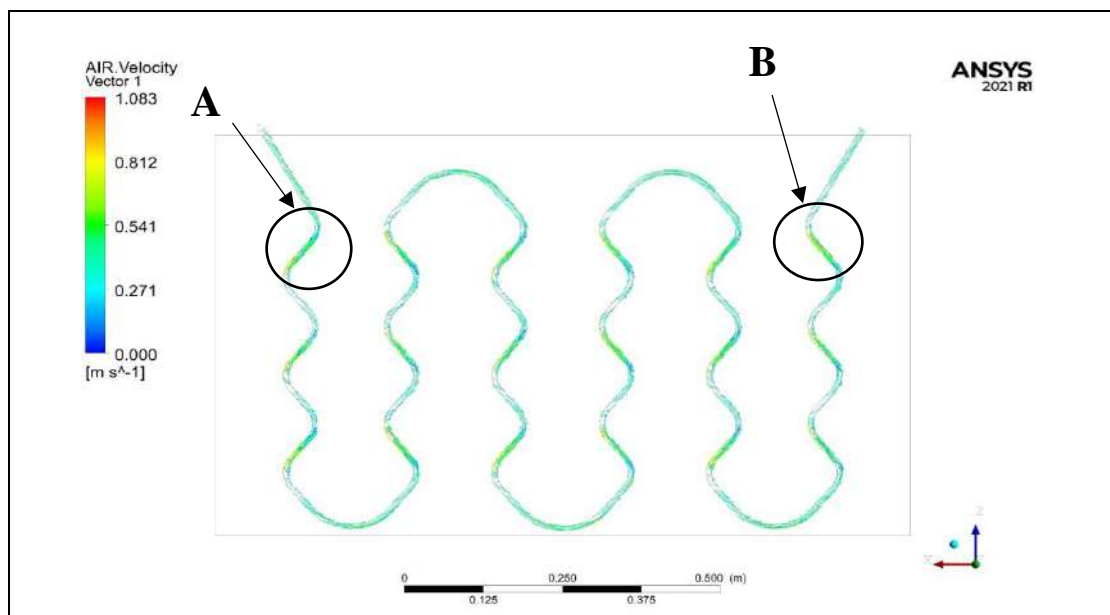
Figure 5-31: Velocity Distribution Contours for the Time from 10:00 Am to 03:00

Pm for Closed System with 2 L/min Water Flowrate with 0.35 L/min Air Injection.

Section A   *Section B*
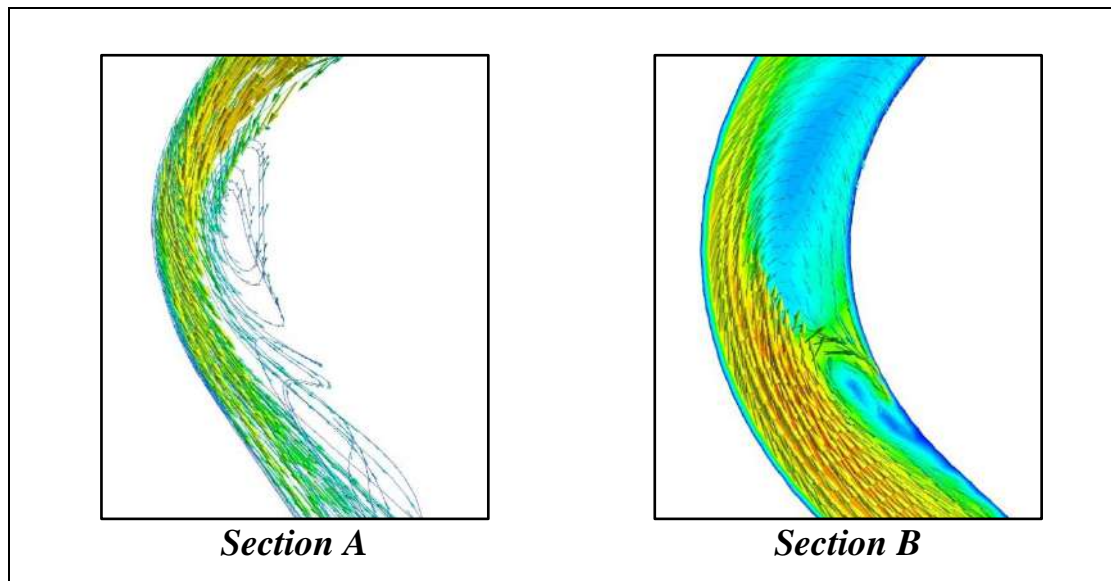
Figure 5-31: Contd.

5.5.2.4 Volume Fraction for Closed System

Each phase occupies space measured in volume fractions, and each phase independently satisfies the principles of conservation of mass and momentum. The ratio of the volume of one phase divided by the overall volume of the mixture flowing through the cross-section per unit of time is known as the volume fraction. The volume fraction for the air/water mixture is presented in the figure below (5.32).

Water volume fraction
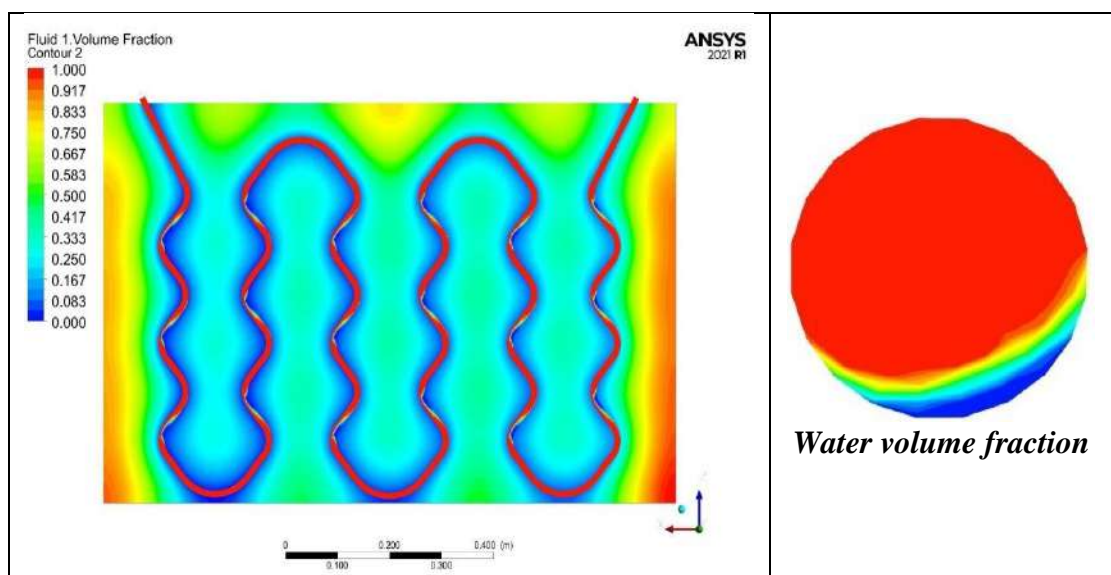
Figure 5-32: Volume Fraction Contours for the Time from 10:00 Am to 03:00 Pm for Closed System with 2 L/min Water Flowrate with 0.35 L/min Air Injection.

5.6 Part II: Experimental Results

The experimental work done in the Karbala city on multi parts, which first divided to two working systems (opened and closed). These systems were tested in four period time each 30 minutes from (10 Am to 3 Pm) with only water as working fluid. After that, the efficiency was calculated to obtain the most efficient case to inject air bubble to it.

5.7 Experimental Results for Opened System Without Air Bubble Injection

The experiments were carried out in four different water flowrates for the opened system to determine the performance of the flat plate solar collector with only water as a working fluid without air injection. With the fluid's entering temperature, incoming solar radiation, and air temperature all known, the exit temperature was determined. this section explores the temperature differential between the inlet and outlet of the water, system pressure drops and the system efficiency, as well as knowing which flowrate is best for the system.

5.7.1 Outlet Temperature for Experimental Opened System

Figure (5.33 a) shows the system's inlet water temperature (T_{in}) to the water outlet temperature (T_{out}) during working hours (10 am to 3 pm) and demonstrates that the maximum value of water outlet temperature when the water flowrate is 0.5 L/min was (32.4 ^{o}C). While figure (5.33 b) compares the water outlet temperature during working hours (10 am to 3 pm) with the system's input water temperature and demonstrates that the maximum amount of outflow temperature was (30.1 ^{o}C) is occurs when the water flowrate was 1 L/min. But the figure (5.33 c) shows the effect of the water flowrate 1.5 L/min on the inlet and outlet temperature during working hours (10 am - 3 pm) and shows the highest amount of outlet temperature is (28.5 ^{o}C). Finally, the effect of the water flowrate 2 L/min

on the inlet and outlet temperature during working hours (10 am - 3 pm) was illustrated in figure (5.33 d), which shows the highest value of water outlet temperature is (28.4 °C). Figure (5.34) show the plate temperature for all flowrates of (0.5, 1, 1.5 and 2) L/min, which illustrate that the average plate temperature was (47.25, 42.08, 39.06 and 37.65) °C respectively. These results shows that the decrees in the amount of discharge with remaining the cross-sectional area of the pipe is constant leads to a decrease in the water flow velocity, and therefore the low velocity of the water leads to an increase in the heat transfer gained from the absorber plate to the pipe then to the fluid, which leads to a rise in the temperature difference between the outlet and inlet water temperature.
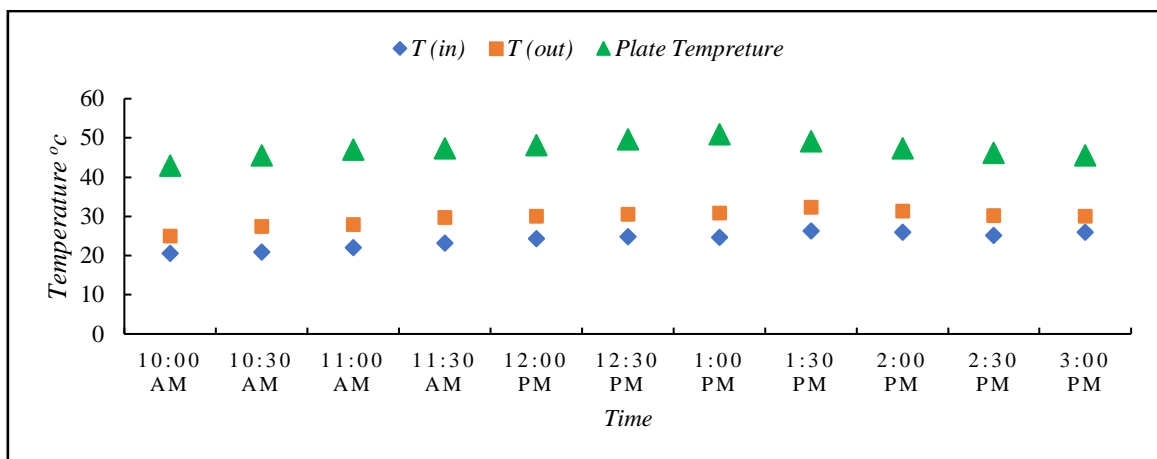
(a)0.5 L/min
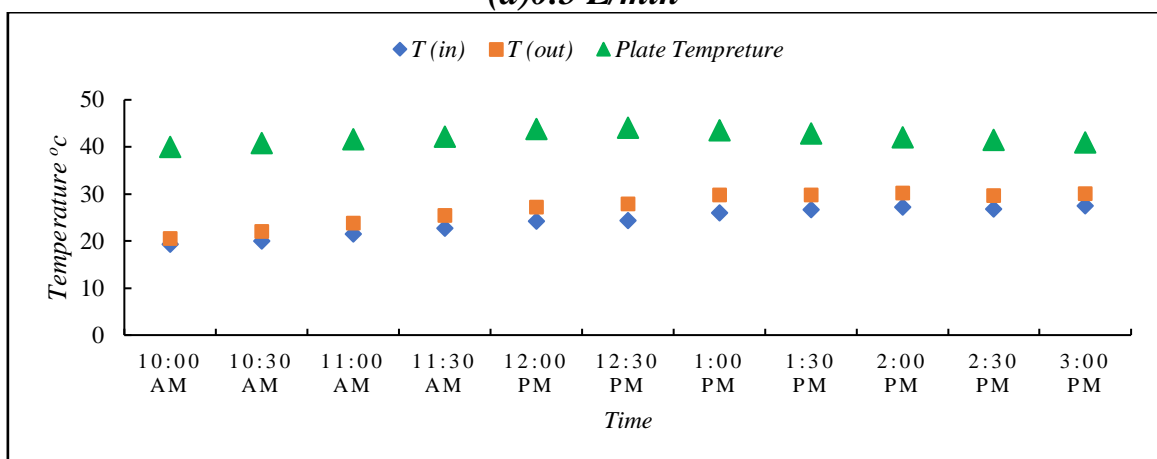
(b) 1 L/min

Figure 5-33 (a, b, c and d): Water Outlet Temperature (°C) for Opened System Without
Air Injection with Time at Different Water Flowrates of (0.5, 1, 1.5 and 2) L/min
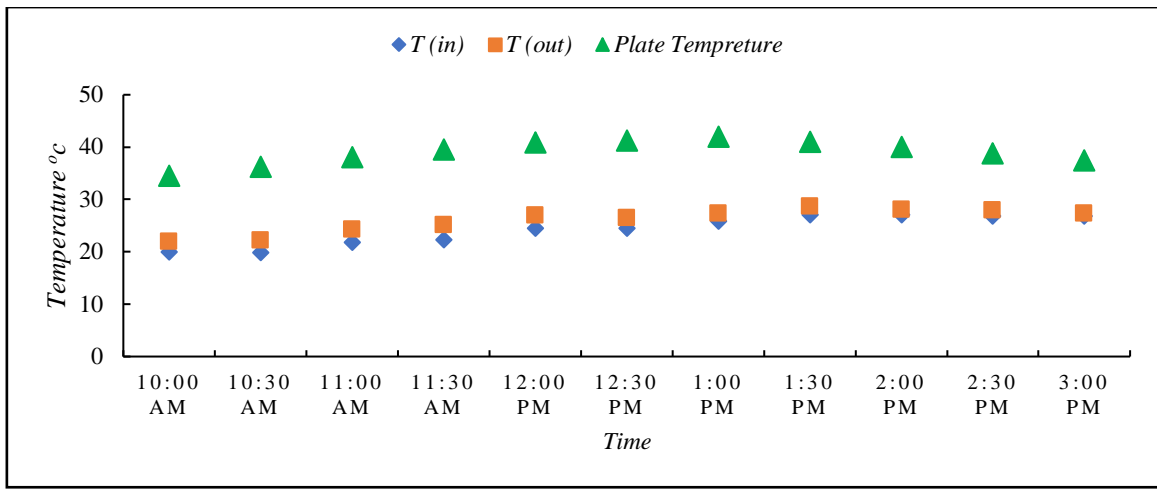
(c) 1.5 L/min
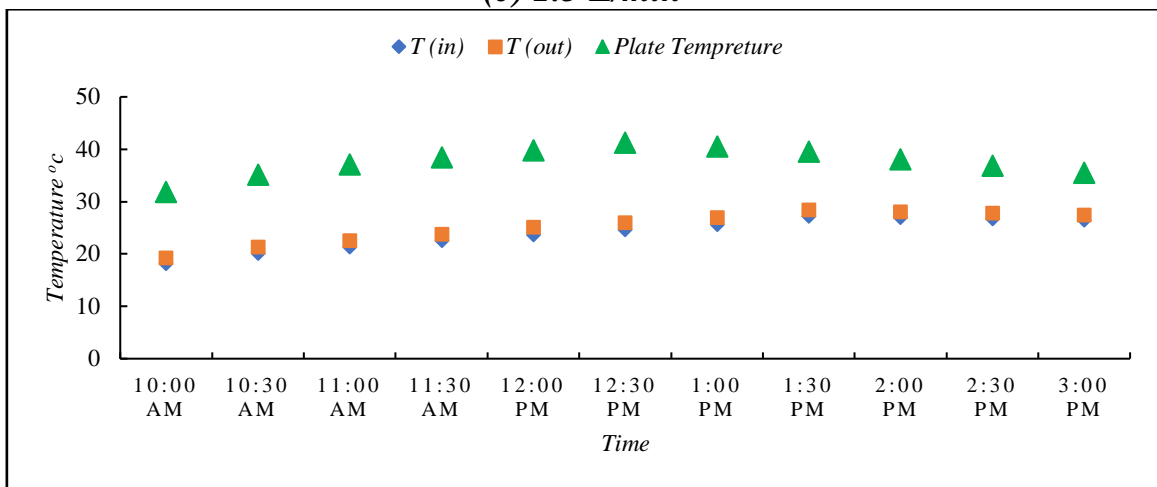
(d) 2 L/min

Figure 5-33: Contd.
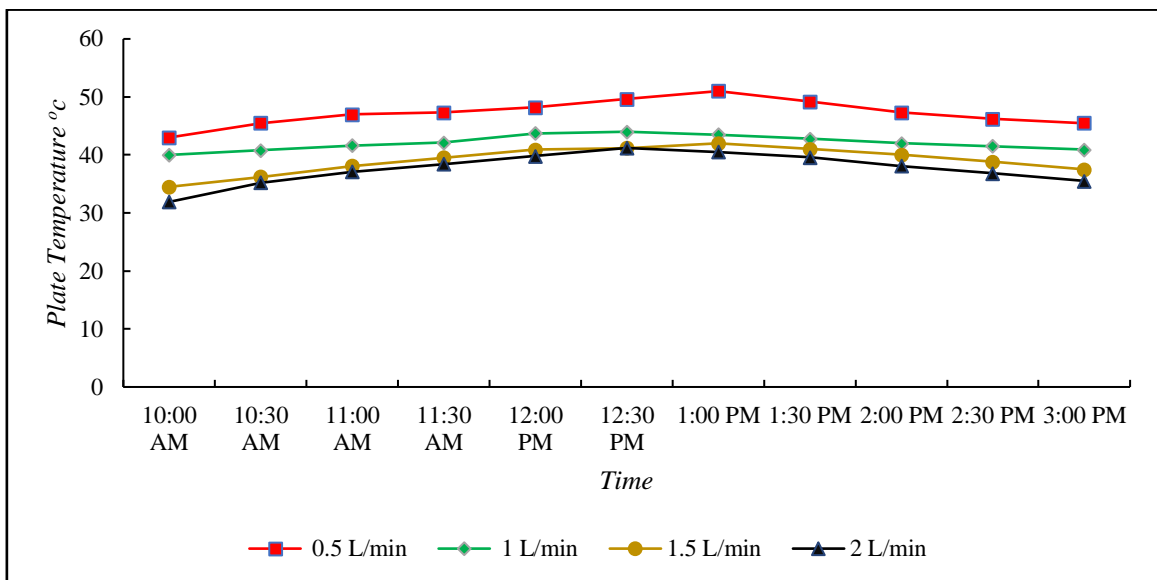
Figure 5-34: Plate Temperature (^oC) for Opened System Without Air Injection with Time

at Different Water Flowrates of (0.5, 1, 1.5 and 2) L/min

Figure (5.35) show the temperature difference with time (10 am - 3pm) for different flowrate of water (0.5,1,1.5, 2) l/min, which it shows that the largest temperature difference was (6.6 oC) at (0.5 L/min) at average solar intensity of (980) W/m2, while the temperature difference for (1, 1.5 and 2) L/min water flowrates were (3.9, 2.8 and 1.4) oC.
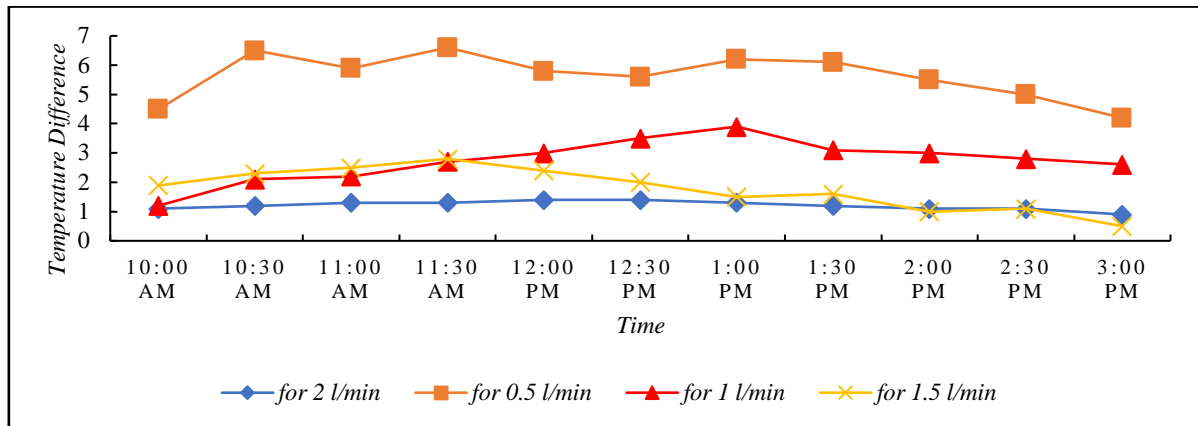
Figure 5-35: The Temperature Difference (^{o}C) *for all Cases of Opened System Without Air Injection with Time at Different Water Flowrate (0.5, 1, 1.5 and 2) L/min*

5.7.2 Pressure Drops for Opened System

The pressure drop was taken at different flow rates and the following was noted that in the figure (5.36). It shows the pressure drop for the different flowrate of water (0.5,1,1.5, 2) L/min which is almost constant for each flowrate at working hours (10 am - 3 pm) and shows the amounts of pressure drops is (5.3, 5.7, 6.13 and 6.65) kpa respectively.
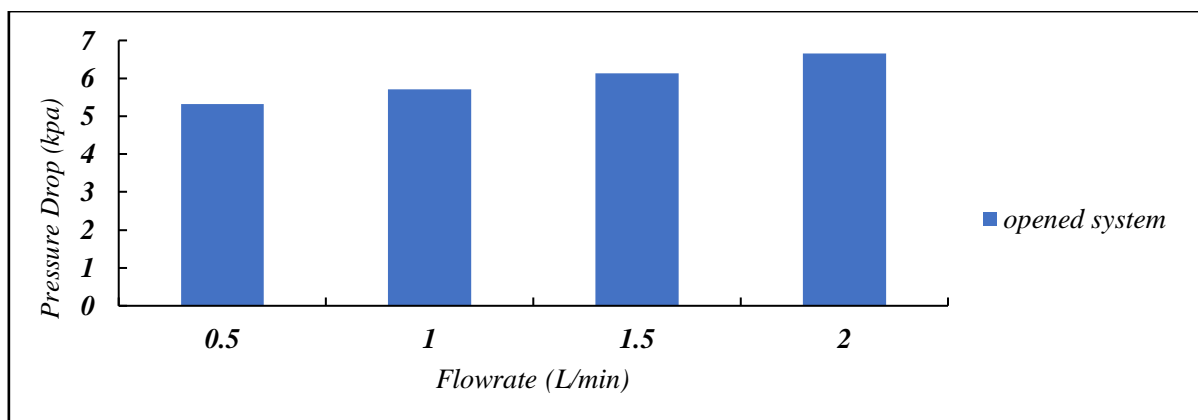
Figure 5-36: The Pressure Drop of all Cases for Opened System Without Air Injection with Different Water Flowrates of (0.5, 1, 1.5 and 2) L/min

5.7.3 Opened System Efficiency

Figure (5.37) shows the efficiencies of the opened system without air injection with different water flowrate (0.5, 1, 1.5 and 2 L/min) during working hours (10 AM- 3PM), which can be observe the average efficiencies is (27.5%, 31.8%, 27.8% and 20.6%) respectively. It was clear that the maximum efficiency will occur with the water flowrate of 1 L/min). Efficiency was calculated for each flow rate to figure out the best case for injecting the air bubble. When the useful energy was calculated and applied to the efficiency equation (3-19) using equation (3-15), it was discovered that the useful energy reached its maximum value when the water flowrate for the opened system was 1 L/min compared to the other flowrates. These results led to the conclusion that the most efficient flow rate for the opened system was 1 L/min.
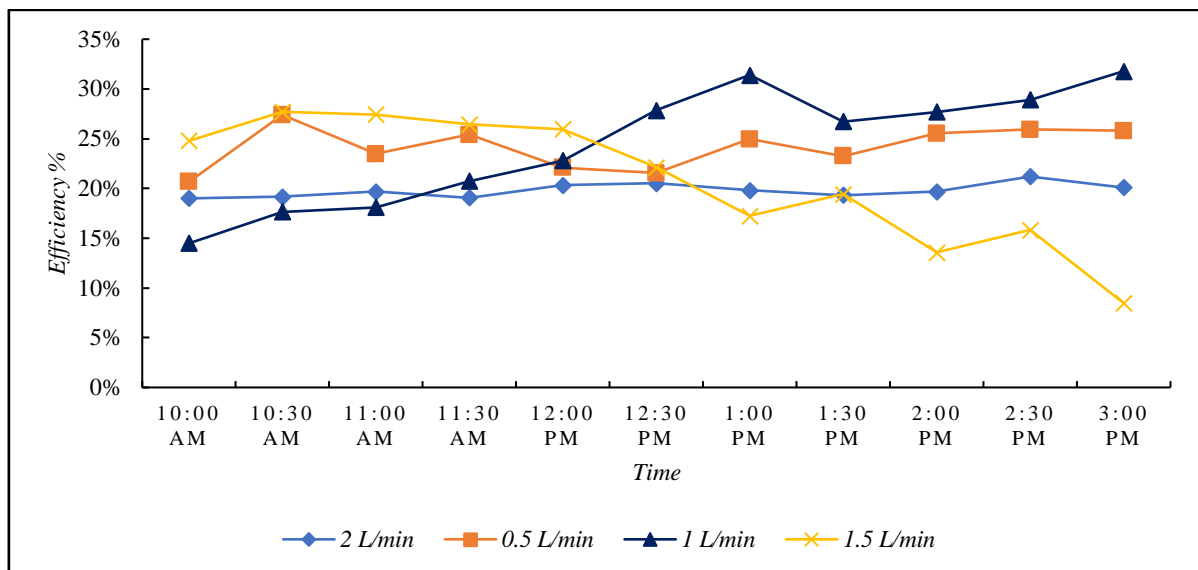
Figure 5-37: The System Efficiency of all Cases for Opened System Without Air Injection with Different Water Flowrates of (0.5, 1, 1.5 and 2) L/min

5.8 Experimental Results for Closed System Without Air Bubble Injection

To find out the performance of the flat plate solar collector using only water as the working fluid, experiments were done in four different water flowrates for the closed system. The outlet temperature (T_{out}) was

measured by taking into account the fluid's inlet temperature (T_{in}), incoming solar radiation, and ambient air temperature. In addition to determining the most efficient water flowrate for the closed system, this part also looks at the temperature difference between the water's inlet and outlet, system pressure drops, and system efficiency.

5.8.1 Outlet Temperature for Experimental Closed System

Figure (5.38 a) shows the effect of the flow (0.5 L/min) on the outlet temperature (T_{out}) during working hours (10 am - 3 pm) compering with the inlet water temperature (T_{in}) and shows the highest amount of outlet temperature is (51.1 ^{o}C). But the figure (5.38 b) shows the effect of the water flowrate (1 L/min) on the inlet and outlet temperature during working hours (10 am - 3 pm) and shows the highest amount of outlet temperature is (35.5 ^{o}C). The figure (5.38 c) illustrates the effect of the flow (1.5 L/min) on the temperature difference during working hours (10 am - 3 pm) and shows the highest amount of outlet temperature is (45.8 ^{o}C). For the water flowrate (2 L/min), the figure (5.38 d) shows the outlet temperature for the system with inlet water temperature during working hours (10 am - 3 pm) and shows the highest amount of outlet temperature is (44.3 ^{o}C). Figure (5.39) show the plate temperature for all flowrates of (0.5, 1, 1.5 and 2) L/min, which illustrate that the average plate temperature was (61.14, 47.74, 52.35 and 54.55) ^{o}C respectively.
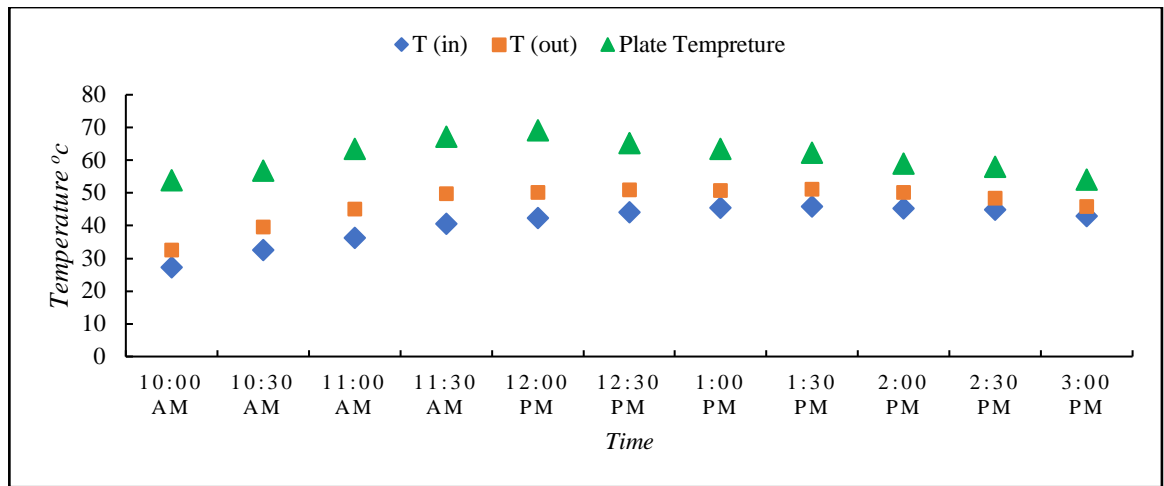
(a) 0.5 L/min
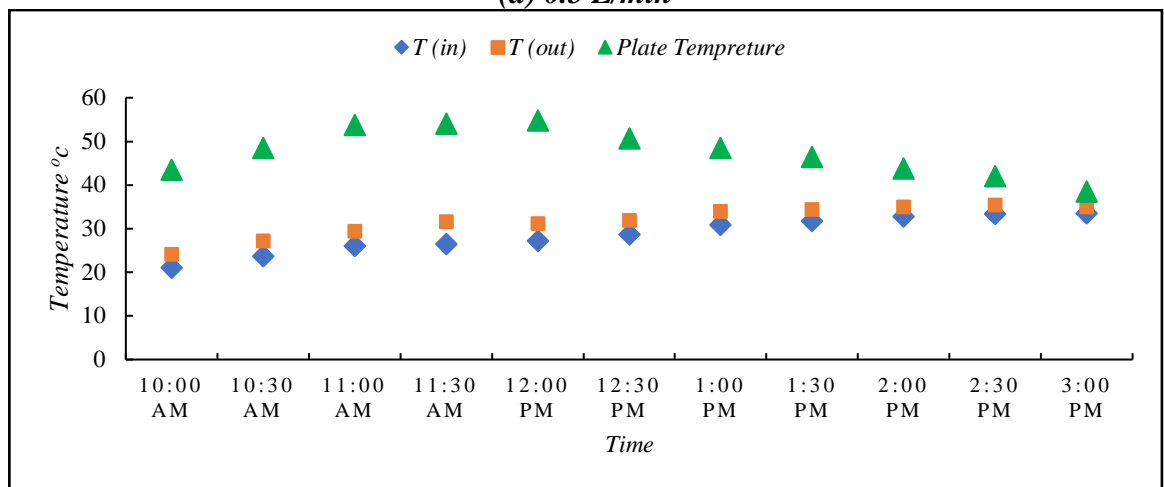
(b) 1 L/min
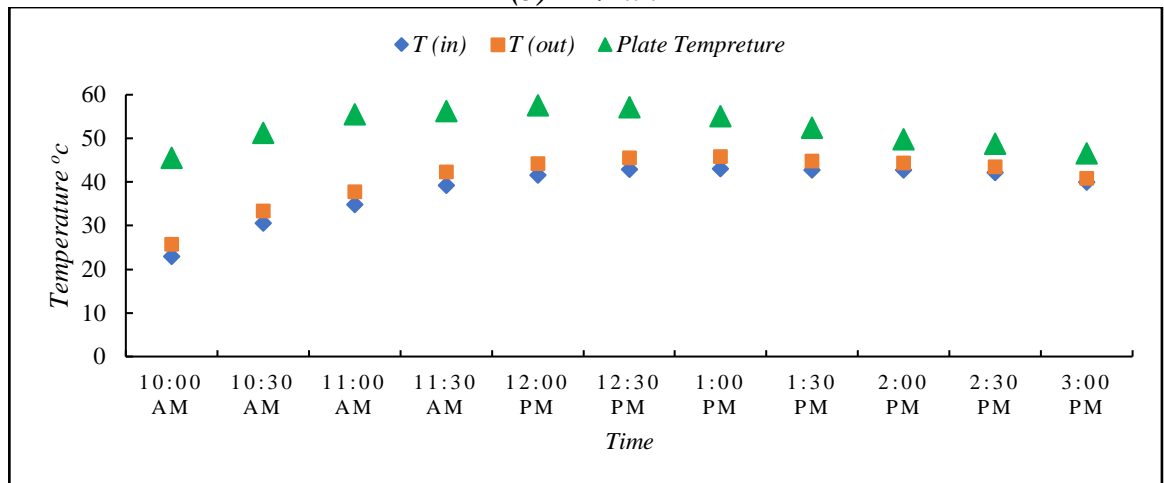
(c) 1.5 L/min

Figure 5-38 (a, b, c and d): Water Outlet Temperature (ᵒC)for Closed System Without Air

Injection with Time at Different Water Flowrates of (0.5, 1, 1.5 and 2) L/min
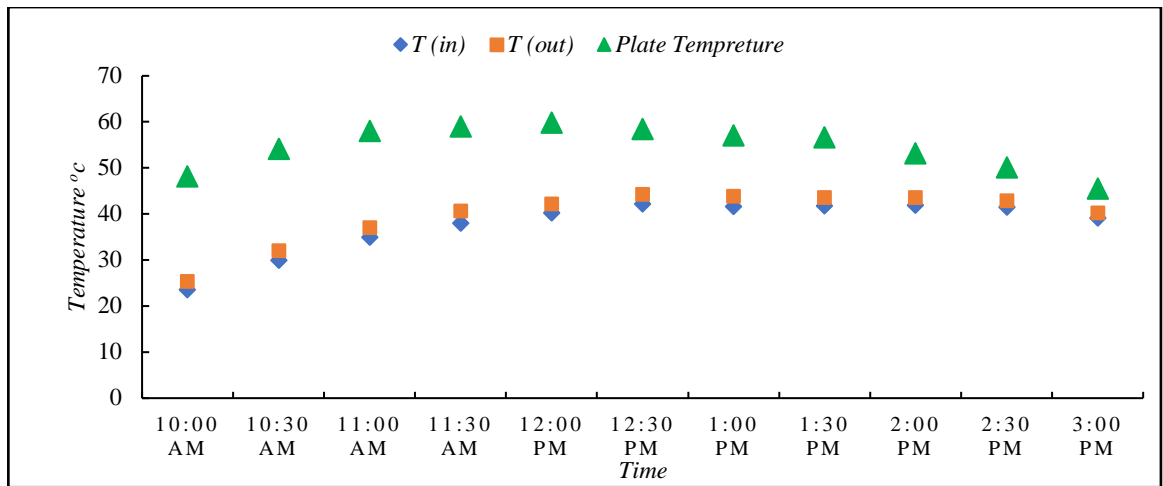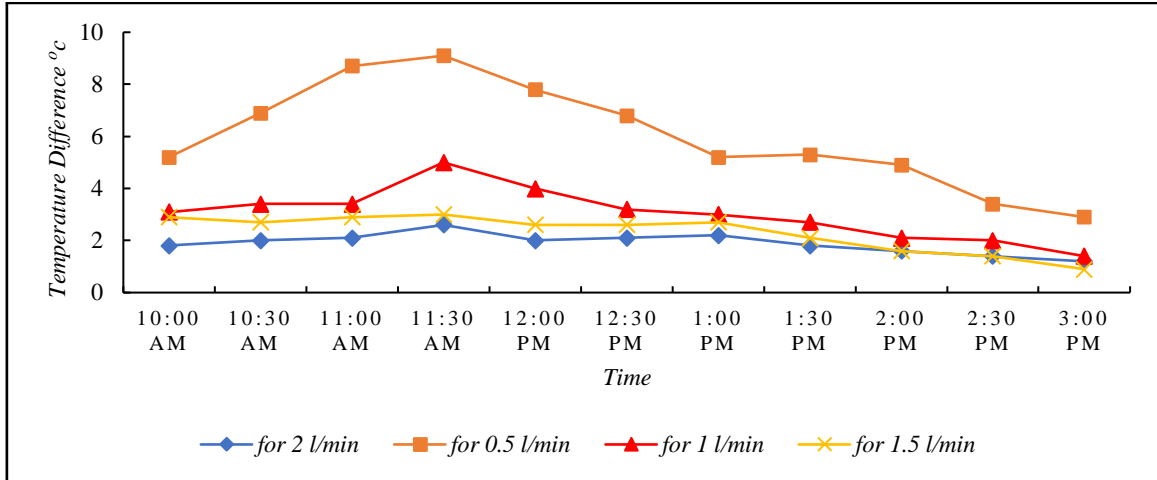
(d) 2 L/min

Figure 5-38: Contd.
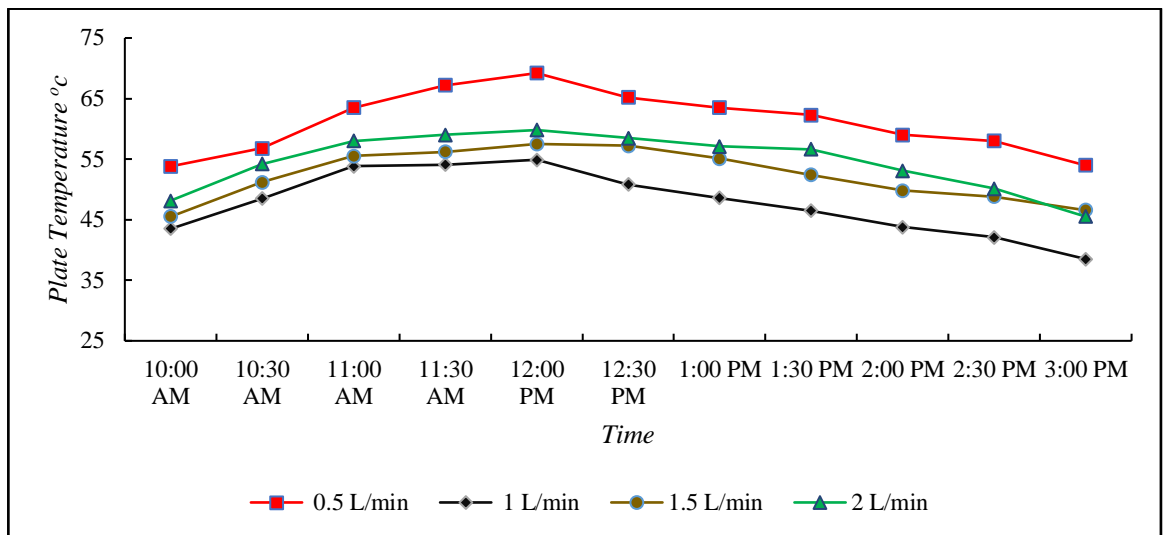
Figure 5-39: Plate Temperature (ᵒC)for Closed System Without Air Injection with Time at Different Water Flowrates of (0.5, 1, 1.5 and 2) L/min

Figure (5.40) show the different flowrate of water (0.5,1,1.5, 2) L/min with the temperature difference at time (10 am - 3pm), which it shows that the largest temperature difference was (9.1 ^{o}C) at (0.5 L/min), while the temperature difference for (1, 1.5 and 2) L/min water flowrates were (3.9, 2.8 and 1.4) ^{o}C at average solar intensity of (1180) W/m^2. These results demonstrated that changes in discharge volume while maintaining a constant pipe cross-sectional area result in a decrease in water flow velocity. As a result, the low water flow velocity increases heat transfer

from the absorber plate to the pipe and then to the fluid, which raises the temperature difference between the outlet and inlet water temperatures.

Figure 5-40: The Temperature Difference (^oC) *for all Cases of Closed System Without Air Injection with Time at Different Water Flowrates of (0.5, 1, 1.5 and 2) L/min*

5.8.2 Pressure Drops for Closed System

The pressure drop was taken at different flow rates and the following was noted that in the figure (5.41). It shows the pressure drop for the different flowrate of water (0.5,1,1.5, 2) L/min which is almost constant at working hours (10 am - 3 pm) for each flowrate and shows the amounts of pressure drops is (5.42, 5.8, 6.12 and 6.78) kpa respectively.
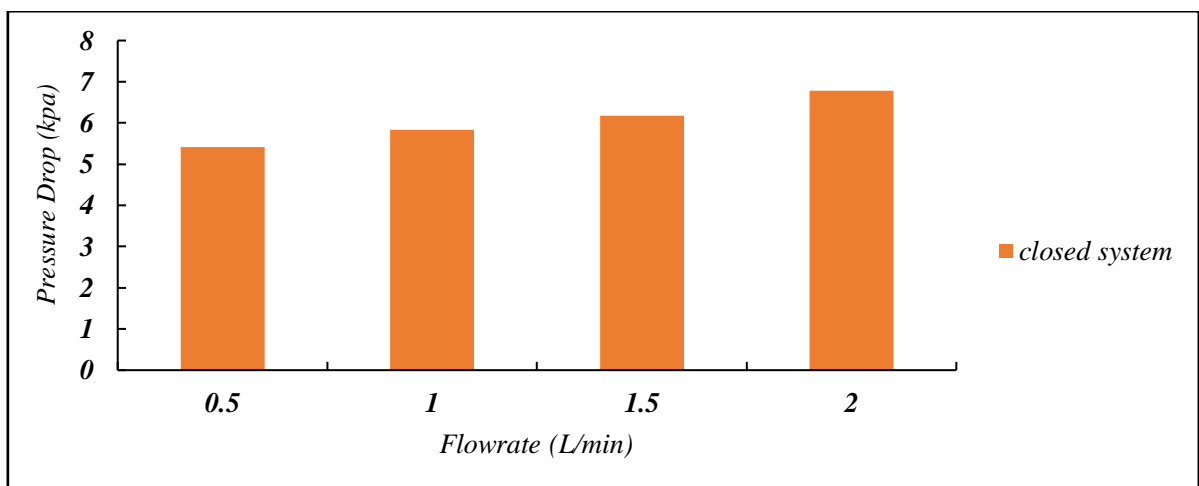
Figure 5-41: The Pressure Drop of all Cases for Closed System Without Air Injection with Different Water Flowrates of (0.5, 1, 1.5 and 2) L/min

5.8.3 Closed System Efficiency

As can be shown in figure (5.42), the average efficiencies are (32.5%, 27.5%, 30.6% and 45.5%) for the closed system without air injection with varying water flowrates of (0.5, 1, 1.5, and 2 L/min) respectively during working hours (10 AM- 3 PM). It was obvious that a water flow rate of 2 L/min would result in the highest efficiency.
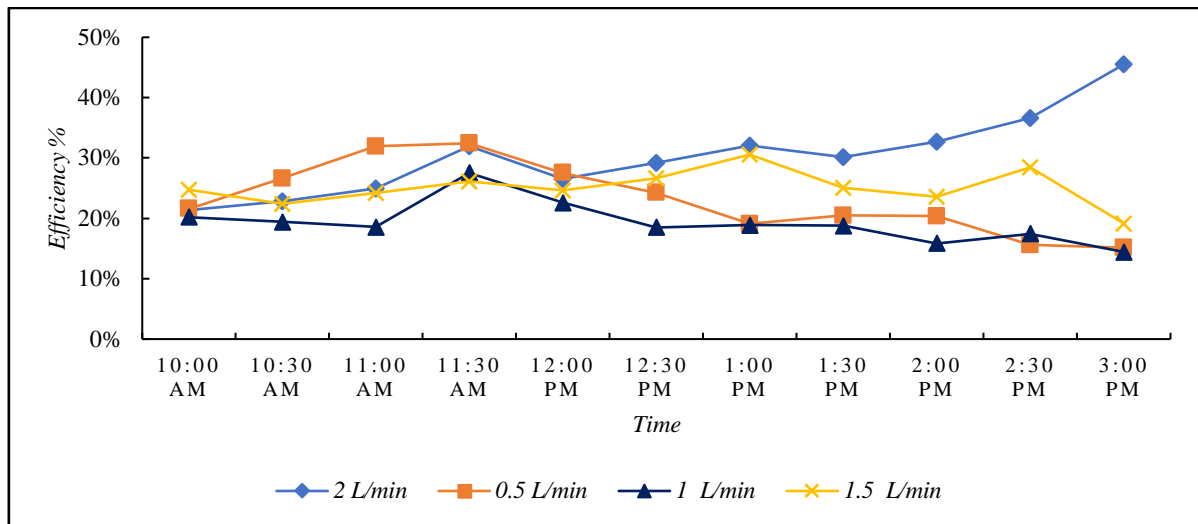
Figure 5-42: The System Efficiency of all Cases for Closed System Without Air Injection with Different Water Flowrate (0.5, 1, 1.5 and 2) L/min

5.9 Experimental Results for Opened and Closed System with Air Bubble Injection

Air bubbles are created inside the test section (wavy pipe) of an inclined flat plate collector by using the Venturi tube. The heat transfer mechanism is improved by the injection of air bubbles in the pipe. After calculating the efficiency for both systems, it shows at the time period every 30 minutes of (10 AM to 3 PM), that the most efficient cases for opened system was when the water flowrate was 1 L/min and when the water flowrate was 2 L/min for closed system with water only as shown in previous figures (5.36 and 5.40). So, air bubble was injected to the both systems at air flowrates of (0.15, 0.25 and 0.35) L/min for opened and closed system according to the analysis results.

5.9.1 Experimental Results for Opened System with Air Bubble Injection
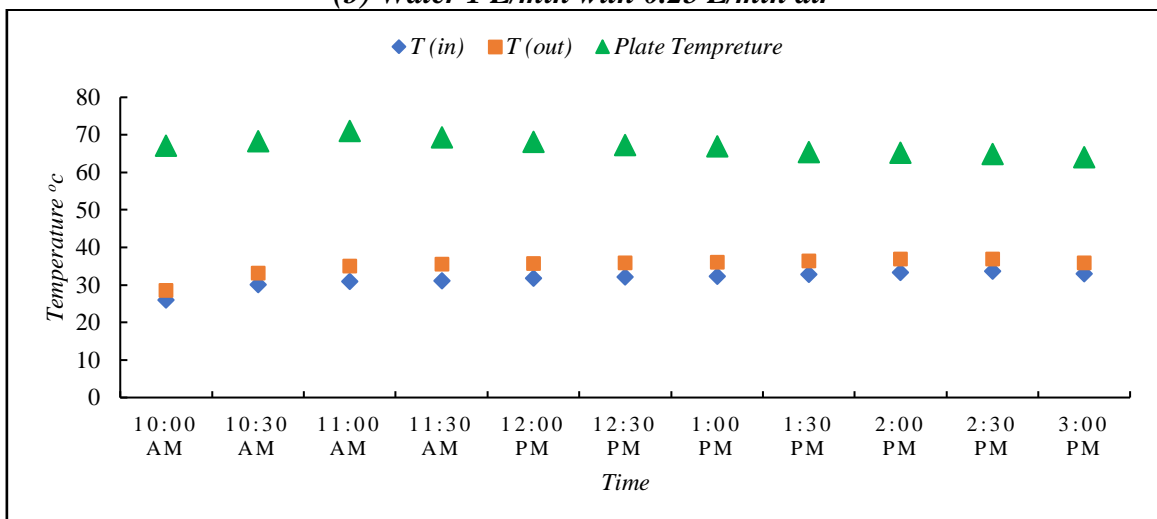
5.9.1.1 Outlet Temperature for Opened System

The influence of water flowrate of (1 L/min) and air flowrate (0.15 L/min) on the water outlet temperature (T_{out}) comparing with the water inlet temperature (T_{in}) during working hours (10 am to 3 pm) is shown in figure (5.43 a), with the largest value of water outlet temperature being (42.2 °C). The figure (5.43 b) shows the effect of the water flowrate of (1 L/min) with air flowrate (0.25 L/min) on the performance of heat exchanger that effect on the water outlet temperature during working hours (10 am - 3 pm) and shows the highest value of outlet temperature is (37.7 °C). Figure (5.43 c) illustrates how the water outlet temperature (T_{out}) compared to the water intake temperature (T_{in}) during working hours (10 am to 3 pm) was affected by the water flowrate of (1 liter per minute) and the air flowrate of (0.35 L/min) and shows the highest value of outlet temperature is (36.8 °C). Figure (5.44) show the plate temperature for all air flowrates of (0.15, 0.25 and 0.35) L/min with 1 L/min water flowrate, which illustrate that the average plate temperature was (71.03, 75.71 and 66.97) °C respectively.
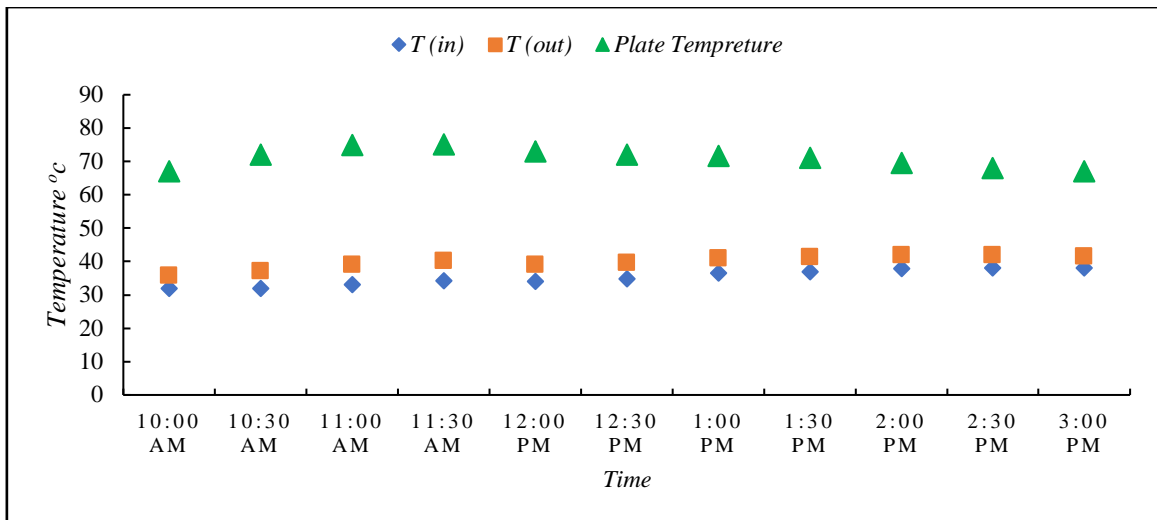
(a)Water 1 L/min with 0.15 L/min air
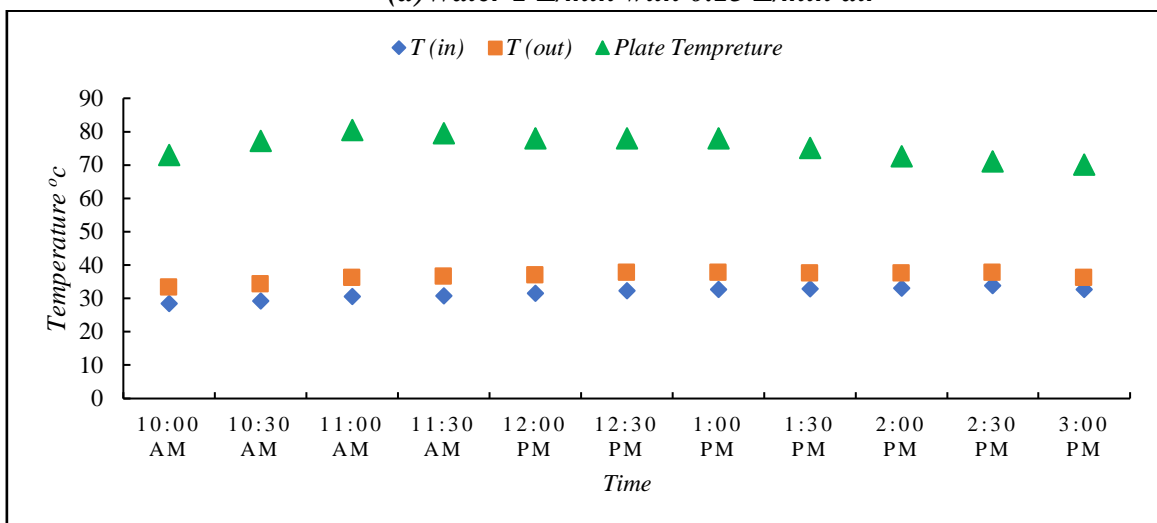
(b) Water 1 L/min with 0.25 L/min air

(c) Water 1 L/min with 0.35 L/min air

Figure 5-43 (a, b and c): Water Outlet Temperature (^{o}C)for Opened System with Air Injection and Time at Different Air Flowrate of (0.15, 0.25 and 0.35 L/min) with (1) L/min Water Flowrate
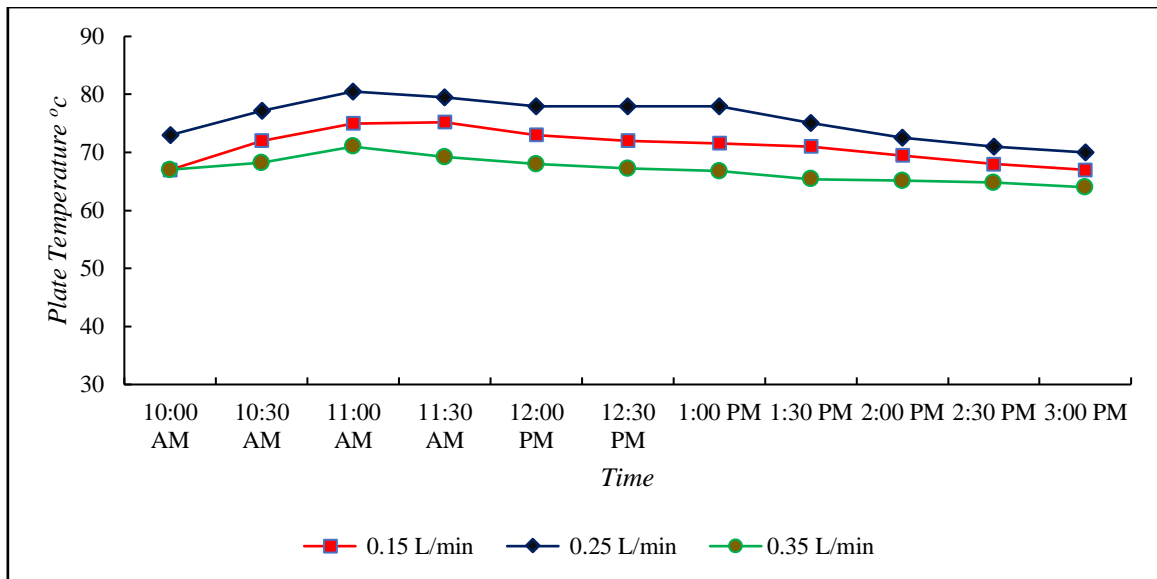
Figure 5-44: Plate Temperature (°C)for Opened System with Air Injection and Time at Different Air Flowrate of (0.15, 0.25 and 0.35 L/min) with (1) L/min Water Flowrate

Figure (5.45) show the different air flowrate (0.15,0.25 and 0.35) L/min for 1 L/min water flowrate with the temperature difference at time (10 am - 3pm), which it shows an enhancement for the temperature difference with respect to the water only at 1 L/min without air injection. The enhancement for temperature difference was (40.98%), (43.10%) and (22.62%) at (0.15,0.25 and 0.35L/min) respectively at average solar intensity of (1100) w/m². This enhancement due to the air bubble influence on the heat transfer process, the air bubbles create more turbulence in the flow, which enhances the performance of heat transfer from the inner surfaces of the tubes that come into contact with the air-water mixture.
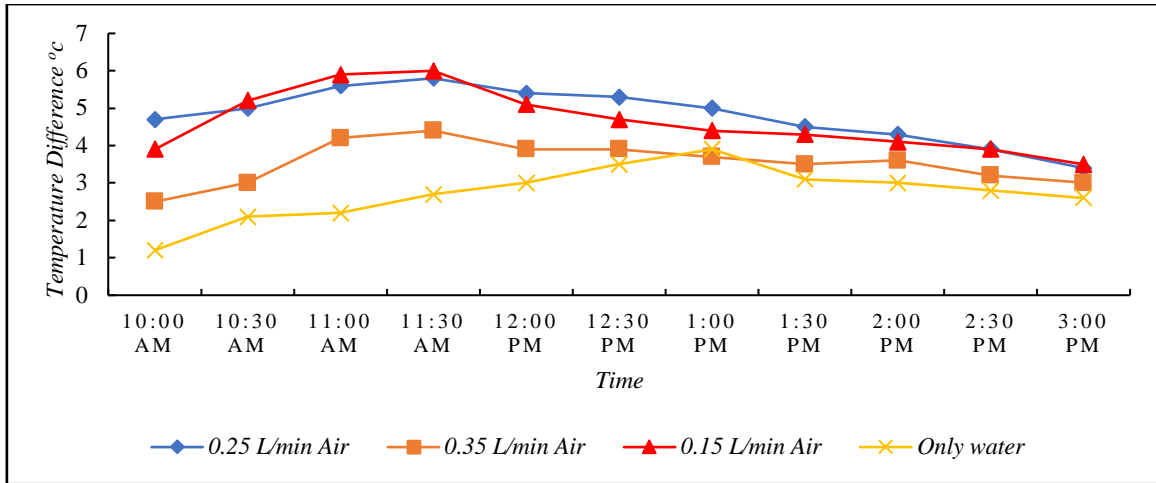
Figure 5-45: The Temperature Difference (^{o}C) *for all Cases in Opened System with Air Injection of (0.15, 0.25 and 0.35 L/min) for 1 L/min Water Flowrate*

5.9.1.2   Pressure Drops for Opened System

The pressure drop was taken at different flow rates and the following was noted that in the figure (5.46). It shows the pressure drop for the different air flowrate (0.15,0.25,0.35) L/min with the pressure drop for 1 L/min water only. The pressure drops with air injection become unstable and fluctuated at working hours (10 am - 3 pm) for each flowrate and shows the amounts of pressure drops is (6.4-11.9) kpa for 0.15 L/min air, (5.4-9.3) Kpa for 0.25 L/min air and (6.07-10.3) kpa for 0.35 L/min air respectively. When air is injected, the discharge value will increase, and thus the pressure drop will increase according to the Hagen-Paseuille equation. Because of the random movement of air bubbles, it leads to pressure disturbance and instability of the readings when air is injected into the system. The least difference in pressure was when injecting air with a discharge of 0.25 liters / minute, as shown in the figure below.
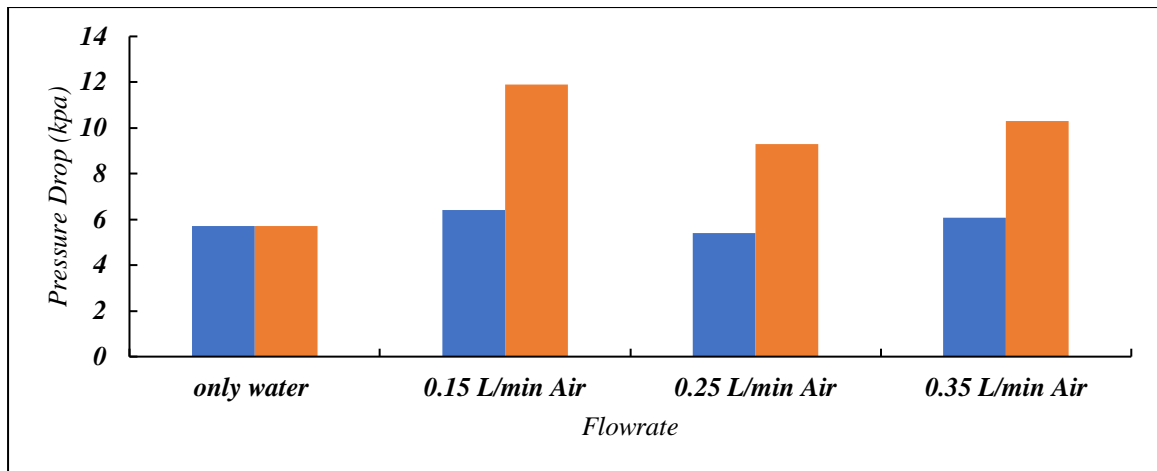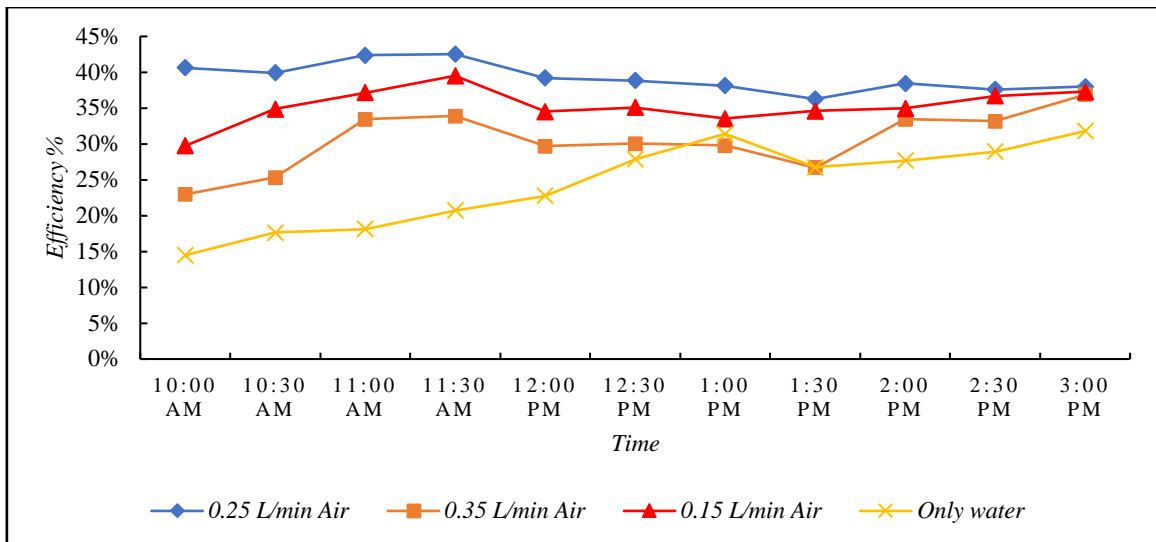
Figure 5-46: The Pressure Drop of all cases in (Opened System with Air Injection at 0.15, 0.25 and 0.35 L/min) for 1 L/min Water Flowrate

5.9.1.3 Opened System Efficiency with Air Bubble Injections

Figure (5.47) show the solar collector efficiencies for different air flowrate (0.15,0.25 and 0.35) L/min for 1 L/min water flowrate with time period of (10 am- 3pm). To figure out the optimum case, efficiency was calculated for each air flowrate (0.15, 0.25, and 0.35) L/min with a water flowrate of 1 L/min. When the useful energy was computed by using equation (3-15) and applied to the efficiency equation (3-19), it was observed that the useful energy reached its highest value when the water flowrate for the opening system was 1 L/min and the air flowrate was 0.25 L/min compared to the other flowrates. Which it shows an enhancement for the system efficiency with respect to the water only at 1 L/min without air injection. the enhancement for system efficiency was (30.89%), (37.92%) and (20.03%) at (0.15, 0.25 and 0.35 L/min) respectively.

Figure 5-47: The System Efficiency for all cases in Opened System with Air Injection of (0.15, 0.25 and 0.35 L/min) for 1 L/min Water Flowrate

5.9.2 Experimental Results for Closed System with Air Bubble Injection

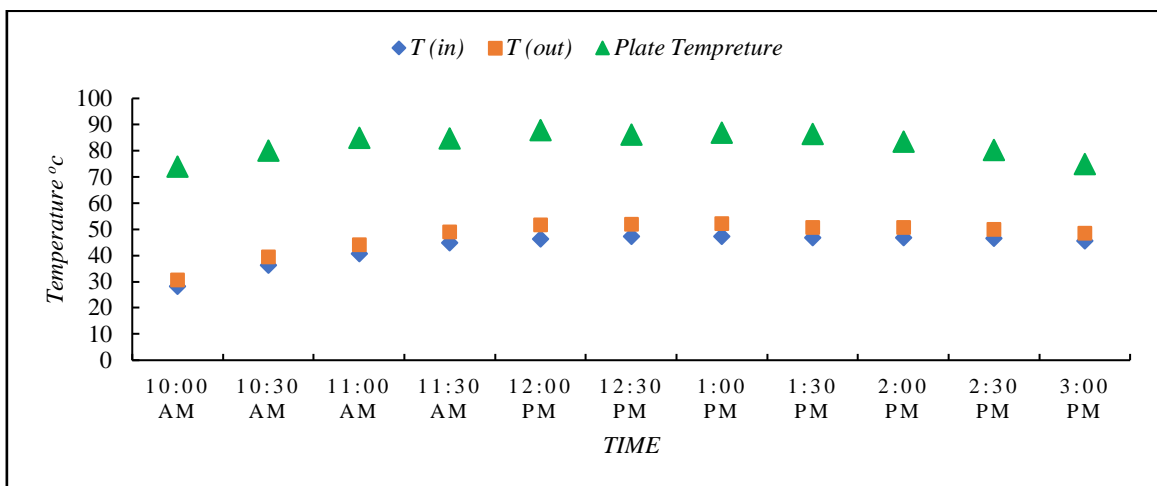### 5.9.2.1 Outlet Temperature for Closed System

The figure (5.48 a) shows the effect of the water flow (2 L/min) with air flowrate (0.15 L/min) on the performance of heat exchange during working hours (10 am - 3 pm) for the outlet water temperature (T_{out}) with the inlet water temperature (T_{in}) and shows the highest value of water outlet temperature is (53.2 °C). While the figure (5.48 b) shows the effect of the water flow (2 L/min) with air flowrate (0.25 L/min) on the outlet water temperature during working hours (10 am - 3 pm) and shows the highest amount of outlet temperature is (51.2 °C). Figure (5.48 c) illustrates how the water outlet temperature (T_{out}) compared to the water intake temperature (T_{in}) during working hours (10 am to 3 pm) was affected by the water flowrate of (2 L/min) and the air flowrate of (0.35 L/min) and shows the highest value of outlet temperature is (52.3 °C). Noted that the average plate temperature was (67.22, 73.15 and 82.80) °C for the above cases, which illustrate in figure (5.49).
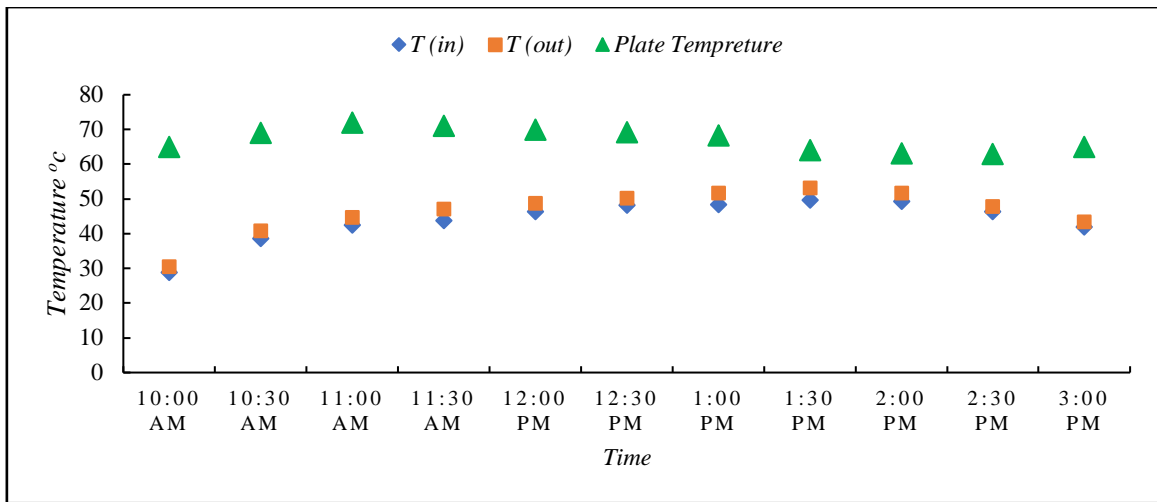
(a) Water 2 L/min with 0.15 L/min air
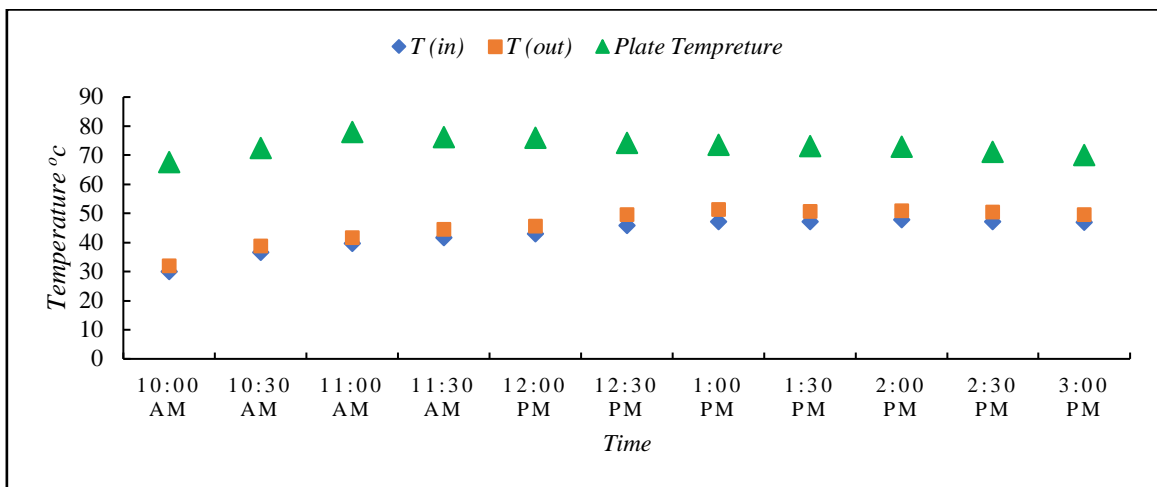
(b) Water 2 L/min with 0.25 L/min air

(c) Water 2 L/min with 0.35 L/min air

Figure 5-48: (a, b and c): Water Outlet Temperature (^{o}C) for Closed System with Air Injection and Time at Different Air Flowrate of (0.15, 0.25 and 0.35 L/min) with (2) L/min Water Flowrate
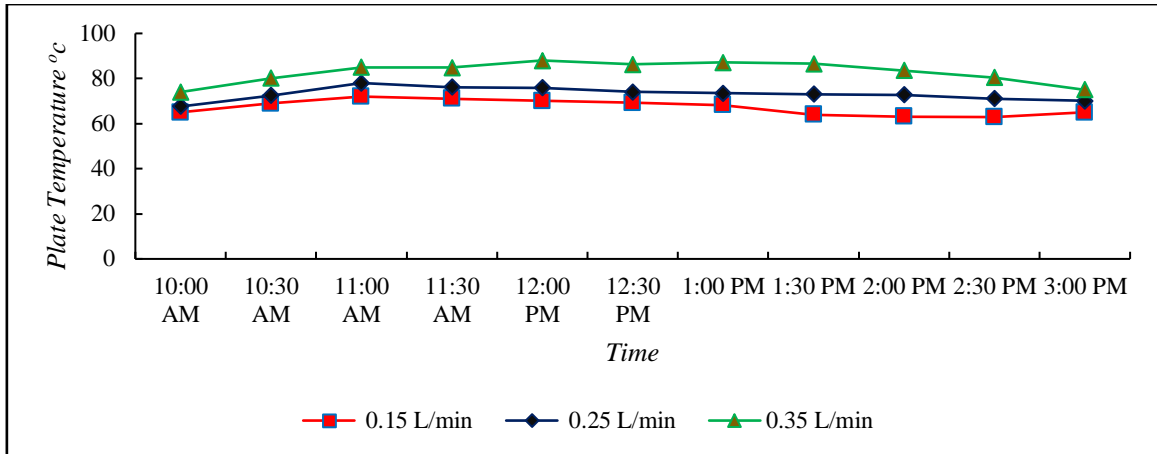
Figure 5-49: Plate Temperature (^{o}C)for Closed System with Air Injection and Time at Different Air Flowrate of (0.15, 0.25 and 0.35 L/min) with (2) L/min Water Flowrate

Figure (5.50) show the different air flowrate (0.15,0.25 and 0.35) L/min for 2 L/min water flowrate with the temperature difference at time (10 am - 3pm), which it shows an enhancement for the temperature difference with respect to the water only at 2 L/min without air injection. The enhancement for temperature difference was (20.00%), (35.20%) and (50.59%) at (0.15,0.25 and 0.35L/min) respectively, at average solar intensity of (1130) W/m^2. The air bubbles' influence on the heat transfer process results in increased flow turbulence, which improves heat transfer from the inner surfaces of tubes that come into contact with the air-water combination.
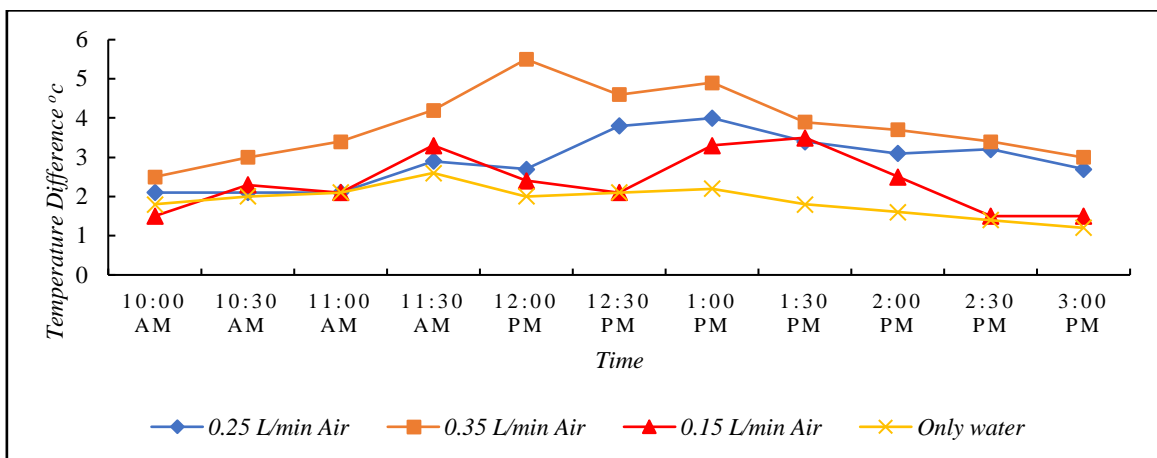
Figure 5-50: The Temperature Difference (^{o}C) for all cases in (Closed System with Air Injection at 0.15, 0.25 and 0.35 L/min) for 2 L/min Water Flowrate

5.9.2.2   Pressure Drops for Closed System

The pressure drop was taken at different flow rates and the following was noted that in the figure (5.51). It shows the pressure drop for the different air flowrate (0.15,0.25,0.35) L/min with the pressure drop for 2 L/min water only. The pressure drops with air injection become unstable and fluctuated at working hours (10 am - 3 pm) for each flowrate and shows the amounts of pressure drops is (6.8-10.2) kpa for 0.15 L/min air, (6.6-9.8) kpa for 0.25 L/min air and (6.5-9.1) kpa for 0.35 L/min air respectively.
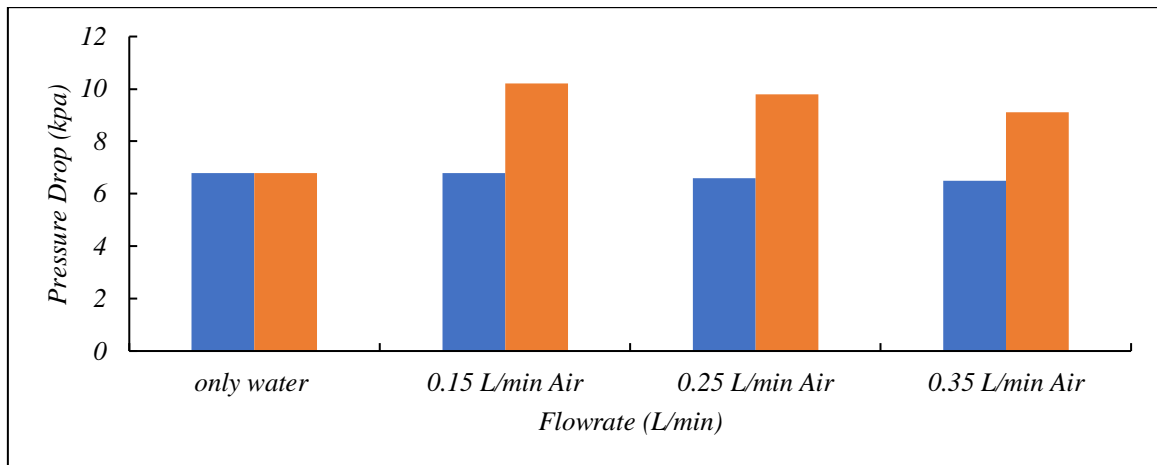
Figure 5.51: The Pressure Drop of all cases in (Closed System with Air Injection at 0.15, 0.25 and 0.35 L/min) with 2 L/min Water Flowrate

5.9.2.3   Closed System Efficiency with Air Bubble Injections

The solar collector efficiencies for various air flowrates (0.15, 0.25, and 0.35 L/min) for 2 L/min water flow rate with the time period (10 am - 3 pm) was illustrated in figure (5.52). Efficiency was computed for each air flowrate (0.15, 0.25, and 0.35 L/min) with a water flowrate of 2 L/min to determine the best case. When the useful energy was calculated using equation (3-15) and applied to the efficiency equation (3-19), it was discovered that when the water flowrate for the closed system was 1 L/min and the air flowrate was 0.35 L/min compared to the other flowrates, the useful energy was at its highest value. which demonstrates an improvement

for the system efficiency compared to the water only at 2 L/min without air injection. It was improved by (24.98%), (37.28%), and (53.71%) at (0.15, 0.25, and 0.35 L/min) respectively.
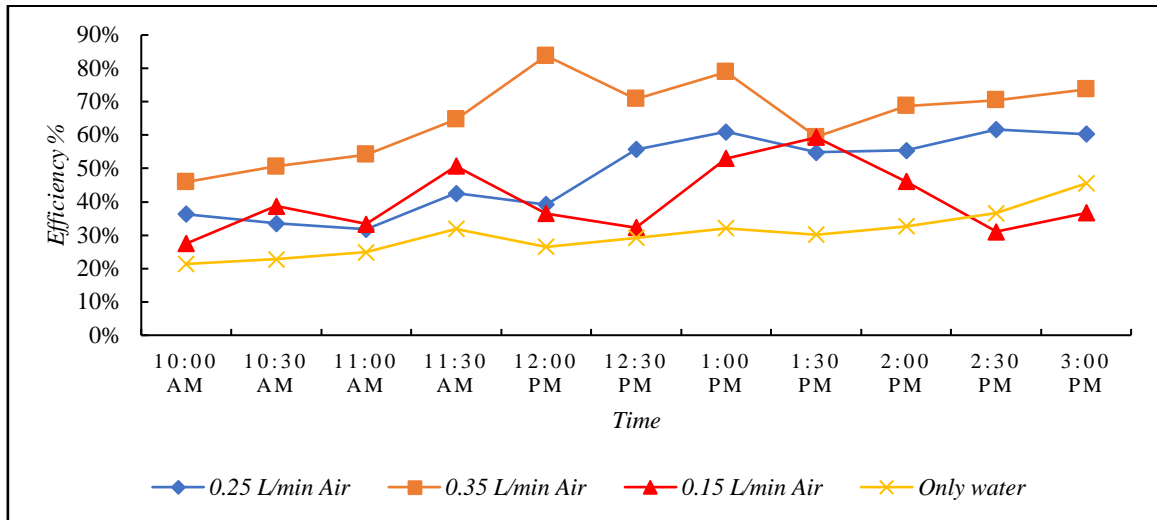

Figure 5-52: The System Efficiency for all cases in Closed System with Air Injection at air flowrate of (0.15, 0.25 and 0.35 L/min) with 2 L/min Water Flowrate
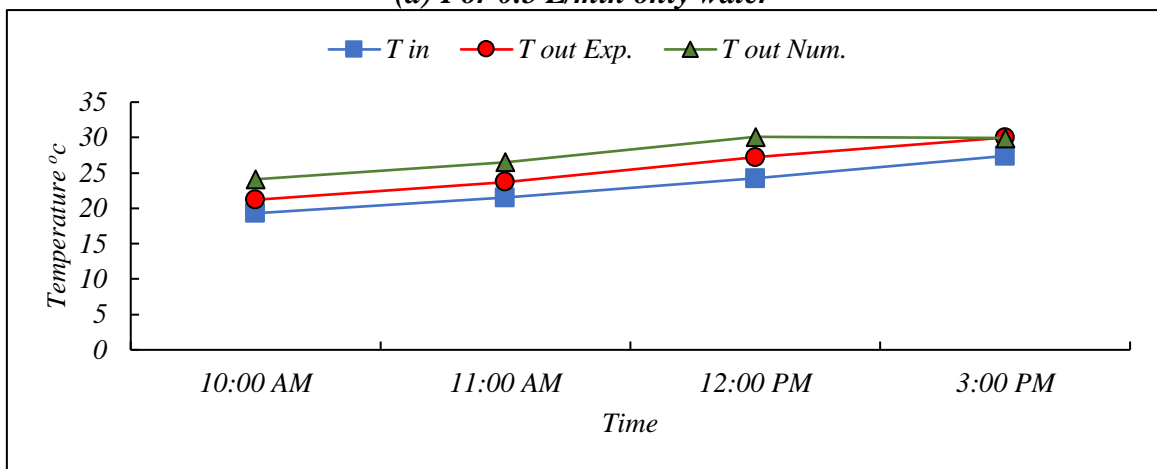
5.10 Comparison Between Experimental and Numerical Results
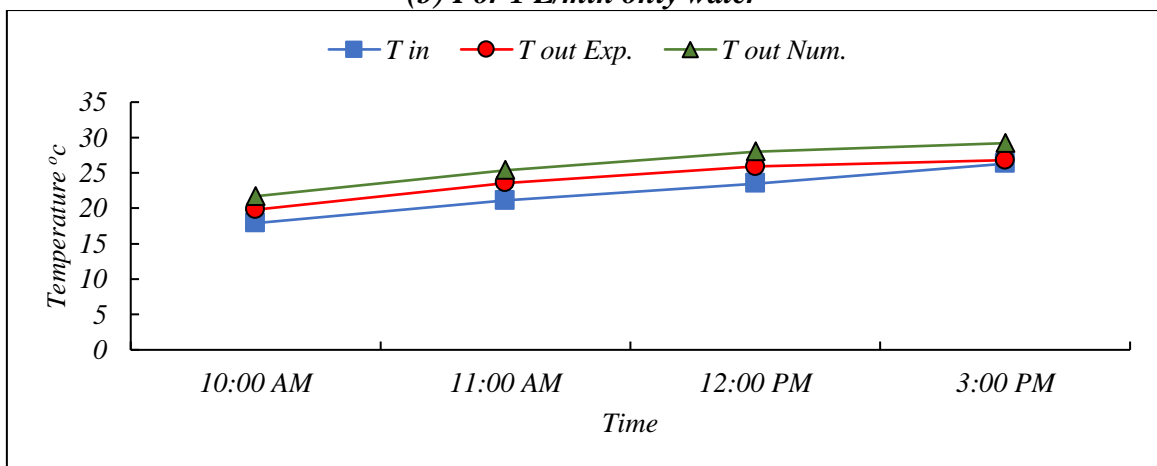
5.10.1 Opened System with and without Air Injection

The results from the experimental and numerical analyses for opened system without air injection were quite similar and did not differ from each other as shown in figure (5.53). The biggest variance rate of 13.5% to 5% occurs at a water flow rate of 0.5 L/min. At 1.5 and 2 L/min, the highest variance rate was 8%. While at 1 L/min, the highest disparity was 12% to 0%.
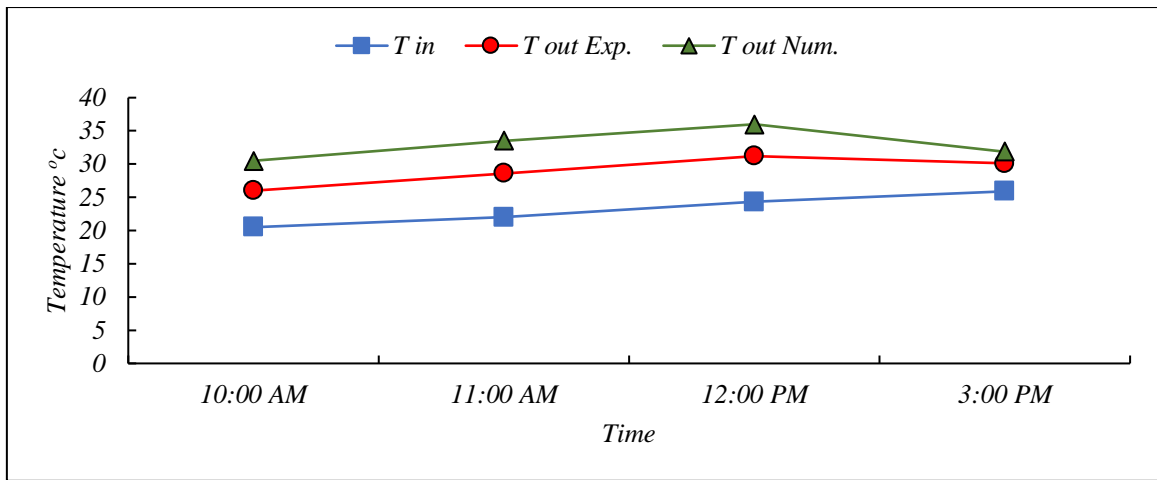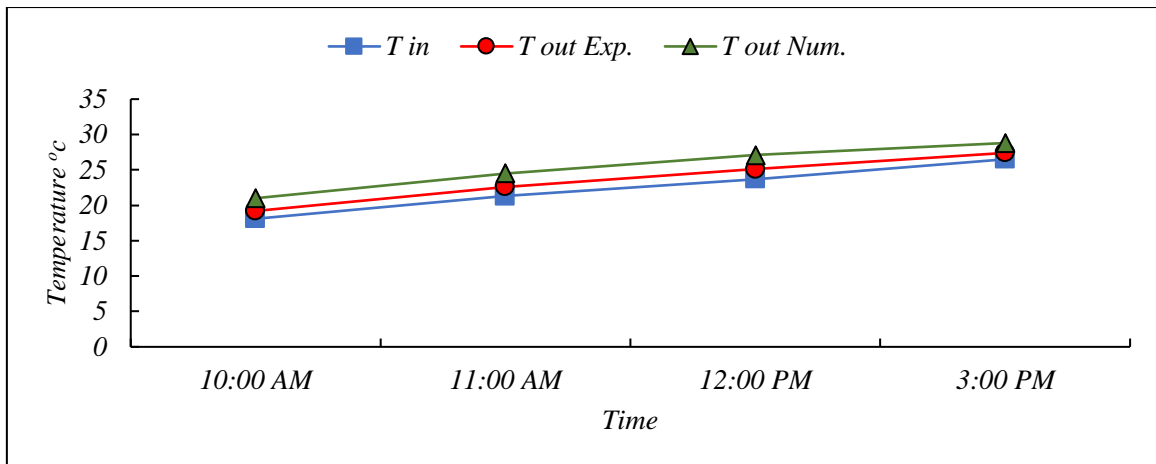
(a) For 0.5 L/min only water

(b) For 1 L/min only water
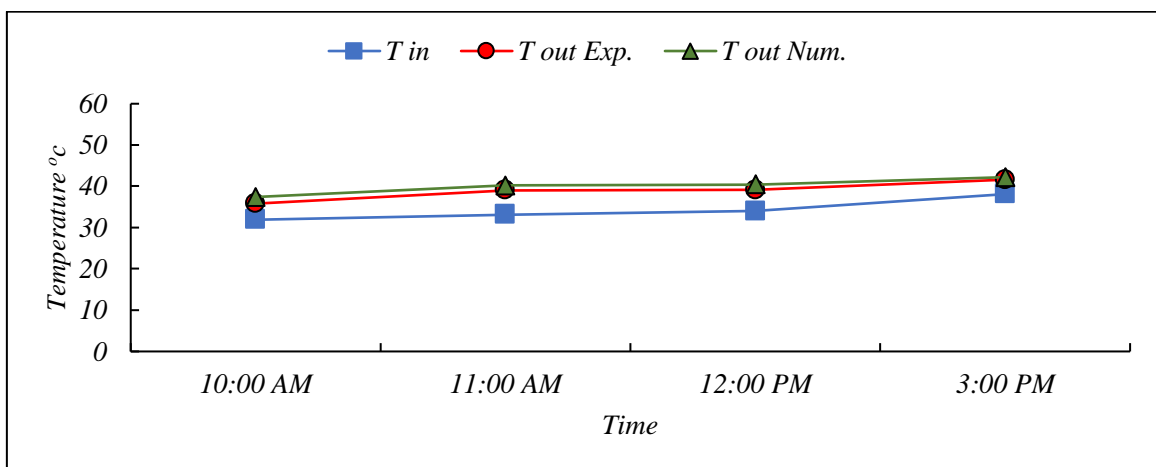

(c) For 1.5 L/min only water

Figure 5-53: Comparison of Outlet Temperature (^{o}C) *between Experimental and Numerical Results for Opened System without Air bubble Injection*

(d) For 2 L/min only water
Figure 5-53: Contd.

For the opened system with air bubble injection, the comparison shows a good agreement between the numerical and experimental results. Which illustrated in figure (5.54) that the largest disparity was 4% for 0.15 L/min air flowrate, with 12% and 8.5% for 0.25 and 0.35 air flowrate respectively.
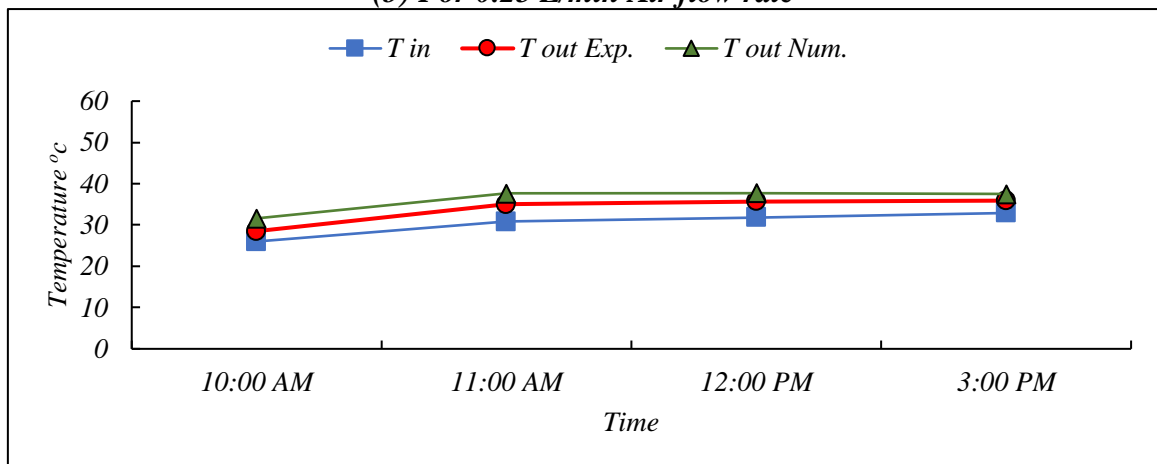

(a) For 0.15 L/min Air flow rate

Figure 5-54: Comparison of Outlet Temperature (^{o}C) between Experimental and Numerical Results for Opened System with Air bubble Injection
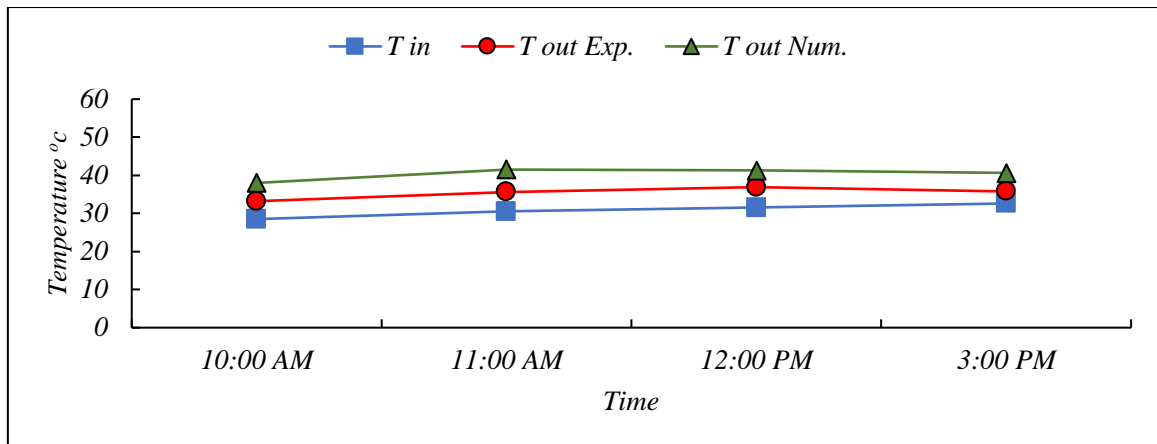
(b) For 0.25 L/min Air flow rate
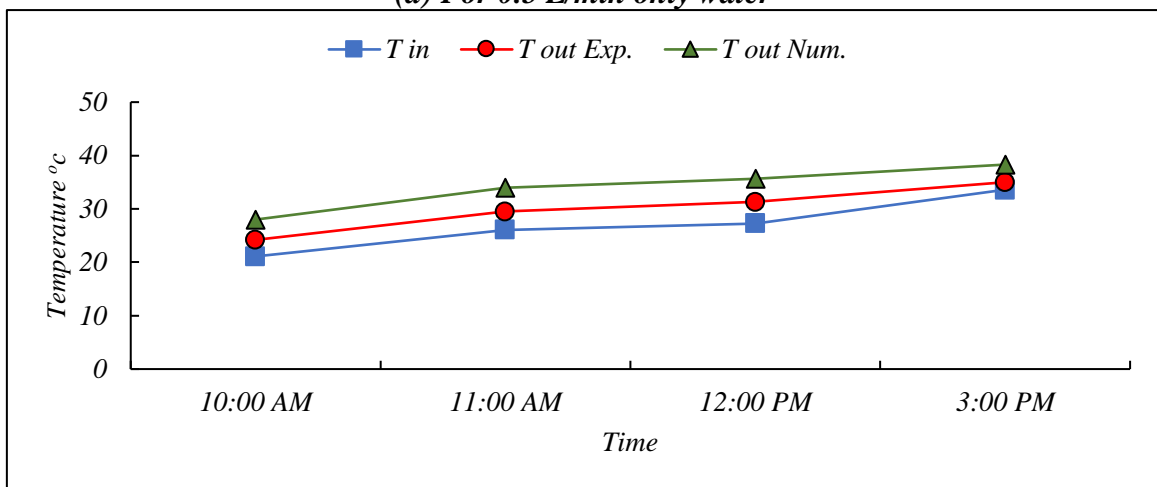

(c) For 0.35 L/min Air flow rate

Figure 5-54: Contd.

5.10.2 Closed System with and without Air Injection

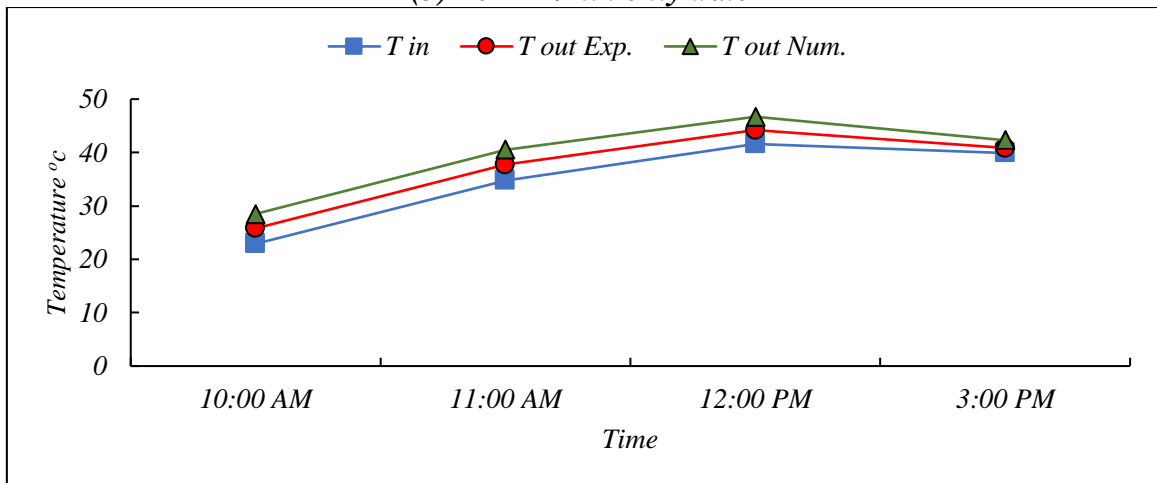For closed system without air injection, both the numerical and experimental results could be compared and they did not significantly differ from one another. For 0.5 L/min water flowrate the biggest difference rate of 13% to 7%. At 1 L/min, the percentage varied from 13% to 8%. The maximum disparity rate is 9 percent at 1.5 L/min. Noted that it reaches 8 % at 2 L/min as shown in figure (5.55).
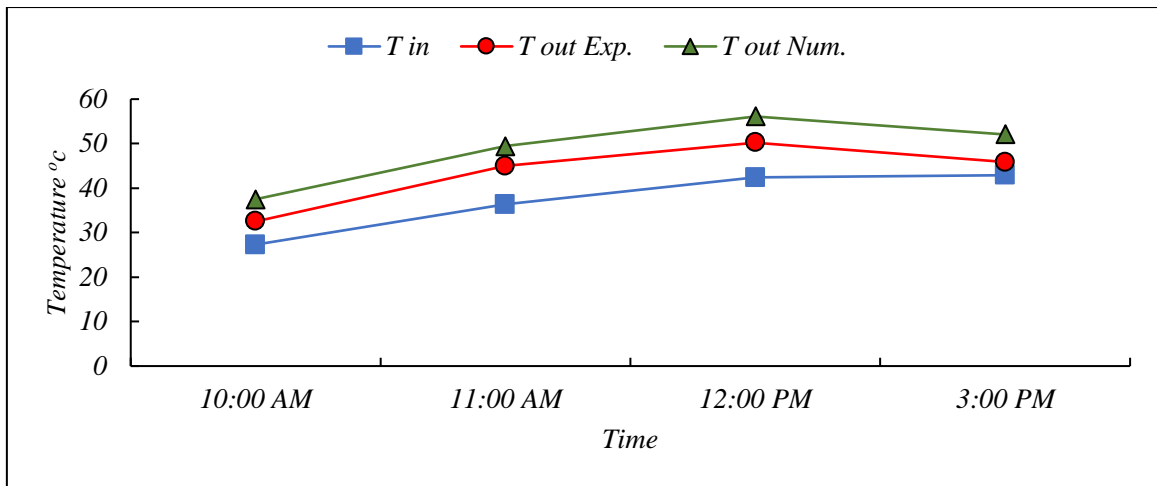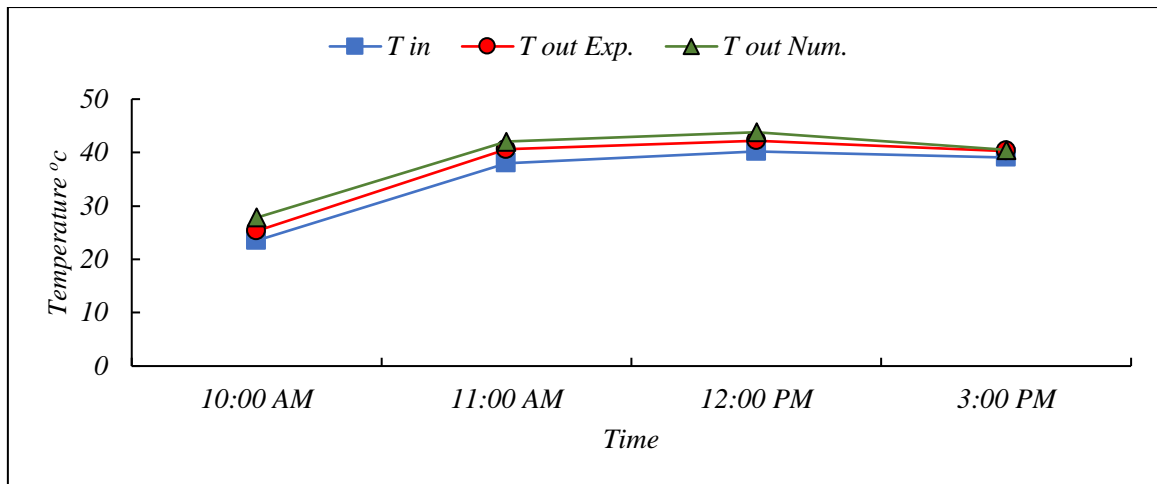
(a) For 0.5 L/min only water

(b) For 1 L/min only water

(c) For 1.5 L/min only water

Figure 5-55: Comparison of Outlet Temperature (^oC) between Experimental and

Numerical Results for Closed System without Air bubble Injection

(d) For 2 L/min only water

Figure 5-55: Contd.

The comparison reveals good agreement between the numerical and experimental results for the closed system with air bubble injection. The biggest variance was 6 % for 0.15 L/min air flowrate, with (13 to 3) percent and (12.5 to 0) % for 0.25 and 0.35 air flowrates, respectively, as shown in figure (5.56).
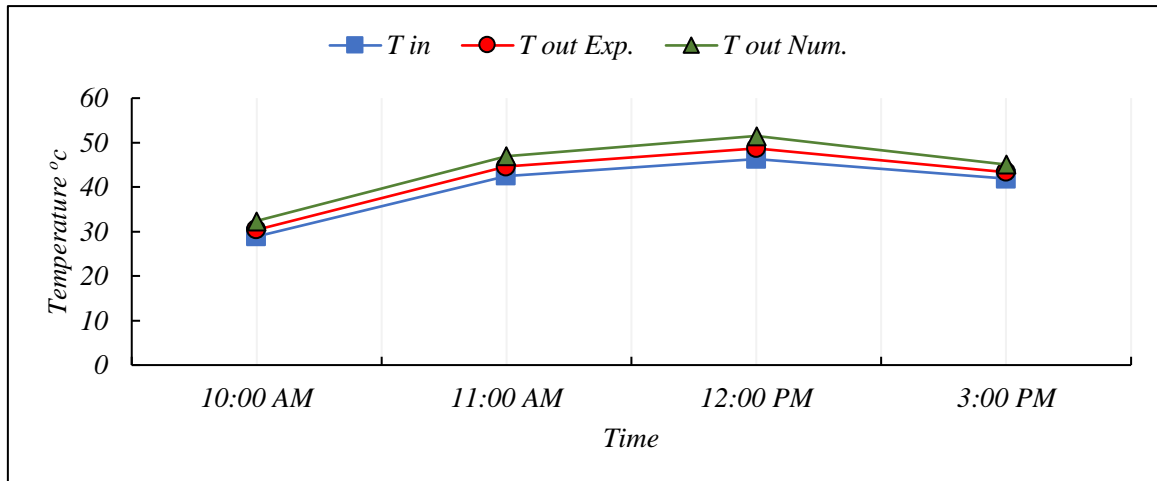

(a) For 0.15 L/min Air flow rate

Figure 5-56: Comparison of Outlet Temperature (^{o}C) *between Experimental and*

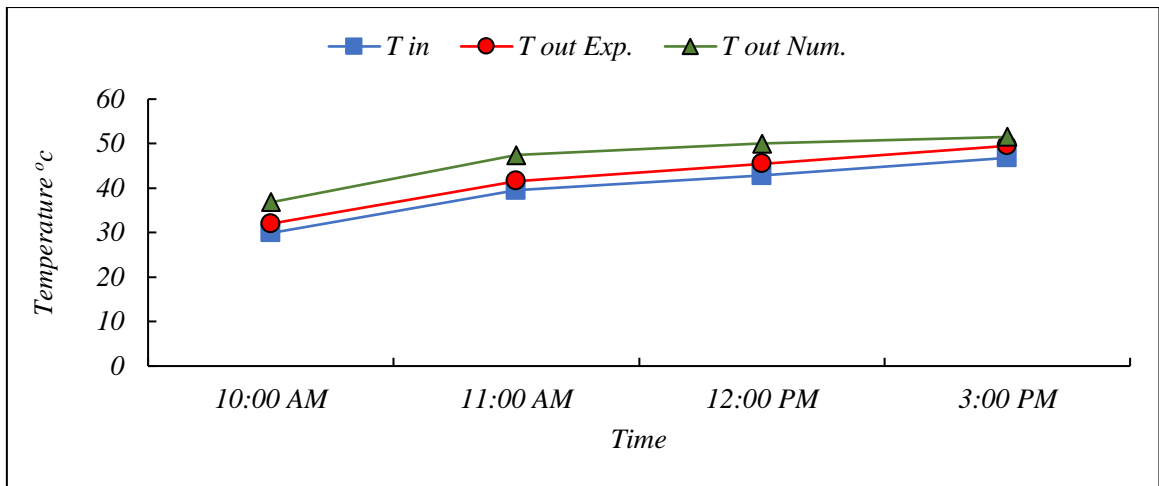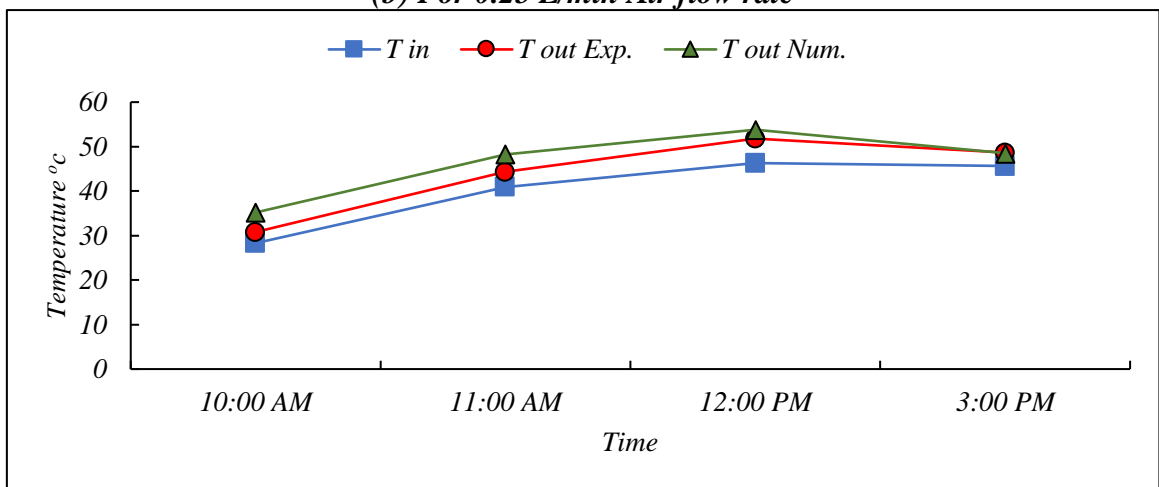*Numerical Results for Closed System with Air bubble Injection*

(b) For 0.25 L/min Air flow rate

(c) For 0.35 L/min Air flowrate
Figure 5-56: Contd.

Chapter SIX

Conclusions and Recommendations

6

Chapter Six

Conclusions and Recommendations

6.1 Conclusions

The wavy solar water collector's performance in single-phase and two-phase flow is described:

1. The calculation shows for the numerical and experimental works that the most efficient case for the opened system when the water flowrate was 1 L/min by an average efficiency (31.8) %, while for the closed system the most efficient case was at 2 L/min for an average efficiency of (45.5) %.

2. The closed system efficiency enhanced by (24.98%), (37.28%), and (53.71%) by adding air flowrate of (0.15, 0.25 and 0.35) L/min respectively.

3. The efficiency enhancement for the opened system after adding air flowrate of (0.15, 0.25 and 0.35) L/min was (30.89%), (37.92%) and (20.03%) respectively.

4. When the working fluid was only water, the pressure drop was almost stable for each flowrate and for the both systems. After injected air to the system, the pressure drop became unstable and fluctuated. It was observed for the opened system that the lowest fluctuating value for the pressure drop was changed between (5.4 - 9.3) Kpa when the air was injected at flowrate of 0.25 L/min with water flowrate of 1 L/min. However, for the closed system when the air was injected at flowrate of 0.35 L/min with water flowrate of 2 L/min, the lowest fluctuating value for the pressure drop was changed between (6.5 – 9.1) kpa.

5. When the water was the only working fluid at flowrate of 1 L/min, the results shows that the average temperature difference for the opened

system was (2.75ºC). In the other hand, the air injection to the system with flowrates of (0.15, 0.25 and 0.35) L/min enhanced the temperature difference to (40.98%), (43.10%) and (22.62%) respectively with the same water flowrate.

6. For the closed system when the water was the only working fluid at flowrate of 2 L/min, the average temperature difference for the system was (2.1 ºC). In comparison, air injection into the system at flowrates of (0.15, 0.25, and 0.35) L/min increased the temperature difference with the same water flowrate to (20.00%), (35.20%) and (50.59%) respectively.

7. Under the same conditions, it was found that there was a reasonable agreement between the numerical simulation from the ANSYS R21 program and the experimental results. The percentage of various results is no more than 13.5%.

6.2 Recommendations for Future Works

The following suggestions are made as further topics of research within the field of this study:

1. Using nanofluid as a working fluid.
2. Using a helical tube instead of a smooth-surface tube to obtain a higher mixing ratio.
3. Using lenses to get more focus on solar radiation.

References

R

References

References

[1] S.A.Kalogirou, "Solar thermal collectors and applications," *Progress in Energy and Combustion Science*, vol.30, no. 3. pp. 231–295, 2004, doi: 10.1016/j.pecs.2004.02.001.

[2] A.Kebede Endalew,"Numerical Modelling and Experimental Validation of Heat Pipe Solar Collector for Water Heating." p. 69, 2012,[Online].Available:https://www.diva-portal.org/smash/get/ diva 2:504099/FULLTEXT01.pdf.

[3] Crisciele Ferreira dos Santos, Arno Krenzinger, Tiago Manea, and Gian Roberto Tirello, "Design and Construction of a System for Controlling the Inlet Temperature in Solar Collector Testing," *Proc. 23rd ABCM Int. Congr. Mech. Eng.*, no. June 2017, 2015, doi: 10.20906/cps/cob-2015-0544.

[4] J. A. Duffie, W. A. Beckman, and J. McGowan, *Solar Engineering of Thermal Processes* , vol. 53, no. 4. 1985.

[5] F. Energy and M. Program, "Solar Water Heating with Low-Cost Plastic Systems." 2009.

[6] "Solar Water Heating." doi: DOE/GO-10096-050 FS 119.

[7] K. Patel, M. Pragna Patel, and M. J. Patel, "REVIEW OF SOLAR WATER HEATING SYSTEMS," *Int. J. Adv. Eng. Technol.*

[8] K.Sam Mathew,"EXPERIMENTAL ANALYSIS OF SOLAR ENHANCED WATER HEATING SYSTEM WITH ENERGY STORAGE," JETIR, 2021. [Online]. Available: www.jetir.org.

[9] H. M. Alkarak, "Feasibility Analysis of a Two-Phase Solar Thermal Water Heater."

[10] S. R. Todkar, U. C. Kapale Co-Supervisor, and A. N. Chapgaon Co-Supervisor, "An Experimental Study on Two Phase (Air-Water) Flow Characteristics in a Horizontal Pipe at Atmospheric

References

Conditions," *Int. J. Eng. Res. Technol.*, vol. 5, 2016, [Online]. Available: http://www.ijert.orgijertv5is010553.

[11] H. Abdulmouti, "Bubbly Two-Phase Flow: Part I- Characteristics, Structures, Behaviors and Flow Patterns," *American Journal of Fluid Dynamics*,vol.4,no.4.pp.194240,2014,doi:10.5923/j.ajfd.20140404. 03.

[12] J. R.Thome and A. Cioncolini, *Two-Phase Flow Pattern Maps for Microchannels*, no. October. 2015.

[13] S. S.Hasan, A. S. Baqir, and H. B. Mahood, "The effect of injected air bubble size on the thermal performance of a vertical shell and helical coiled tube heat exchanger," *Energy Eng. J. Assoc. Energy Eng.*,vol.118,no.6,pp.15951609,2021,doi:10.32604/EE.2021.01743 3.

[14] J. Ma,W. Sun, J. Ji, Y. Zhang, A. Zhang, and W. Fan, "Experimental and theoretical study of the efficiency of a dual-function solar collector," *Appl. Therm. Eng.*, vol. 31, no. 10, pp. 1751–1756, 2011, doi: 10.1016/j.applthermaleng.2011.02.019.

[15] "A high absorbance material for solar collectors'.pdf." .

[16] R. Bakari, R. J. A. Minja, and K. N. Njau, "Effect of Glass Thickness on Performance of Flat Plate Solar Collectors for Fruits Drying," *J. Energy*, vol. 2014, pp. 1–8, 2014, doi: 10.1155/2014/247287.

[17] S. Hossain, A. W. Abbas, J. Selvaraj, F. Ahmed, and N. B. A. Rahim, "Experiment of a flat plate solar water heater collector with modified design and thermal performance analysis," in *Applied Mechanics and Materials*,2014,vol.624,pp.332338,doi:10.4028/www.scientific.net/ AMM.624.332.

[18] A. Noghrehabadi, E. Hajidavaloo, and M. Moravej, "Experimental investigation of efficiency of square flat-plate solar collector using SiO2/water nanofluid," *Case Stud. Therm. Eng.*, vol. 8, pp. 378–386,

References

Sep. 2016, doi: 10.1016/j.csite.2016.08.006.

[19] W.M.Hashim, A.T.Shomran,H.A.Jurmut,T.S.Gaaz,A.A.H. Kadhum, and A. A.Al-Amiery, "Case study on solar water heating for flat plate collector," *Case Stud. Therm. Eng.*, vol. 12, pp. 666–671, Sep. 2018, doi: 10.1016/j.csite.2018.09.002.

[20] E.Nshimyumuremyi and W. Junqi, "Thermal efficiency and cost analysis of solar water heater made in Rwanda," *Energy Explor. Exploit.*,vol.37,no.3,pp.11471161,May2019,doi:10.1177/014459871 8815240.

[21] M.Moravej, M. R. Saffarian, L. K. B. Li, M. H. Doranehgard, and Q. Xiong, "Experimental investigation of circular flat-panel collector performance with spiral pipes," *J. Therm. Anal. Calorim.*, vol. 140, no. 3, pp. 1229–1236, 2020, doi: 10.1007/s10973-019-08879-1.

[22] M. R. Saffarian, M. Moravej, and M. H. Doranehgard, "Heat transfer enhancement in a flat plate solar collector with different flow path shapes using nanofluid," *Renew. Energy*, vol. 146, pp. 2316–2329, Feb. 2020, doi: 10.1016/j.renene.2019.08.081.

[23] M.R.Mohammad, D. A. Alazawi, and A. T. Mohammad, "Case study on spiral solar collector performance with lens," *AIMS Energy*, vol. 8, no. 5, pp. 859–868, 2020, doi: 10.3934/ENERGY.2020.5.859.

[24] U.Muthuraman *et al.*, "Energy and Economic Analysis of Curved, Straight, and Spiral Flow Flat-Plate Solar Water Collector," *Int. J. Photoenergy*, vol. 2021, 2021, doi: 10.1155/2021/5547274.

[25] A.Baylar,M.C.Aydin, M. Unsal, and F. Ozkan, "Numerical modeling of venturi flows for determining air injection rates using fluent V6.2," *Math.Comput.Appl.*,vol.14,no.2,pp.97108,2009,doi:10.3390/mca14 020097.

[26] A.Moosavi, M. Abbasalizadeh, and H. Sadighi Dizaji, "Optimization of heat transfer and pressure drop characteristics via air bubble

References

injection inside a shell and coiled tube heat exchanger," *Exp. Therm. FluidSci.*,vol.78,pp.19,Nov.2016,doi:10.1016/j.expthermflusci.2016.05.011.

[27] V. Panthalookaran and J. P. George, "Experimental Study on Cooling of Solar Collectors Using Air-water Mixture," *Energy Procedia*, vol. 91, pp. 303–311, 2016, doi: 10.1016/j.egypro.2016.06.222.

[28] M.Mahdi Heyhat, A. Abdi, and A. Jafarzad, "Performance evaluation and exergy analysis of a double pipe heat exchanger under air bubble injection," *Appl. Therm. Eng.*, vol. 143, pp. 582–593, Oct. 2018, doi: 10.1016/j.applthermaleng.2018.07.129.

[29]H.B.M.AhmedR.Kreem,AliBaqir,*TemperatureDistributionMeasurements along Helical Coiled Tube Heat Exchanger with Effect of Air Injection*. .

[30] V.Shemelin and T.Matuska,"Performance modelling of dual air/water collector in solar water and space heating application," *Int. J. Photoenergy*, vol. 2019, 2019, doi: 10.1155/2019/8560193.

[31] H.Q.Mohammed, A. S. Baqir, and H. S. K. Hasan, "Effects of Air Bubble Injection on the Efficiency of a Flat Plate Solar Collector: An Experimental Study for the Open Flow System," 2020.

[32] S.L.Ghashim and A. M. Flayh, "Experimental investigation of heat transfer enhancement in heat exchanger due to air bubbles injection," *J. King Saud Univ. - Eng. Sci.*, vol. 33, no. 7, pp. 517–524, Nov. 2021, doi: 10.1016/j.jksues.2020.06.006.

[33] S. A. Jawad, F. L. Rashid, and Z. A. A. Ridha, "Thermal Performance of Spiral Flat Plate Solar Water Collector," *Int. J. Heat Technol.*, vol. 40, no. 1, pp. 183–192, Feb. 2022, doi: 10.18280/ijht.400122.

[34] "ANSYS Fluent Theory Guide," *http://www.ansys.com*, p. 814, 2013.

[35] M.B.AL_Mudhafar, "Investigation of Solar Chimney Performance in

References
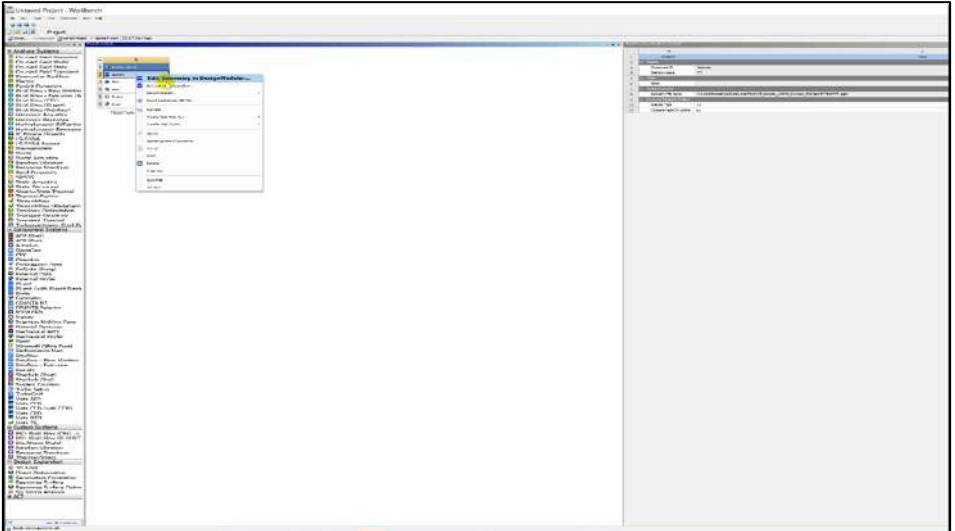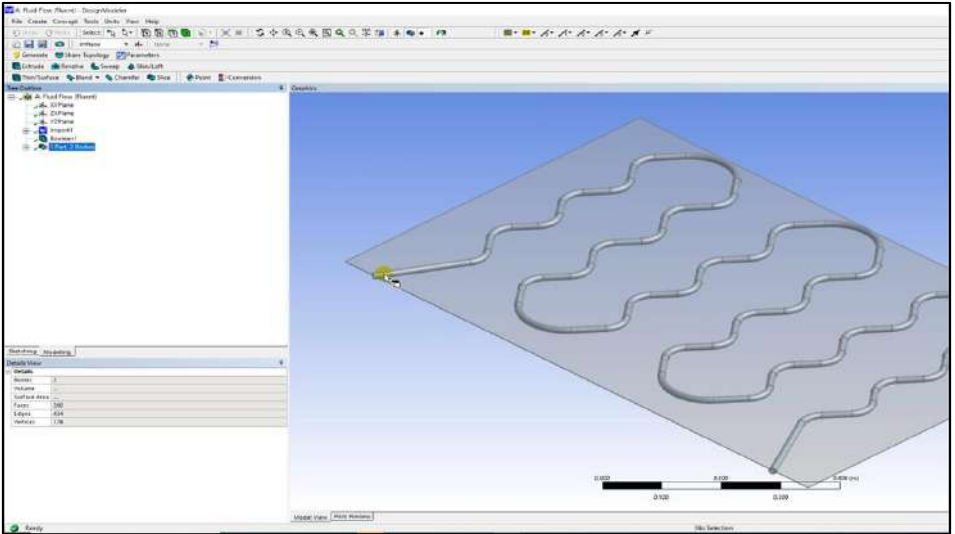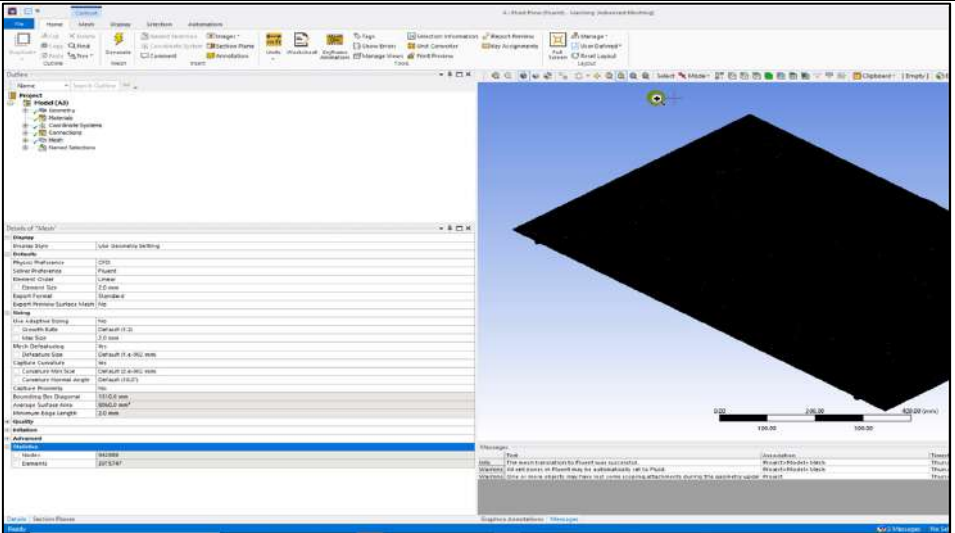
the Holly Kerbala," College of Engineering /University of Kerbala, 2016.

[36] Http://www.ansys.com, *ANSYS Fluent Theory Guide*. 2013.

[37] J.V Madan and O. M. Sirse, "Experimental Study On Efficiency Of Solar Collector At Nagpur (India) During Winter," *Int. J. Sci. Technol. Res.*, vol. 4, p. 8, 2015, [Online]. Available: www.ijstr.org.

[38] S.A. Jawad, "Effect of Air Bubble Injection on the Performance of a Solar Thermal Spiral Water Collector," University of Baghdad, 2022.

[39] L.Xing,H.Yeung, J. Shen, and Y. Cao, "Experimental study on severe slugging mitigation by applying wavy pipes," *Chem. Eng. Res.Des.*,vol.91,no.1,pp.1828,2013,doi:10.1016/j.cherd.2012.06.020

[40] H.S.Khwayyir, A. S. Baqir, and H. Q. Mohammed, "Effect of air bubble injection on the thermal performance of a flat plate solar collector,"*Therm.Sci.Eng.Prog.*,vol.17,Jun.2020,doi:10.1016/j.tsep.2019.100476.

Appendix

Ansys Fluent Setups

A

Ansys Fluent Setups

Opining the Program and Choosing Fluent	
Calling the Draw from the Solid Work Program	
Applying the Mesh	
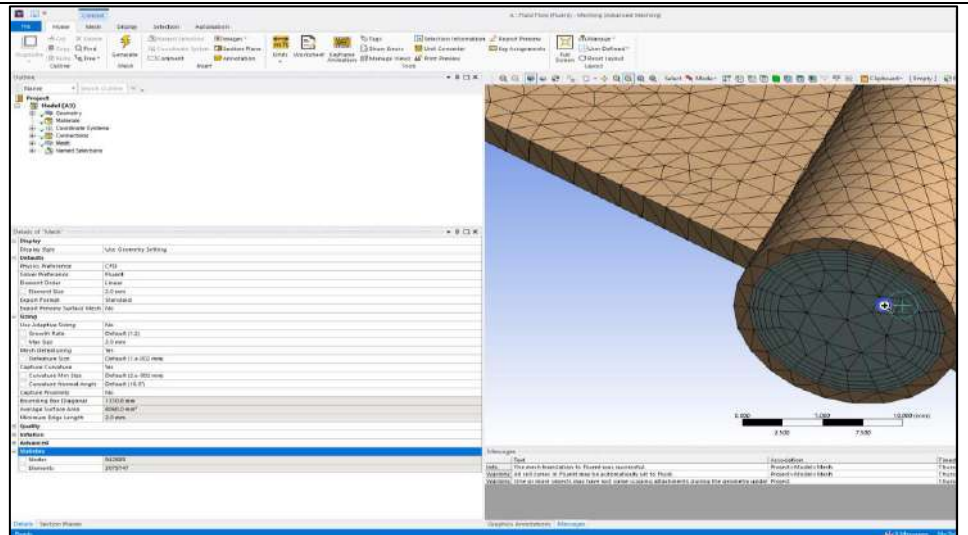
Mesh properties	
Entering to the Fluent Setup	
Insert the Acceleration Values and Choosing Steady State	
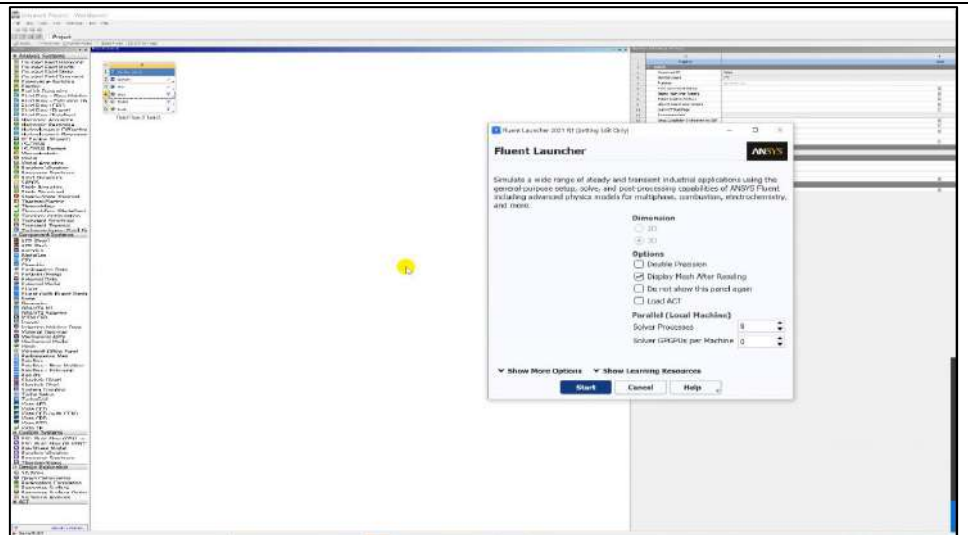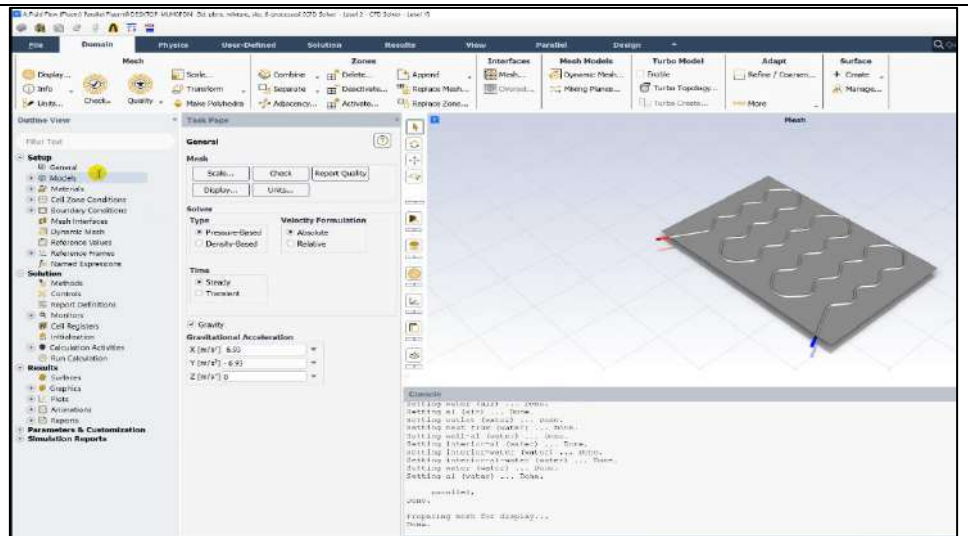
Choosing the Governing Equations	
Choosing Mixture Model	
Choosing the Phases Properties	
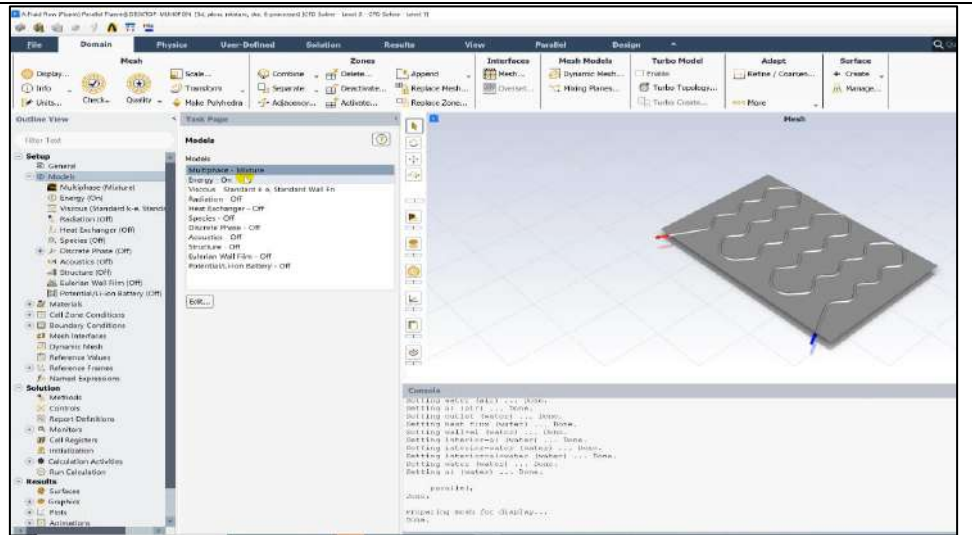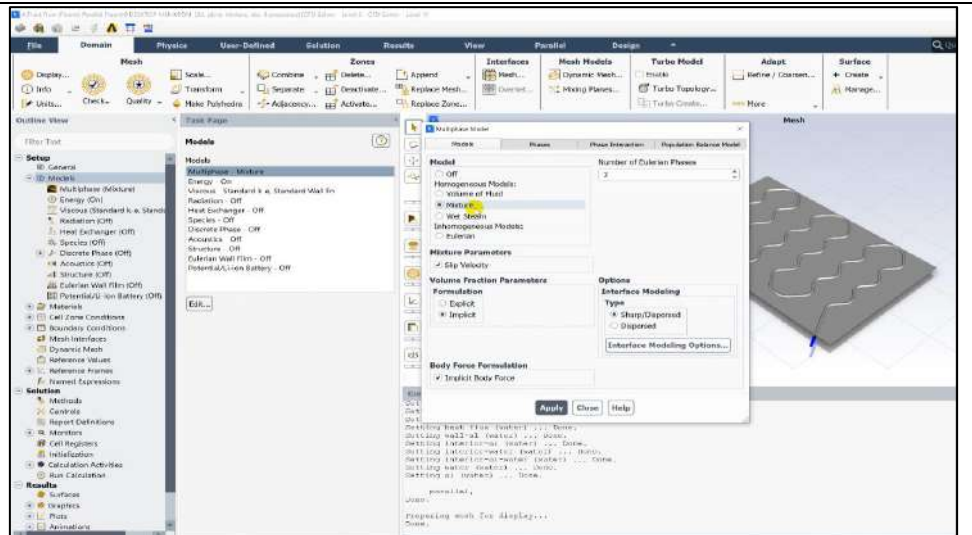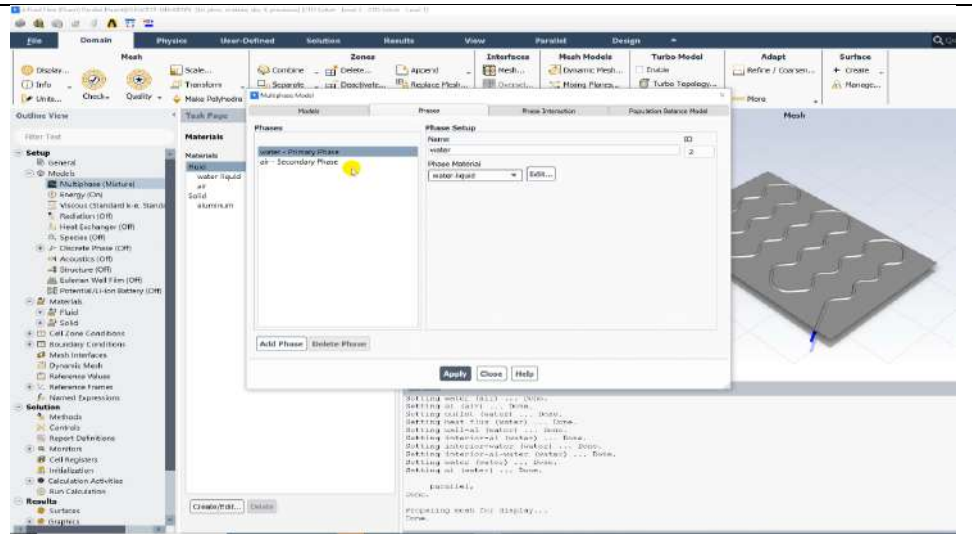
Inserting the Material Properties	
Choosing the Boundary Conditions and Putting the Heat Flux Value	
Putting the Inlet Boundary 1- Water Mass Flowrate Value	
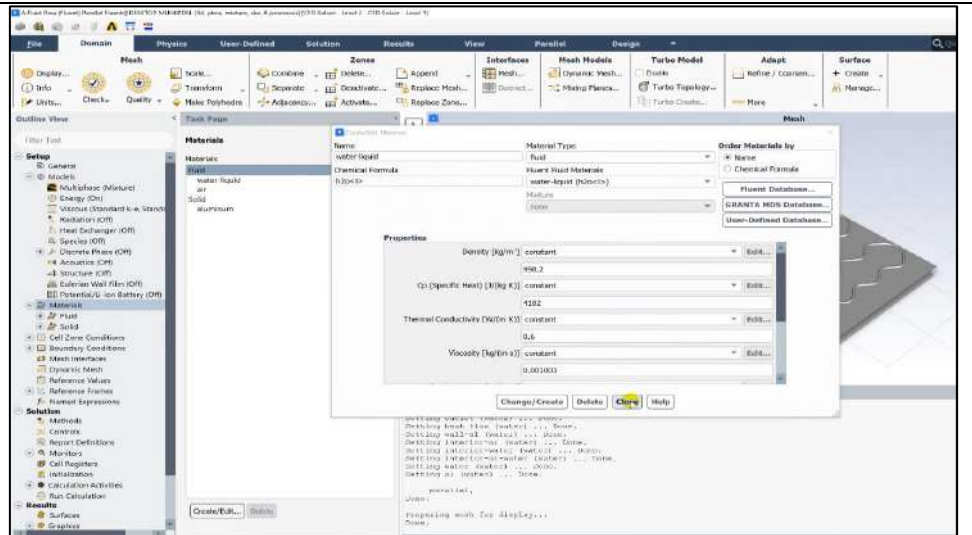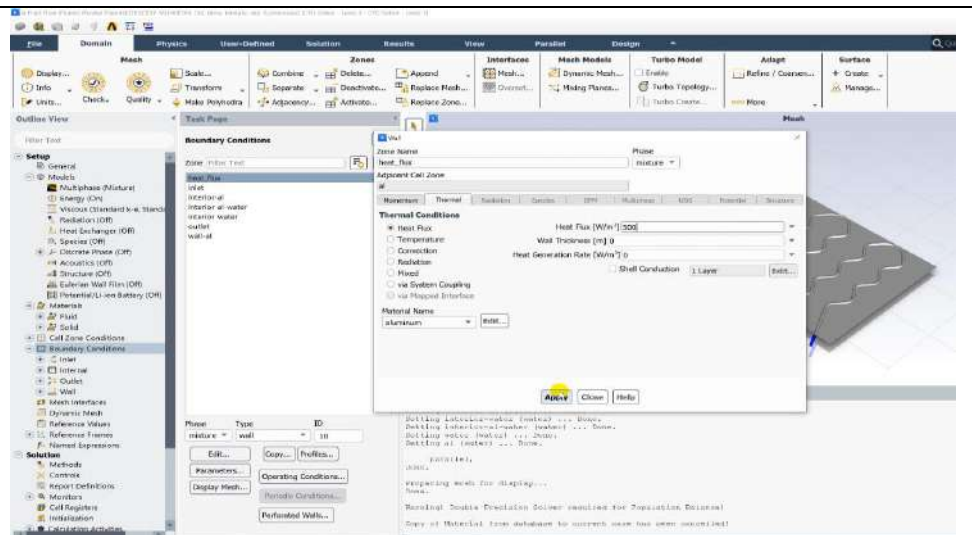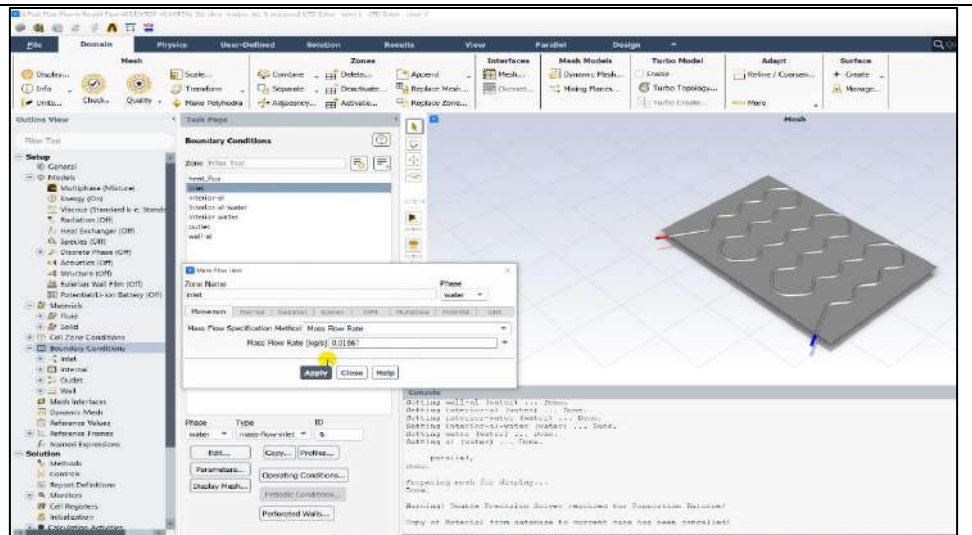
2- Air Mass Flowrate Value	
3- Completing the Mixture Values	
Insert the Outlet Boundary	
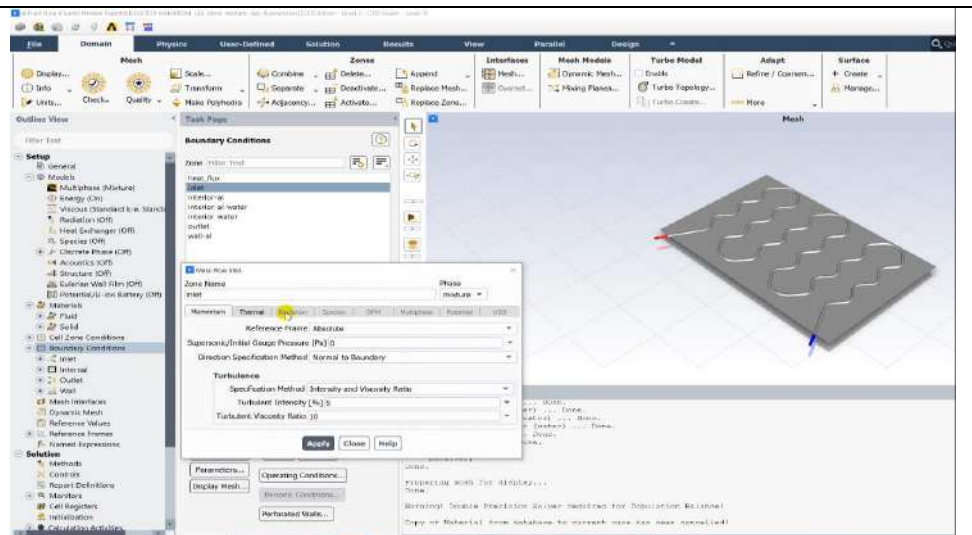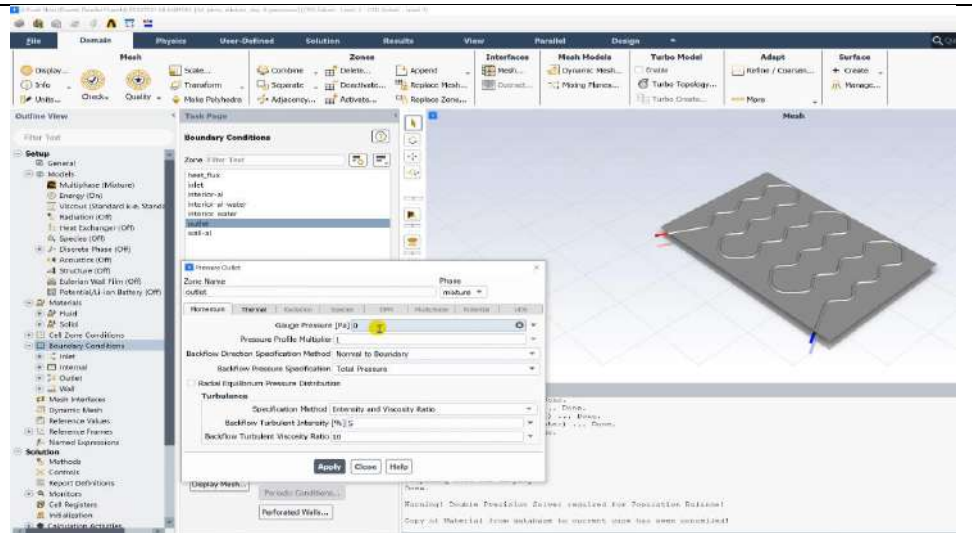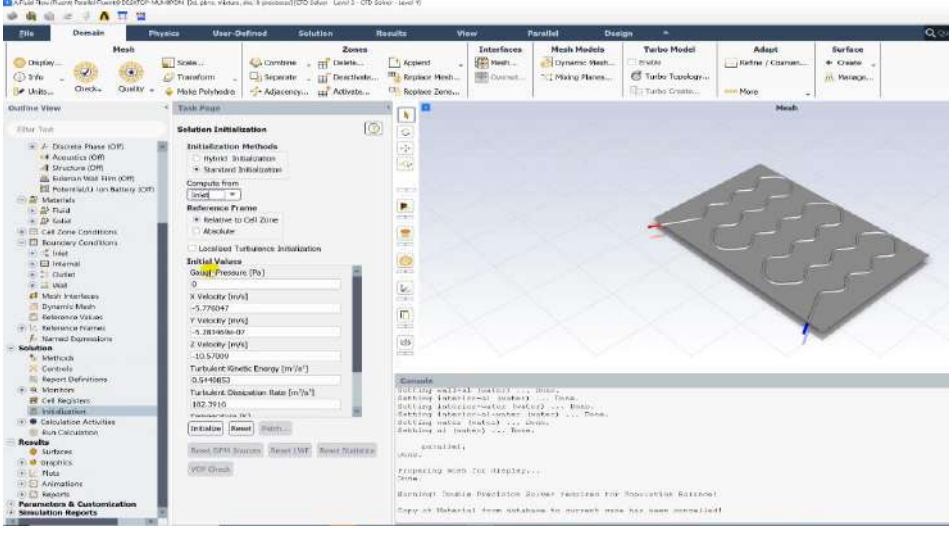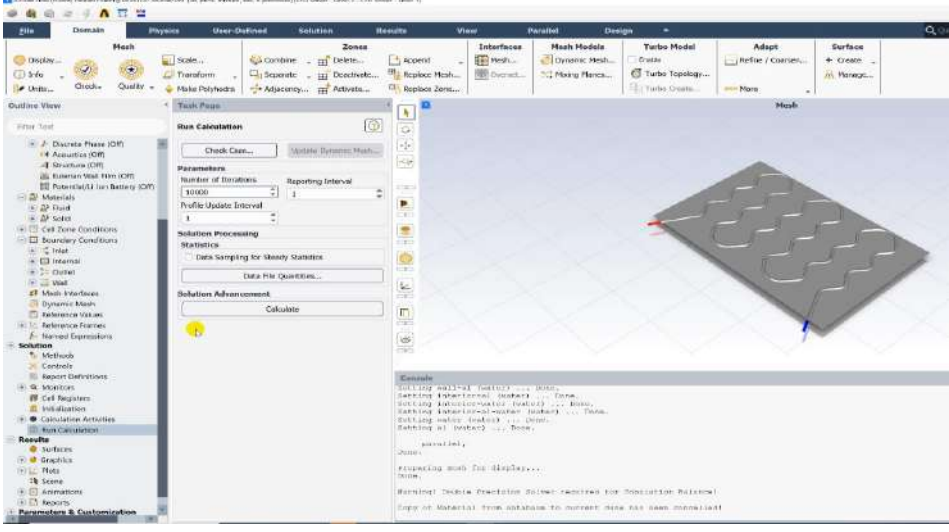
Making Initialization from the Inlet	
Run the Calculations	

Appendix

Calibrations

B

REPUBLIC OF IRAQ

MINISTRY OF SCIENCE & TECHNOLOGY

RENEWABLE ENERGY DIRECTORATE

جمهورية العراق

وزارة العلوم والتكنولوجيا

دائرة الطاقات المتجددة

معاً لمساندة قواتنا المسلحة الباسلة لدحر الإرهاب

العدد: ط م / ٦٥٠ ع

التاريخ: ٢٠٢٢/٣/١٢

الى/ جامعة كربلاء/ كلية الهندسة

م/أبداء مساعدة

تحية طيبة :

اشارة الى كتابكم العدد د ع ٦٣٦/٦ في ٢٠٢٢/٢/١٥ الخاص بابداء المساعدة لطالب الماجستير (محمد محسن جاسم) في قسم الهندسة الميكانيكية نرفق لكم طيا نتائج الفحص والمعايرة الخاصة ببحثه .

١- تم اجراء فحص ومعايرة لجهاز قياس شدة الاشعاع الشمسي من خلال المقارنة بين قراءات شدة الاشعاع الشمسي لجهاز قياس شدة الاشعاع الشمسي المطلوب فحصه (%10+-): es132Data (T 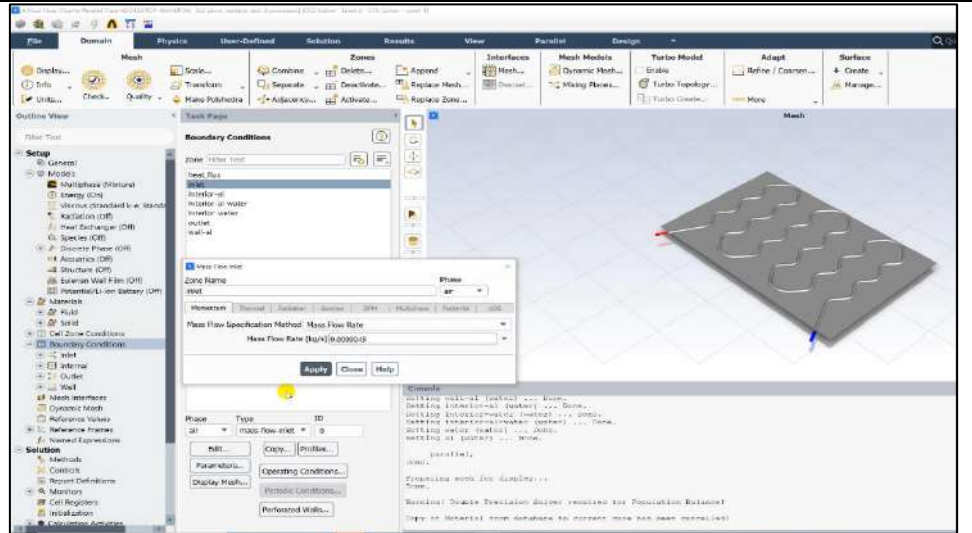logging solar power meter accuracy) والذي يحمل الرقم التسلسلي (160001732) مع قراءات جهاز قياس شدة الاشعاع الشمسي معتمد لدينا علما ان القراءات كانت بوضع الاجهزة الافقي وجد ان هناك فروقات في القراءات بعد انجاز المعايرة تعزى الى نسبة الخطا المصنعية للجهاز البالغة (%10+-) وكما موضح في الجدول رقم (1) المرفق طيا .

٢- تم فحص جهاز(12channels SD Data Logger) الذي يحمل الرقم (H.297840) من خلال مقارنة القراءات مع جهاز معتمد لدينا ومن خلال استخدام فرن حراري حيث وجد ان القراءات كانت متقاربة الى حد ما والفرق البسيط يعزى الى الاختلاف في مدى نسبة الخطا من جهاز الى اخر وكما موضح في الجدول رقم (2) المرفق طيا . علما ان انتاج هذا النوع من الاجهزة لا يمكن معايرته حيث يخضع لمعايير دولية قياسية .

مع التقدير

د.فلاح ابراهيم العطار

معاون المدير العام

٢٠٢٢/٣/٩

نسخه منه/الى

قسم التخطيط والمتابعة/شعبة المعلومات مع الاوليات

Table (1) : Comparison between Standard solar Power meter and
TES 132 Data Logging Solar power meter Accuracy: (± (10 %) under testing

No.	Time	Solar Power meter W/m^2 Standard	TES 132 Solar Power meter W/m^2 under testing
1	10:06	648	649
2	10:48	735	733
3	11:30	765	776
4	11:54	795	801
5	12:25	790	784

Table (2): Comparison between two Data Logger ; the Standard Data logger and
Data Logger under the testing

Time	Data Logger under testing ($^\circ$ C)	Data Logger Standard ($^\circ$ C)
10:30:59	307.3	308.3
10:35:59	299.3	300.1
10:40:59	283	283.6
10:45:59	266	266.5
10:50:59	249.4	249.7
10:55:59	233.4	234
11:00:59	218.9	219.4
11:05:59	205.4	205.8
11:10:59	192.8	193.4
11:15:59	181.2	181.9
11:20:59	170.4	171.2
11:25:59	160.3	161.3
11:30:59	126.1	123.3
11:35:59	102.6	102.6
11:40:59	86.4	86.6
11:45:59	74.9	75.3
11:50:59	66.2	66.4
11:55:59	59.1	59.4
12:00:59	53.6	53.9
12:05:59	49	49.2
12:10:59	45.3	45.6
12:15:59	42.2	42.4
12:20:59	39.4	39.8
12:25:59	26.4	26.5
12:30:59	23.9	25.3
12:35:59	20.1	21.2

REPUBLIC OF IRAQ

MINISTRY OF SCIENCE & TECHNOLOGY

RENEWABLE ENERGY DIRECTORATE

وزارة العلوم و التكنولوجيا
Ministry Of Science & Technology

جمهورية العراق

وزارة العلوم والتكنولوجيا

دائرة الطاقات المتجددة

العدد: ط م ٢٠٩

التاريخ: ١٩ / ٤ / ٢٠٢١

إلى/ جامعة كربلاء-كلية الهندسة

م/ معايرة أجهزة قياس

تحية طيبة

إشارة إلى كتابكم المرقم بالعدد (د.ع/١١٤٦/٦ في ٢٠٢١/٤/١٥)، بخصوص إبداء المساعدة لطالب الدراسات العليا / الماجستير **(محمد محسن جاسم)**، تم إجراء المعايرة للأجهزة والمعدات المدرجة تفاصيلها في أدناه في مختبراتنا بتاريخ ٢٠٢١/٤/١٩ وهي جاهزة للاستخدام.

شاكرين تعاونكم معنا .. مع فائق التقدير

الأجهزة التي تم معايرتها:

١-جهاز قياس شدة الإشعاع الشمسي العدد / ١

٢-جهاز قياس درجة الحرارة العدد /١

٣-جهاز قياس سرع الرياح العدد /١

٤-متحسس درجة الحرارة T/C k طول ١ متر العدد /١

دائرة
الطاقات المتجددة

د. فلاح إبراهيم العطار

ع/المدير العام

٢٠٢١/٤/١٩

نسخة منه إلى/

مركز تخطيط وإدارة الطاقة مع الأوليات .... للتفضل بالاطلاع مع التقدير

قسم التخطيط والمتابعة .... للتفضل بالاطلاع مع التقدير

جمهورية العراق

العدد : ٨٤٨١

التاريخ م : ٤/ ١-٢٠١٨

هـ : / /

وزارة التخطيط

الجهاز المركزي للتقييس والسيطرة النوعية

الدائرة : التقييس

القسم : المقاييس

إلى /جامعة كربلاء ـ كلية الهندسة ـ الموارد البشرية

م / معايرة اجهزة

يهدي الجهاز أطيب تحياته ....

أشارة إلى كتابكم ذي العدد د/٣/ ٢٠٩٤ في ٢٠٢١/٨/١ نود اعلامكم الاتي :

١ـ تمت معايرة الجهاز العائد لكم وكانت النتائج كما مبينة في شهادة المعايرة و ينبغي الاخذ بنظر الاعتبار النتائج و التصحيحات عند القياس علما ان المعايرة نافذة لمدة سنة .

٢ـ نعتذر عن معايرة الاجهزة الواردة في الفقرات (٣، ٤، ٥) لعدم وجود الامكانية في الوقت الحاضر .

٣ـ تم تسديد أجور المعايرة البالغة (٧٧٠٠٠) سبعة وسبعون الف دينار فقط بموجب وصل القبض المرقم (٣٥٠٨٣) في ٢٠٢١/٨/٣ .

الاجهزة :

Data Loger مع مزدوج حراري نوع (K) عدد /٧

مع التقدير ....

المرافقات /

شهادة معايرة عدد (١) فقط .

المهندسة

خلود خالد شكري

عن/ مدير عام دائرة التقييس

٤/ ١٠ /٢٠٢١

نسخة منه إلى /

- مكتب المدير العام /للتفضل بالاطلاع ..... مع التقدير
- شعبة القياسات الفيزياوية لطفا.

هناء محمد قادر

العراق ـ بغداد ـ الجادرية ـ ص . ب (١٢٠٢٢) ـ البريد الالكتروني : www.cosqc.gov.iq

هاتف / ٨٤ / ٨٣ / ٨٢ / ٧٨ / ٨١ / ٧٧٨٥١٨٠ / تلفاكس ٧٧٦١٩٨١   cosqc@cosqc.gov.iq

Calibration Certificate
Central Organization for Standardization and Quality Control (COSQC)
Metrology Department - Physics Section (FOR-TC-012)
P.O. Box13032 Aljadriya street, Baghdad , Tel:7785180 - E-Mail : cosqc@cosqc.gov.iq

Certificate No.: PHT   677 / 2021

Date of issue :   12/08/2021

Customer	
Name:	جامعة كربلاء / كلية الهندسة
Address:	العراق - كربلاء المقدسة

Item under calibration				
Description:	Temperature Recorder 12 CH With TC (K)	Res. :	0.1	° C
Manufacturer:	LUTRON			
Model:	BTM - 4208SD			
Serial number:	I.144597			
Other identification:	(-200 ------- 1370) °C			
Date of reception:	Order no. : (260) , Date of Reception : 3/08/2021			
Condition of reception:	As Found			

Standard(s) used in the calibration		
Description:	Digital Nano volt / Micro Ohm meter	PT100
Manufacturer:	Agilent	———
Model:	34420A	———
Serial number:	MY42000734	(1 , 3)
Other identification:	ID : PHT-01- 17	ID : PHT-01-84 , 86

Calibration information	
Date of calibration:	10/08/2021 , Due to: 10/08/2022
Place of calibration:	PH LAB. 1
Method(s) of calibration:	Calibration method using - PROC-TC-012 (C)
Calibrated quantity:	Temprature ° C
Results of calibration:	Attached a complete result in Annex **1** of this certificate
Measurement uncertainty:	The reported expanded uncertainty is based on UKAS M3003 Standard and the standard Uncertainty multiplied by coverage factor k=2 to give confidence level of 95%
Metrological traceability:	The traceability of measurement results to the SI units is assured by the National standard maintained at Central Organization for standardization and Quality Control through calibration at :- UME /CER. NO (G1KS-0127)
Environmental conditions of calibration:	Temp. 37.51° C RH. 23.5%
Observations, opinions or recommendations:	The results in Annex 1 should be taken into consideration

Approved by:

Eng
Moyasser Ali Taher
Head Of Physics Section
12/08/2021

1 of 2

Ref. Proc.Tc-012

Calibration Certificate

Central Organization for Standardization and Quality Control

Metrology Department - Physics Section   (FOR-TC-012)

P.O. Box13032 Aljadriya street, Baghdad , Tel:7785180 - - E-Mail : cosqc@cosqc.gov.iq

Certificate No.: PHT   677 / 2021

Date of issue :   12/08/2021

Annex 1

Results

The results of the measurements are given on table below.

TC No.	Set. Value $C°$	Ref. (R) $C°$	UUC (M) $C°$	Error (M)-(R) $C°$	Uncertainty ± $C°$
TC 1	25	25.01	25.9	0.85	1.04
TC 2	35	34.98	35.7	0.74	0.95
TC 3	45	45.04	45.8	0.76	0.88
TC 4	55	55.01	55.80	0.79	0.92
TC 5	65	65.02	65.70	0.68	0.79
TC 6	75	23.02	23.40	0.38	0.45
TC 7	95	94.19	95.00	0.81	0.94

Calibrated by :

Khalid Naser

12/08/2021

Revised by :

Hanaa Mohammed

12/08/2021

Approved by:

Moyasser Ali Taher

12/08/2021

2 of 2

This certificate is issued in accordance with the laboratory accrediation requirements.It provides tracibility of measurement to recognized national standards,and to the units of measurement realized at the COSQC or other recognized national standards laboratories.This certificate may not be reproduced other than in full by photographic process.This certificate refers only to the particular item submitted for calibration

Ref. Proc.Tc-012

Appendix

Publication

C

The 3rd International Conference on Electromechanical Engineering & its Applications

ICEMEA-2022

ACCEPTANCE LETTER

Dear, [Zahraa Mohammed Kadhum, Mohammed Wahhab Aljibory, and Farhan Lafta Rashid]

We are pleased to inform you that your manuscript entitled (Experimental study to investigate the influence of air bubble injection on solar water collector performance) has been accepted for oral presentation at the 3rd International Conference on Electromechanical Engineering and its Applications (ICEMEA-2022) to be held on July 19th – 20th, 2022 at the University of Technology, Baghdad, Iraq. Decision was made upon double-blind review process. The exact date, time and place of your presentation will be posted at the conference website.

On behalf of the organizing committee of ICEMEA 2022, we are looking forward to seeing you at the University of Technology, Baghdad, Iraq. If you have any further questions, please do not hesitate to contact us.

Sincerely,

The Chairman of ICEMEA-2022
Professor Dr. Hosham Salim

+964-7736-833726
eme.icemea@uotechnology.edu.iq
https://eme.uotechnology.edu.iq/icemea

6th International Conference on Engineering Sciences

ICES 2022

ID-Code: ICES-63

Authors: Zahraa Mohammed Kadhum, Mohammed Wahhab Aljibory, Farhan Lafta Rashid

Date: 20/11/2022

Dear Authors,

On behalf of the scientific and organizing committees of the 6th International Conference on Engineering Sciences (ICES 2022), I am pleased to inform you that your manuscript entitled **"Numerical and Experimental Investigations for the Thermal Performance of Flat Plate Solar Water Collector with Air Bubble Injections."** has been accepted for publication in the conference proceedings of ICES2022. The accepted paper will be published in the AIP Conference Proceedings which is indexed in the Scopus Journals database. The 6th ICES will be held on 21-22 December 2022 .Thank you for your interest in participating in the 6th ICES.

Best Regards

L. Sh. Rash

Prof. Dr. Laith Sh. Rasheed
Chair of the Organizing Committee -ICES
Dean of Engineering College at Kerbala University

+964-771-5907020

ices@uokerbala.edu.iq

https://sites.google.com/view/ices-2022/home

Acceptance Letter

Author(s) : Zahraa Mohammed Kadhum[1] ,Mohammed Wahhab Aljibory[1] ,Farhan Lafta Rashid[3]

Affiliation : Mechanical Engineering Department, University of Kerbala, Karbala 56001, Iraq[1] ,Petroleum Engineering Department, University of Kerbala, Karbala 56001, Iraq[2]

Email of Corresponding Author : zahraa.khadim@s.uokerbala.edu.iq

Dear (author) We are pleased to inform you that your manuscript

Numerical Simulation for the Effect of Air Bubble Injection

after being peer- reviewed , has been accepted for participating in the

4th INTERNATIONAL SCIENTIFIC CONFERENCE OF ALKAFEEL UNIVERSITY , ISCKU 2022

in Al-Najaf Al-Ashraf, Iraq ,December 20th -21st , 2022 . Given that your manuscript will be published after passing. the conference Scopus-indexed journals requirements

With Best Regards

N. ALDAHAN

Prof. Dr. N. Al-Dahan

Rector of Alkafeel University

Scopus

AIP Publishing

University of Alkafeel

ان المحاكاة العددية بواسطة برنامج ANSYS FLUENT والنتائج التجريبية للنموذج كانت لها نسبة توافق جيدة إلى حد ما تحت نفس الظروف. بالنسبة للنظام المفتوح (مع أو بدون حقن فقاعات الهواء)، فإن النسبة المئوية القصوى للاختلاف في النتائج كانت لا تزيد عن 13.5٪. ومع ذلك، بالنسبة للنظام المغلق (مع وبدون حقن فقاعات الهواء)، فإن اقصى اختلاف في النتائج كانت النسبة المئوية لا تزيد عن 13٪.

المستخلص

قدمت هذه الدراسة طريقتين للتحقيق (عدديا وعمليا) استخدمت فيهما آلية فنجوري لحقن فقاعات هواء في أنبوب مموج لتجميع المياه بالطاقة الشمسية لتحسين أدائه الحراري. تسمح هذه التقنية للهواء بالتحرك عبر الأنابيب، والاختلاط بالماء ثم التدفق معًا داخل أنبوب تجميع الطاقة الشمسية. تم استخدام نظامين في كل جزء، نظام مفتوح ومغلق. تم إنجاز الجزء العددي من خلال رسم النموذج الهندسي باستخدام برنامج SOLID WORKS 2021، بعدها تم اجراء المحاكاة باستخدام برنامج ANSYS 21. بينما تم تنفيذ الجزء العملي من خلال إنشاء مجمع تسخين المياه بالطاقة الشمسية بأبعاد (120x80x24) سم3 مائلة بزاوية 45 درجة وتشمل أنبوب نحاسي مموج بقطر 0.0125 م وبطول 8 م مطلي باللون الأسود المطفأ.

تم بناء جهاز الاختبار في مدينة كربلاء لمعرفة تأثير حقن الفقاعات الهوائية تحت الظروف الجوية لمدينة كربلاء المقدسة في العراق مع خط عرض وخط طول 32.616 درجة شمالا و44.0249 درجة شرقا خلال الأشهر الأولى من العام (كانون الثاني، شباط، آذار ونيسان). تم استخدام الماء كسائل عمل بمعدلات تدفق متعددة لتحديد كفاءة المجمع لكل نظام، ثم تم حقن فقاعات الهواء بعدة تصريفات لمعدل تدفق المياه الأكثر كفاءة لكل نظام (مغلق ومفتوح)، وبالتالي معرفة أفضل معدل تدفق خليط الهواء والماء لكل نظام.

في هذا العمل، تمت محاكاة واختبار أربعة عشر حالة لمعرفة أداء المجمع والحالة الأكثر كفاءة، والتي تتكون من أربعة مستويات مختلفة لمعدلات تدفق المياه فقط (0.5، 1، 1.5، 2) لتر/دقيقة كسائل عمل. للنظام المفتوح والمغلق. تم حقن فقاعات الهواء بثلاث معدلات تدفق هواء (0.15، 0.25 و0.35) لتر / دقيقة مختلطة مع تدفق الماء الأكثر كفاءة في كل نظام.

وبعد ذلك، تم حساب كفاءة النظام بعد إجراء الاختبارات العددية والتجريبية لمعدلات تدفق المياه الأربعة لكلا النظامين. حيث أوضحت النتائج أن الحالة الأكثر كفاءة للنظام المفتوح حدثت عندما كان معدل تدفق المياه 1 لتر / دقيقة، بمتوسط كفاءة (31.8) ٪، في حين أن الحالة الأكثر كفاءة للنظام المغلق كانت 2 لتر / دقيقة، مع بمتوسط كفاءة (45.5) ٪.

كما أظهرت النتائج انه عند حقن ثلاث معدلات تدفق مختلفة للهواء في عند أفضل حالة لكل نظام بأن هنالك تحسن لكفاءة النظام المغلق بنسبة (24.98٪) و (37.28٪) و (53.71٪)، فيما تعززت كفاءة النظام المفتوح بنسبة (30.89٪) و (37.92٪) و (20.03٪) بعد ذلك. إضافة الهواء بمعدلات تدفق (0.15، 0.25، 0.35) لتر / دقيقة على التوالي.

جمهورية العراق
وزارة التعليم العالي و البحث العلمي
جامعة كربلاء
كلية الهندسة
قسم الهندسة الميكانيكية

تصميم وبناء مجمع جديد للمياه بالطاقة الشمسية باستخدام حقن الفقاعات الهوائية

رسالة مقدمة الى مجلس كلية الهندسة / جامعة كربلاء وهي جزء من متطلبات نيل

درجة الماجستير في علوم الهندسة الميكانيكية

من قبل:

زهراء محمد كاظم

بكالوريوس 2012

باشراف :

أ.م .د. محمد وهاب الجبوري

أ. م .د. فرحان لفتة رشيد

2023 م   **1444 هـ**